

Journal Pre-proof

Physics of the nuclear pore complex: Theory, modeling and experiment

Bart W. Hoogenboom, Loren E. Hough, Edward A. Lemke, Roderick Y.H. Lim, Patrick R. Onck, Anton Zilman



PII: S0370-1573(21)00110-1
DOI: <https://doi.org/10.1016/j.physrep.2021.03.003>
Reference: PLREP 2164

To appear in: *Physics Reports*

Received date : 19 August 2019
Revised date : 1 February 2021
Accepted date : 12 March 2021

Please cite this article as: B.W. Hoogenboom, L.E. Hough, E.A. Lemke et al., Physics of the nuclear pore complex: Theory, modeling and experiment, *Physics Reports* (2021), doi: <https://doi.org/10.1016/j.physrep.2021.03.003>.

This is a PDF file of an article that has undergone enhancements after acceptance, such as the addition of a cover page and metadata, and formatting for readability, but it is not yet the definitive version of record. This version will undergo additional copyediting, typesetting and review before it is published in its final form, but we are providing this version to give early visibility of the article. Please note that, during the production process, errors may be discovered which could affect the content, and all legal disclaimers that apply to the journal pertain.

© 2021 Published by Elsevier B.V.

1
2
3
4
5 1
6
7 2 **Physics of the Nuclear Pore Complex: Theory,**
8
9 3 **Modeling and Experiment**
10
11 4

12 5 Bart W. Hoogenboom^{1,+}, Loren E. Hough², Edward A. Lemke³, Roderick Y. H. Lim⁴, Patrick R. Onck⁵,
13 6 Anton Zilman^{6,*}
14 7

15 8 *Author affiliations:*
16 9

17 10 ¹ *London Centre for Nanotechnology and Department of Physics and Astronomy,*
18 11 *University College London, London WC1E 6BT, United Kingdom*
19 12

20 13 ² *Department of Physics and BioFrontiers Institute, University of Colorado, Boulder CO 80309,*
21 14 *United States of America*
22 15

23 16 ³ *Biocenter Mainz, Departments of Biology and Chemistry, Johannes Gutenberg University and Institute*
24 17 *of Molecular Biology, 55128 Mainz, Germany*
25 18

26 19 ⁴ *Biozentrum and the Swiss Nanoscience Institute, University of Basel, 4056 Basel, Switzerland*
27 20

28 21 ⁵ *Zernike Institute for Advanced Materials, University of Groningen, 9747 AG Groningen,*
29 22 *The Netherlands*
30 23

31 24 ⁶ *Department of Physics and Institute for Biomedical Engineering (IBME),*
32 25 *University of Toronto, Toronto, ON M5S 1A7, Canada*
33 26
34 27
35 28
36 29

37 30 * zilmana@physics.utoronto.ca (corresponding author)
38 31

39 32 + b.hoogenboom@ucl.ac.uk (co-corresponding author)
40 33
41 34
42 35
43
44
45
46
47
48
49
50
51
52
53
54
55
56
57
58
59
60
61
62
63
64
65

1
2
3
4
5 1
6
7 2 **Table of Contents**
8 3
9
10 4

10	4	1. Introduction	4
11	5	2. Biological function, molecular components and architecture of the NPC	8
12	6	3. Physics of the intrinsically disordered proteins of the Nuclear Pore Complex and their interactions with transport proteins	12
13	7		
14	8	3.1. The gatekeeper of the NPC: FG nup assembly in the NPC	12
15	9	3.2. Physics of FG nups on the single molecule level	13
16	10	3.2.1 Theoretical background	14
17	11	3.2.2 Simulation approaches and methods	17
18	12	3.2.3 Analysis of experimental data using theoretical and computational models	18
19	13	3.3. Collective effects in assemblies of FG nups	20
20	14	3.3.1. Bulk phases and phase transitions of FG nups	20
21	15	3.3.2. Assemblies of FG nups grafted to planar surfaces	23
22	16	3.3.3. FG nups in NPC mimicking synthetic nanopores	26
23	17	3.4. Interactions of FG nups with transport proteins	30
24	18	3.4.1. Quantification of interactions between FG nups and transport proteins: thermodynamics	31
25	19		
26	20	3.4.2 Kinetics of the FG nup- transport protein interaction	34
27	21	3.4.3. Morphologies of multi-chain assemblies of FG nups and transport proteins in solution	35
28	22		
29	23	3.4.4. Assemblies of transport proteins and surface grafted FG nups	38
30	24	3.4.5. Transport proteins in FG nups assemblies in nanopores	41
31	25	3.5. Biophysical insights into the morphology of transport channel of intact NPCs	42
32	26	4. From structure to transport	46
33	27	4.1. Transport dynamics of the transport proteins within NPC-like FG nup assemblies <i>in vitro</i> .	47
34	28		
35	29	4.1.3. Diffusion of transport proteins within FG nup assemblies.	47
36	30	4.1.4. Nanochannel mimics of the NPC.	50
37	31	4.1.4.1. Theoretical background: diffusion through nanochannels.	51
38	32	4.1.4.2. Specificity of NPC mimics at the single molecule level	54
39	33	4.1.4.3. Effective potential in FG nup functionalized nanopores	55
40	34	4.1.4.4. Transport protein crowding inside the channel	57
41	35	4.2. Physical insights into transport by NPCs in the cell	59

1			
2			
3			
4	1	4.2.3. Passive permeability barrier of the NPC	59
5			
6	2	4.2.4. Kinetics and energetics of the facilitated transport through NPCs in cells.	62
7			
8	3	3.4.2. Effects of transport protein crowding on NPC transport	67
9			
10	4	4.3. Nucleo-cytoplasmic transport cycle as a pump	69
11	5	5. Conclusions and Discussion	72
12			
13	6		
14	7		
15			
16			
17			
18			
19			
20			
21			
22			
23			
24			
25			
26			
27			
28			
29			
30			
31			
32			
33			
34			
35			
36			
37			
38			
39			
40			
41			
42			
43			
44			
45			
46			
47			
48			
49			
50			
51			
52			
53			
54			
55			
56			
57			
58			
59			
60			
61			
62			
63			
64			
65			

Abstract

The hallmark of eukaryotic cells is the nucleus that contains the genome, enclosed by a physical barrier known as the nuclear envelope (NE). On the one hand, this compartmentalization endows the eukaryotic cells with high regulatory complexity and flexibility. On the other hand, it poses a tremendous logistic and energetic problem of transporting millions of molecules per second across the nuclear envelope, to facilitate their biological function in all compartments of the cell. Therefore, eukaryotes have evolved a molecular “nanomachine” known as the Nuclear Pore Complex (NPC).

Embedded in the nuclear envelope, NPCs control and regulate all the bi-directional transport between the cell nucleus and the cytoplasm. NPCs combine high molecular specificity of transport with high throughput and speed, and are highly robust with respect to molecular noise and structural perturbations. Remarkably, the functional mechanisms of NPC transport are highly conserved among eukaryotes, from yeast to humans, despite significant differences in the molecular components among various species.

The NPC is the largest macromolecular complex in the cell. Yet, despite its significant complexity, it has become clear that its principles of operation can be largely understood based on fundamental physical concepts, as have emerged from a combination of experimental methods of molecular cell biology, biophysics, nanoscience and theoretical and computational modeling. Indeed, many aspects of NPC function can be recapitulated in artificial mimics with a drastically reduced complexity compared to biological pores.

We review the current physical understanding of the NPC architecture and function, with the focus on the critical analysis of experimental studies in cells and artificial NPC mimics through the lens of theoretical and computational models. We also discuss the connections between the emerging concepts of NPC operation and other areas of biophysics and bionanotechnology.

Keywords: Nuclear pore complex, intrinsically disordered proteins, nanochannels, stochastic transport, crowding, biomimetic, multivalency, diffusion, molecular modelling, molecular dynamics

1. Introduction

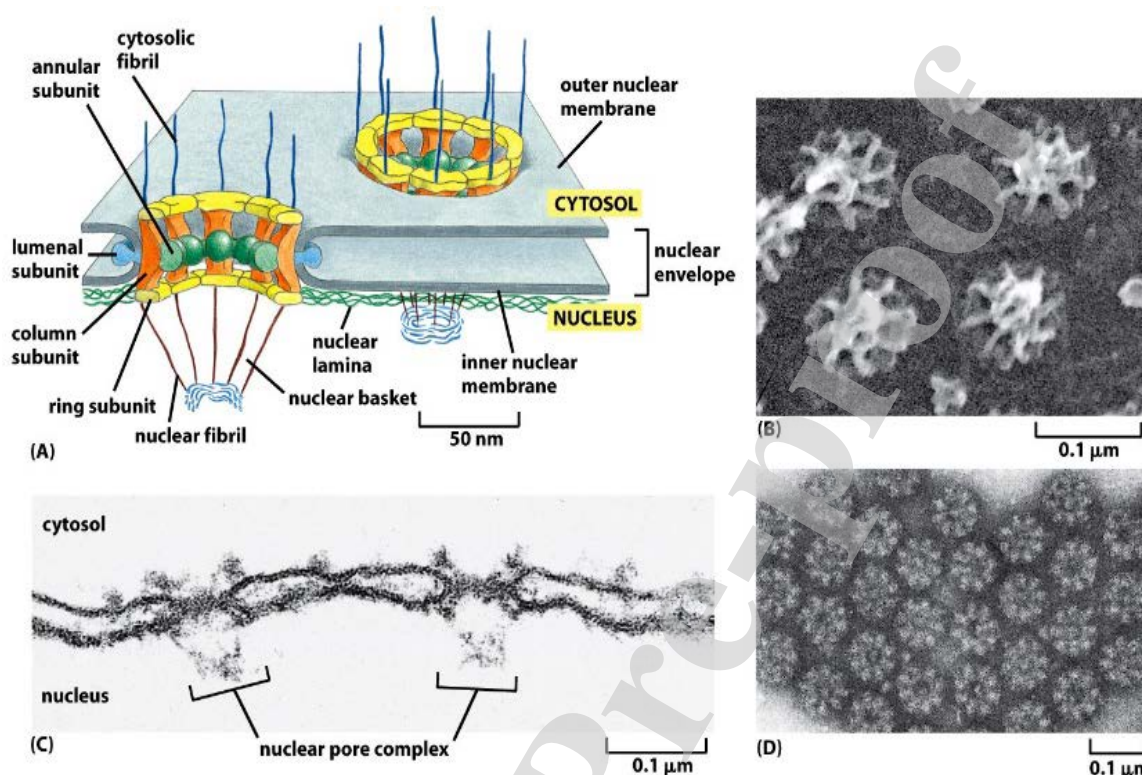


Figure 1. (A) The nucleus is encapsulated by a nuclear envelope that comprises two lipid bilayers with an approximate overall thickness of 40 nm. NPCs perforate the nuclear envelope and mediate molecular transport between the nucleus and the cytoplasm. (B-D) Electron microscopy images showing nucleoplasmic, and cytoplasmic sides of a nuclear envelope of a *Xenopus* frog perforated by NPCs. Note the eightfold symmetry of the structure (D) and the nuclear basket structure (B,C) **Reproduced from [1], permission pending.**

Eukaryotic organisms comprise one of the tree main branches of life, alongside with bacteria and archaea. Eukaryotic cells are highly morphologically and functionally diverse, and occur as unicellular micro-organisms (such as yeast) or as essential building blocks of tissues of complex organisms (such as humans). Nevertheless, they are universally characterized by the sequestration of their genome inside the cell nucleus (a feature from which they derive their name). This separation is achieved by a complex barrier of approximately 40 nm thickness, known as the nuclear envelope [1], which consists of two lipid membranes pierced or decorated by various proteins. The evolutionary origin of the nucleus and its subcomponents are still not fully understood [2,3]. Functionally, segregation of the nuclear DNA enables significantly more complex spatial and temporal regulation of intra-cellular processes compared to prokaryotes (e.g. bacteria), where the genome is directly accessible by most regulatory molecules [4]. On the other hand, sequestration of the DNA in the nucleus implies the need to regulate macromolecular transport across the nuclear envelope. Typical import cargoes include transcription factors, seeking access to the DNA in the nucleus, while typical export cargoes include mRNAs seeking access to the ribosomes in the cytoplasm [5]. Under normal operating conditions, millions of proteinaceous and nucleic acid molecules must cross the envelope per second in both directions [6].

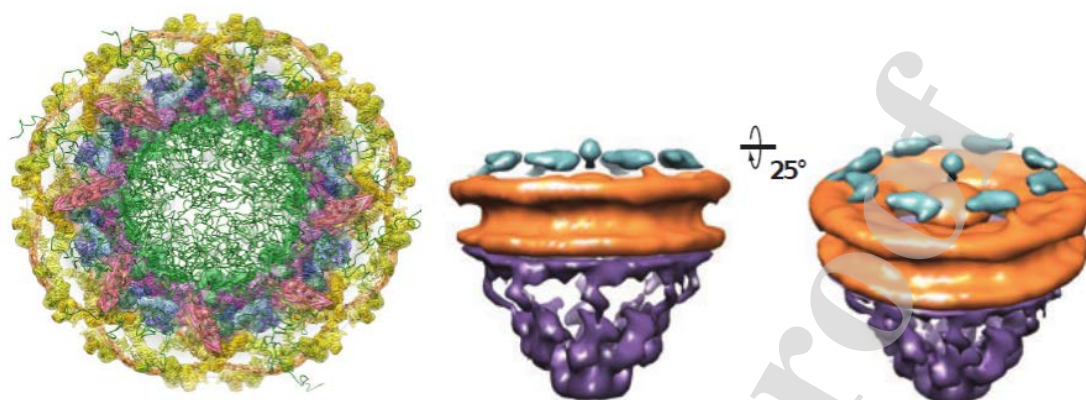


Figure 2. Electron tomography structure of the NPC from different angles. The orange/yellow-labeled proteins form a ring-shaped structure that anchors the NPC to the nuclear envelope of the thickness of ~40 nm and that serves as the scaffold for the attachment of intrinsically disordered polypeptides, here schematically depicted in green. The purple structure is the nuclear basket. While the structure of the scaffold is now known to a high precision, the distribution of the intrinsically disordered domains in the passageway is much less defined. The diameter of the internal passageway is approximately 35-59 nm, and the overall length is ~100 nm, (including the basket). Note that the cytoplasmic filaments are not well resolved. Adapted from [7] and [8], permission pending.

All this multifarious bi-directional transport proceeds through molecular filtering “machines” termed nuclear pore complexes (NPCs) (see Figure 1). Altogether, several hundred to several thousands of NPCs perforate the nuclear envelope, depending on the cell type, with a typical flux of hundreds of molecules per second per NPC. Each transport event takes from several milliseconds to hundreds of milliseconds depending on the cargo type. In spite of the high throughput, molecular transport through the NPC is remarkably specific, rapid and robust with respect to molecular noise and structural perturbations [5,6,9].

As the sole conduit of nucleocytoplasmic transport, the NPC is a keystone component of multiple transport and regulatory processes in health and disease, such as gene regulation and signaling. Not surprisingly, dysregulation of NPC function is implicated in a number of diseases, from viral infections to cancer and neurodegenerative diseases [10–17].

The overall architecture and transport mechanism of the NPC is functionally conserved among species, although specific molecular details can vary [2,3,18–22]. Notably, many of the NPC properties have been recapitulated *in vitro* in simplified functionalized molecular assemblies and nanopore devices that mimic aspects of NPC architecture and function [23–28]. These observations suggest that NPC function relies on universal design features, and might largely be understood from fundamental physical principles.

The structure, architecture and functional mechanism of the NPC is unique amongst different cellular transporters [5,9], as detailed in the following sections. NPCs are assembled from multiple

1
2
3
4 1 copies of approximately thirty different proteins termed nucleoporins. With a combined molecular
5 2 mass of 60-125 MDa (depending on the species), NPCs constitute the largest macromolecular
6 3 complexes in the cell [8,29,30]. In comparison, the ribosome, the protein synthesizing apparatus,
7 4 is about two orders of magnitude smaller than the NPC. Approximately half of these proteins form
8 5 a structure that perforates the nuclear envelope and forms the aqueous transport channel of the
9 6 NPC. Recent structural studies using X-ray crystallography and electron microscopy/tomography,
10 7 as well as mass-spectrometry and cross-linking, have provided detailed insights on how Nature
11 8 assembles this giant “jigsaw puzzle” (Figure 2) [7,31–36].
12 9

13 10 The internal structure of the transport channel is equally unique. Its walls are decorated with
14 11 multiple nucleoporins that contain highly flexible and dynamic intrinsically disordered regions
15 12 (IDRs), which form the transport environment within the NPC passageway (IDRs are also known
16 13 as natively unfolded or “unstructured” protein domains) [5,6,9,37–41]. The disordered nature of
17 14 the nucleoporins within NPC passageway makes it challenging to experimentally probe their
18 15 behavior at the relevant nanometer length and millisecond time scales. A major drawback arises
19 16 from the high spatial and temporal mobility of the IDRs making them largely inaccessible to
20 17 classical methods, such as X-ray crystallography and (cryo)-electron tomography, as these rely on
21 18 ensemble averaging of individual conformations to obtain structural information. Although
22 19 alternative techniques, such as atomic force microscopy (AFM), super-resolution microscopy ,
23 20 intra-cellular FRET and fluorescence correlation spectroscopy, have started to resolve the
24 21 morphology and the dynamics of the transport channel in intact NPCs [42–48], much of our
25 22 knowledge about the nuclear pore still derives from *in vitro* studies of its components and their
26 23 assemblies, interpreted via computational and theoretical models. As a result, computational and
27 24 theoretical modeling have been a key part in understanding the role of the intrinsically disordered
28 25 protein domains in the NPC function.
29 26

30 27 Theoretical models have enabled rigorous investigation of various ideas and concepts of NPC
31 28 function, facilitating quantitative interpretations of experimental data and providing predictions to
32 29 guide the development of future experiments. To develop an adequate description of the NPC
33 30 machinery, ongoing efforts have drawn upon a rich combination of ideas, theoretical concepts and
34 31 simulation techniques. These span equilibrium and non-equilibrium statistical mechanics,
35 32 stochastic process theory, polymer physics, and simulation techniques ranging from explicit
36 33 atomistic molecular dynamics to coarse grained polymer models [49–63]. In combination,
37 34 biophysical techniques and theoretical approaches are starting to reveal fundamental insights into
38 35 the organization and the dynamics of the NPC at the nanoscale.
39 36

40 37 Besides its fundamental biological importance, the NPC also has served as a case study for the
41 38 application of physical approaches to understanding of noise-dominated phenomena that occur in
42 39 highly fluctuating nanoscale macromolecular assemblies in extremely complex biological
43 40 molecular complexes. This review describes the recent advances in the understanding of the NPC,
44
45
46
47
48
49
50
51
52
53
54
55
56
57
58
59
60
61
62
63
64
65

1
2
3
4 1 with the focus on the physical concepts, approaches and tools. In Section 2, we introduce the main
5 2 structural and functional features of the NPC. Section 3 describes our current understanding of the
6 3 biophysics of the interactions between the transport proteins and the intrinsically disordered
7 4 proteins of the NPC, and how these interactions shape the internal morphology of the NPC
8 5 passageway. Section 4 deals with the kinetics and dynamics of the NPC transport, based on the
9 6 discussion on Section 3. We conclude with discussion in Section 5.
10 7
11
12
13
14
15
16
17
18
19
20
21
22
23
24
25
26
27
28
29
30
31
32
33
34
35
36
37
38
39
40
41
42
43
44
45
46
47
48
49
50
51
52
53
54
55
56
57
58
59
60
61
62
63
64
65

2. Biological function, molecular components and architecture of the NPC

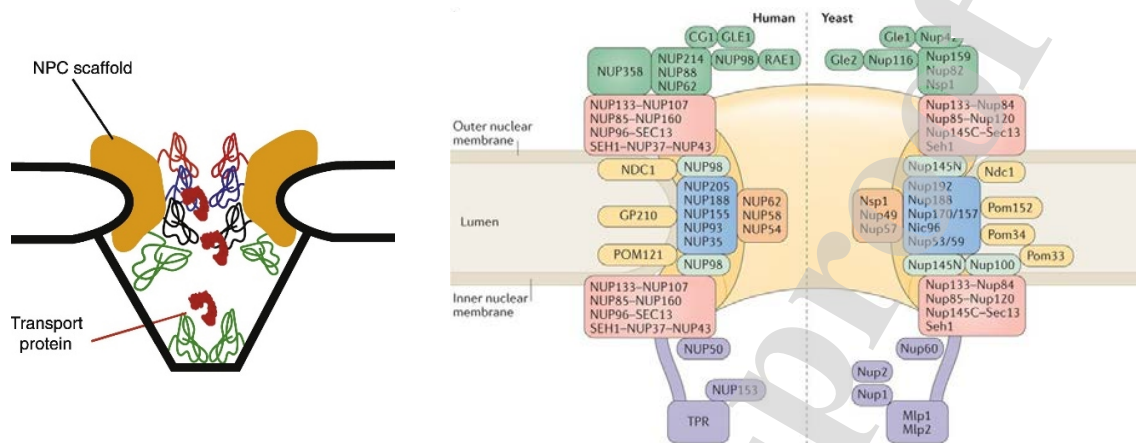


Figure 3. Schematic rendering of the NPC structure. Left: Schematic illustration of the NPC cross-section. Yellow color denotes the structural scaffold of the NPC embedded in the nuclear envelope. Wiggly lines of different color denote different FG nups. Transport proteins are indicated in red. Adapted from [56], permission pending. Right: Schematic diagram of the locations of various molecular components of the NPC. The major human FG nups are Nup98, Nup62, Nup153 and Nup214. The major yeast FG nups are Nup100, Nup116, Nsp1, Nup1 and Nup2. Adapted from [31], permission pending.

NPC is capable of transporting a variety of cargoes of different sizes and molecular characteristics [5,6,9,12]. These range from small molecules, such as ions, proteins such as transcription factors and histones, to large protein complexes, such as proteasomes, ribosomal subunits, and messenger RNAs (mRNA); the latter are exported from the nucleus packaged with proteins into what are known as messenger ribonucleoproteins (mRNPs) and can reach the size of tens of nanometers [64–66]. This transport versatility makes the NPC stand out from other cellular transporters such as ion pumps, metabolic transporters and porins, which are typically highly specialized to transport specific molecules [1]; consequently, it also stands out in terms of size and transport mechanism. One of the most striking and unique characteristic of the NPC is its ability to combine this transport versatility with high selectivity, throughput and relative robustness to structural perturbations [5,6,67–69].

The NPC is anchored to the nuclear envelope by a structural scaffold that forms a passageway with an inner diameter of about 35-50 nm (depending on the species) as illustrated in Figure 2 and Figure 3. Recent advances in electron tomography, X-ray crystallography and mass spectroscopy have resulted in the models of the pore scaffold approaching atomic resolution [7,31–35,70,71]. The structure of the scaffold will not be the focus of this review.

The passageway of this pore is lined by numerous proteins that possess intrinsically disordered regions (IDRs) that are rich in hydrophobic Phenylalanine(F)-Glycine(G) amino-acid “patches” from which they derive their name - FG nucleoporins or FG nups, in short [5,72]. These proteins

1 are end-grafted to the inner walls of the pore typically via small folded terminal domains [5,9].
2 Unlike the more familiar structured proteins, the intrinsically disordered regions of the FG nups
3 do not fold into defined three-dimensional structures. Hence, in many respects they behave as
4 conventional polymers [37,39,53,56,57,73,74]. We return to the molecular and the biophysical
5 description of these molecules below. Each NPC contains about 200-300 FG nups per pore, spread
6 among 10-15 different types that can differ in their amino acid sequence and localization within
7 the NPC [9,10,19,22]. These chain-like molecules create a milieu within the NPC passageway that
8 enables transport of a wide variety of cargoes through the same pore in both directions. This
9 reliance on disorder also implies that, unlike other transporters, the NPC does not possess a gate
10 that transitions between well defined “closed” and “open” conformations during a transport event.

11
12 Despite this versatility, NPC is strictly selective and efficiently limits the transport only to
13 appropriate cargoes. This combination of flexibility and selectivity of transport through the NPC
14 is achieved through a two-layer regulation of transport specificity and kinetics. This is illustrated
15 in Figure 4 for the example of the nuclear import cycle, which concentrates cargoes such as
16 transcription factors inside the nucleus [6,9].

17
18 The first level of import regulation involves the binding of macromolecular cargoes in the
19 cytoplasm to soluble transport proteins known as Importins/Transportins or Karyopherins
20 (depending on the species); or more generally as nuclear transport receptors (NTRs). Throughout
21 this review we will refer to them either as “transport proteins” or NTRs interchangeably. The
22 function of these transport proteins is to recognize and bind specific cargoes in the cytoplasm
23 through a short peptide motif on the cargo known as the nuclear localization sequence (NLS). The
24 binding of cargoes to transport proteins can be regulated through the use of adaptor proteins,
25 conformational changes and chemical modifications of the cargo (such as phosphorylation),
26 thereby providing the first layer of regulation of cargo recognition and transport [5,9,10].

27
28 The second layer of transport selectivity relies on multiple but relatively weak binding interactions
29 between the transport proteins with the FG nups, which facilitates the entry and the eventual
30 translocation of the cargo-NTR complex through the NPC passageway [9]. By contrast, the NPC
31 hinders the entry and translocation of macromolecules that do not bind to the transport proteins
32 and do not bind directly to the FG nups: whereas ions and small molecules (up to a few nanometers)
33 like ATP can freely translocate through the NPC by diffusion, larger molecules and particles are
34 progressively hindered from entering and translocating through the NPC with increasing size [75–
35 77].

36
37 Inside the NPC passageway, the translocation of transport protein/cargo complexes is primarily a
38 diffusive process, driven by thermal fluctuations and facilitated by the interactions with the FG
39 nups [6,78–80]. Each individual translocation of a transport protein/cargo complex occurs without
40 requiring direct input of energy, e.g., in the form of ATP or GTP hydrolysis, and typically takes

on the order of several milliseconds [78,81]. Yet, macroscopically, NPC translocation is a part of the transport cycle that operates as a thermodynamic pump that concentrates cargoes inside the nucleus against their chemical potential gradient. Once the transport protein/cargo complex reaches the nucleus, the cargo is released from the transport protein through binding of the transport protein with RanGTP, which acts as a molecular switch that unilaterally releases the cargo from the transport protein (and thus from the NPC) into the nucleus [79,82]. The RanGTP-bound transport protein is free to translocate back to the cytoplasm, as illustrated in Figure 4 [6,9]. In addition, RanGTP is also known to catalyze the release of some of the transport proteins from the FG nups located at the nuclear basket, further enhancing the transport efficiency [43,80,83,84].

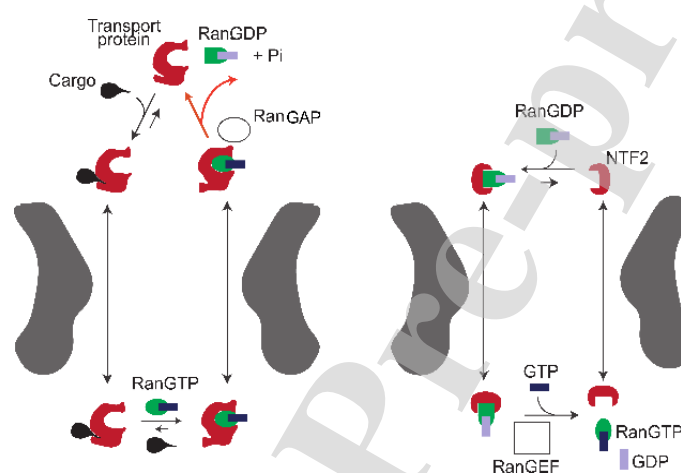


Figure 4. Schematic illustration of the import cycle of the NPC. Left: Cargo import cycle. Right: Ran cycle. See text for explanation. With the exception of GTP hydrolysis by RanGAP in the cytoplasm (red arrows), all the processes are thermodynamically reversible. Additional details are provided in Section 4.3. Adapted from [6], permission pending.

In the case of nuclear import, cargo concentrates in the nucleus at higher levels than in the cytoplasm (e.g. [85–89]), which ultimately requires the input of energy provided by the hydrolysis of a Ran bound GTP molecule and the accompanying conversion of RanGTP to RanGDP. This non-equilibrium step of the import cycle occurs in the cytoplasm, catalyzed by the cytoplasmic protein RanGAP (an abbreviation of “GTPase activating protein”). The energy obtained from the hydrolysis is used to overcome the binding of Ran to the transport protein, resulting in their detachment. After the release, the transport protein becomes available to bind the next cargo for nuclear import. Notably, in the operational NPC transport cycle, energy input in the form of GTP hydrolysis is not directly coupled to any molecular rearrangement of the NPC, unlike in many other familiar molecular motors and pumps (such as processive motors, ion exchangers, and ATPases) [90].

As a consequence, the nuclear import cycle scheme shown in Figure 4 uses one molecule of GTP and exports one Ran molecule from the nucleus to the cytoplasm per each cargo transported to the

1
2
3
4 1 nucleus. (For transport proteins, such as Importin- β that use an adapter, Importin- α , to bind the
5 2 cargo, the energy cost is two GTP molecules [5]). To maintain the concentration gradient of
6 3 RanGTP across the nuclear envelope and thus the transport directionality, RanGDP needs to be
7 4 shuttled back to the nucleus and converted back to GTP, as follows. Firstly, a specialized
8 5 transporter, nuclear transport factor 2 (NTF2), re-imports the RanGDP molecule into the nucleus
9 6 through a reversible energy-independent diffusion-based translocation through the NPC. There,
10 7 GDP in RanGDP is substituted by GTP – a process catalyzed by the nuclear protein by Ran guanine
11 8 exchange factor GEF (RanGEF; also known as RCC1) using GTP available in the cell.
12 9 Importantly, with the exception of the GTP hydrolysis at the NTR release stage, all other transport
13 10 and binding processes in the cycle are thermodynamically reversible. In summary, GTP hydrolysis
14 11 powers the directional flow of cargoes into the nucleus that is rectified by the asymmetry in
15 12 RanGAP and RanGEF localization between the nucleus and the cytoplasm. We return to the
16 13 energetics and directionality of nuclear transport in Section 4.3.

17 14
18 15 As mentioned above, a most remarkable feature of the NPC is its ability to combine high transport
19 16 selectivity with high speed of transport. Individual protein import/export events typically occur on
20 17 millisecond time scales [78,81,91], and the transport times of even very large cargoes such as
21 18 mRNPs are typically on the sub-second scale [66,92,93]. Notably, unlike other transporters, NPC
22 19 translocation is not restricted to only one cargo at a time. Instead, the passageway of the NPC is
23 20 typically crowded with multiple transport proteins, some of which are bound to cargoes and others
24 21 not, some directed towards the cytoplasm, others to the nucleus. Overall, each NPC can contain
25 22 hundreds of transport proteins at any given time, while transporting hundreds of cargoes per second
26 23 [7,43,83,85]. It remains puzzling that the NPC can maintain its selectivity and its continuous, fast,
27 24 parallel and bidirectional transport, in spite of this crowding.

28 25
29 26 Another remarkable aspect of NPC transport is its robustness with respect to deletion of its
30 27 components. While several pore-specific constituent proteins are indispensable for cell viability
31 28 and NPC transport functionality, a substantial fraction of the FG nups can be deleted (in yeast),
32 29 resulting in no to mild defects in transport functionality [41,67,68,94]. In another manifestation of
33 30 this structural robustness, transport defects caused by deletion of barrier-forming FG nups in one
34 31 species (*Xenopus*) could be rescued by expression of functionally homologous FG nups from
35 32 another species (yeast) [94].

36 33
37 34 Faced with this complexity, a number of different models have evolved in the field to address
38 35 different aspects of NPC operation, ranging in focus from the general principles of the molecular
39 36 transport on the nanoscale as revealed in *in vitro* NPC mimics, to the emphasis on the particular
40 37 molecular mechanisms and structures as central to NPC transport [49,50,84,95–103]. Based on
41 38 these ideas, the combined experimental and the theoretical work of the last decade has started to
42 39 provide a comprehensive physical picture of NPC organization and function, within which
43 40 molecular details and functional principles fall into place.

1
2
3
4 1
5
6 2 This review focuses on and elaborates this physical picture, with the emphasis on the following
7 3 key questions about the NPC:
8
9 4

- 10 5 • What key physical principles and variables capture NPC function and how do they relate
11 6 to the molecular architecture?
- 12 6 • What is the spatial organization of the FG nups inside the NPC passageway, and how does
13 7 it define the transport properties?
- 14 8 • How can NPCs combine high selectivity with high speed and throughput in bi-directional
15 9 transport under highly crowded conditions?
- 16 9 • How can the design principles of the NPC be mimicked and exploited by artificial nano-
17 10 devices for protein sensing, sorting and transport?
18 11
19 11
20 12

21 22 23 13 3. Physics of the intrinsically disordered proteins of the Nuclear Pore 24 14 Complex and their interactions with transport proteins 25 15

26 15 27 16 3.1. The gatekeeper of the NPC: FG nup assembly in the NPC 28 17 29 17

30 18 As mentioned above, the intrinsically disordered polymer-like FG nup domains are at the core of
31 19 the NPC transport mechanism. Overall, the FG nup protein family contains 10-15 different
32 20 subtypes that can vary in length and molecular sequence [5,7,9,41,62,63]. Within closely related
33 21 species (such as vertebrates), individual FG nup types can have close homologues, but there can
34 21 be large differences in sequence between distant species such as vertebrates and yeast [2,3,104].
35 22 In all species, the intrinsically disordered domains of these proteins harbor multiple hydrophobic
36 23 Phenylalanine-Glycine (FG) repeat motifs in their sequence [5,6]. The FG motifs are typically
37 24 interspersed by spacers that contain mostly neutral but also a small fraction of charged amino acids,
38 25 typically with zero or slightly positive overall charge [10,63,101,105]. The FG repeats are an
39 26 evolutionarily conserved motif of the FG nups, and they play a crucial role in the structure and
40 27 function of the NPC. Generally, it has been noted that FG motifs commonly appear in the FG nup
41 28 sequence either alone or in “patches” such as FGFG, FxFG or GLFG combinations, and
42 29 occasionally as GF or single F amino acids. Although classification of the groups of FG nups based
43 30 on these features has been discussed, the functional role of these differences is currently not fully
44 31 understood [41,72,101,106] In current approaches, especially computational ones, the FG motif is
45 32 commonly considered as the minimal “functional” unit responsible for the FG nup roles in NPC
46 33 transport, but further studies are required. We return to this question in more detail in the following
47 34 sections.
48 35
49 35
50 36
51 36
52 36
53 36
54 36

55 36
56 37 Most importantly, FG motifs are the main mediators of the interactions between the FG nups and
57 38 the transport proteins, crucial for NPC permeability and selectivity, predominantly through
58 39 hydrophobic interactions between Phenylalanines and hydrophobic grooves on the surface of the
59 39
60
61
62
63
64
65

1 transport proteins [9,10,95,96,105–107]. FG motifs are also hypothesized to be largely responsible
2 for intra- and inter-chain interactions between the FG nups, and thus potentially for shaping the
3 morphology and the permeability of the FG nup assembly [97,101,108,109]. However, recent
4 research shows that other interactions, such as electrostatic, cation- π , $\pi - \pi$ can participate both
5 in the interactions between FG nups and FG nup-transport protein interactions [63,67,96,105,110–
6 112].

7
8 Functionally, FG nups play a twofold role: they form a template for the binding of cargo-carrying
9 transport proteins in the NPC while simultaneously forming a permeability barrier against
10 macromolecules that do not specifically bind the FG motifs. The exact nature of this barrier has
11 been extensively debated, in particular whether it is based mainly on entropic forces
12 [73,75,102,113] or whether it arises from breaking the attractive FG-FG interactions between the
13 chains [97,109]. In general, the balance between the role of the chain entropy versus chain cohesion
14 in the barrier has been unclear; and more recent studies emphasize that both are likely to play an
15 important role [56,57,108,114].

16 17 3.2. Physics of FG nups on the single molecule level

18
19
20 FG nups, and IDRs in general, elude investigation by classical structural biology techniques, such
21 as X-ray crystallography and electron microscopy because they lack a well-defined, ordered
22 conformation [33,37,39]. Broadly speaking, at equilibrium the flexible IDRs populate a large
23 ensemble of different conformations, much like classical polymeric molecules [39,115,116].
24 Although some disordered domains can retain a significant propensity for particular secondary
25 structures [117,118], the experimentally studied FG nups exhibit conformational ensembles that
26 closely resemble polymer coils [73,101,103,119]. Accordingly, polymer physics concepts and
27 tools have become key in elucidating the biophysics of IDRs and the FG nups. Experimentally
28 observed FG nup behavior has been recapitulated in computational and theoretical models of
29 different degrees of coarse-graining.

30
31 The conformational ensemble of a polymer-like molecule can be characterized by the moments of
32 the spatial distribution of the monomer positions of the polymers [120,121]. Two variables that
33 characterize the chain dimensions in space are widely used in the interpretation of experimental
34 measurements: the average end-to-end distance R_E and the radius of gyration R_G . For a polymer of
35 N monomers, with the monomer positions denoted as \vec{R}_i , these closely related quantities are
36 defined as
37

$$R_E^2 = \langle (\vec{R}_1 - \vec{R}_N)^2 \rangle, \quad R_G^2 = \frac{1}{N} \sum_{i=1}^N \langle (\vec{R}_i - \vec{R}_c)^2 \rangle \quad (1)$$

where $\vec{R}_c = \frac{1}{N} \sum_i \vec{R}_i$ is the coordinate of the geometrical center of the chain and the averaging $\langle \dots \rangle$ is performed over the distribution of the conformational ensemble of the polymer [120]. Closely related to R_G (within a factor of 0.7-1.4 [120,122]) is the hydrodynamic radius (also known as the Stokes radius) R_S , defined as $R_S = \frac{k_B T}{6\pi\eta D}$, where D is the diffusion coefficient of the molecule in space and η is the viscosity of the fluid.

As the name suggests, R_E is a measure of the average distance between the two ends of the polymer molecule, and R_G quantifies its average overall dimension in space. Experimentally, R_E can be inferred, for instance, from Förster resonance energy transfer (FRET) between fluorescent labels at the chain ends, and R_G by small-angle X-ray scattering (SAXS) [123–125]. The hydrodynamic radius of the chain R_S can be inferred from dynamic light scattering (DLS) [126] or/and from a comparison with reference proteins by size exclusion chromatography [101], as well as from conventional light scattering, analytical centrifugation and microfluidic diffusional sizing.

Generally, the average dimensions of polymer molecules in solution are determined by the balance between, on one hand, their ensemble entropy and inter-monomer steric repulsion within the chain (which favor more extended structures), and, on the other hand, attractive intra-chain interactions (which favor more compact conformations) [121,127–129]. Although classical polymer physics was largely developed for homopolymers – and FG nup sequences are quite heterogeneous – the insights from simple polymer concepts have turned out to be very helpful for the analysis and interpretation of FG nup behavior (and other disordered proteins) [39,56,57,73,101,108,130].

3.2.1 Theoretical background

In a simple classical Flory-type mean field theory [121,127], the free energy of a polymer chain of N monomers is

$$\frac{F(N,R)}{k_B T} \simeq \frac{R^2}{2b^2 N} + f(n)R^3 \quad (2)$$

where R is the size of the polymer coil in space, b is the monomer size and n is the average monomer density inside the chain $n \simeq N/R^3$. The first term roughly approximates the configurational ensemble entropy of a chain that performs a random walk in space, stretched to a size R [121]. The second term describes the free energy of a “gas” of monomers that is contained within the spatial volume occupied by the chain. In the spirit of the virial expansion, the free energy density is $f(n) \simeq \frac{1}{2} B n^2 +$ higher order terms in n . The coefficient B is roughly proportional to

1 the second virial coefficient of the monomer-monomer interaction [120,131]. It includes the steric
2 repulsion between the monomers, also known as the “excluded volume” interactions, and attractive
3 interactions that make B more negative. Microscopically, monomer-monomer interactions can
4 arise from many molecular sources: hydrophobic, electrostatic and others, such as $\pi - \pi$ and
5 cation- π interactions between the aromatic rings of the Phenylalanines, as mentioned above. It is
6 convenient to write it as $B = v_0(1 - \chi_c)$ where $v_0 \sim b^3$ is the excluded volume of a monomer
7 and χ_c characterizes the strength of the averaged self-cohesive attractive interactions within the
8 chain, subsuming all molecular details; in the polymer physics literature, $\chi_c/2$ is known as the
9 Flory parameter [127]. The equilibrium chain size R is determined through the minimization of
10 the free energy of Equation (2) with respect to R . The simple heuristic Flory theory can be derived
11 using a number of different approximations using both lattice construction and continuous space.
12 Although exact methods and simulations can modify the Flory theory predictions, in many cases
13 it serves as a very good approximation, and has been the staple of the analysis of polymer chain
14 behavior, and more recently protein IDRs [131,132].
15
16
17
18
19

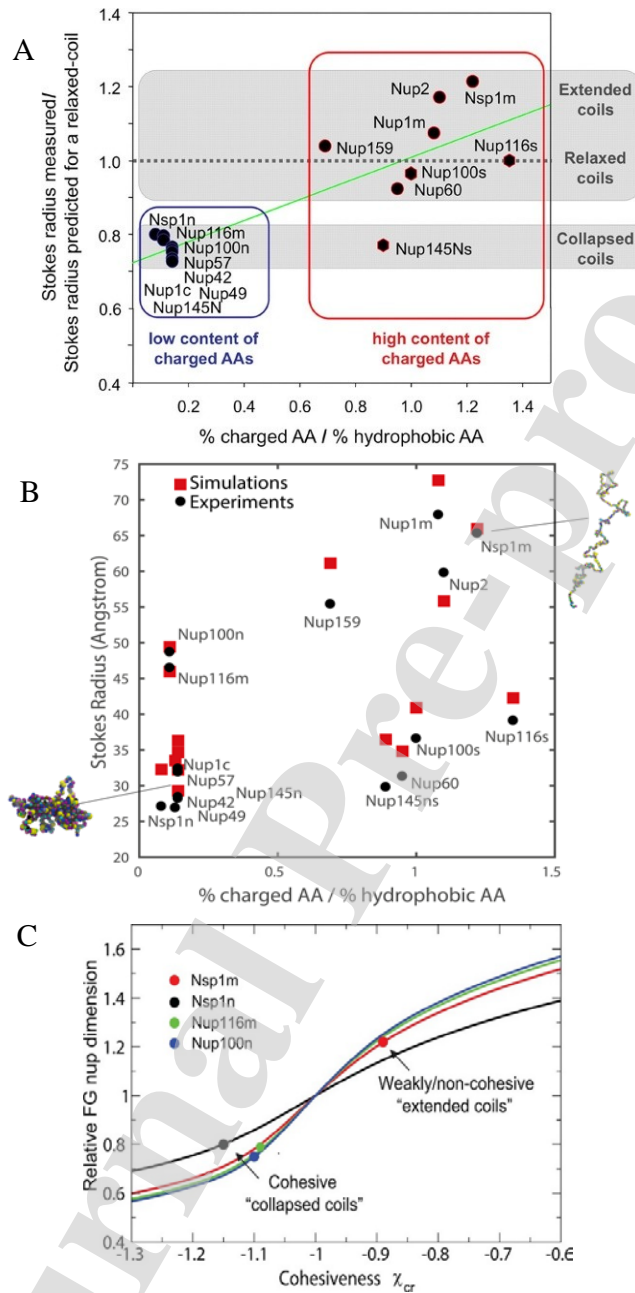


Figure 5. Dimensions of different FG nup chains. A: Classification of different FG nups based on their compactness as a function of the hydrophobic-to-charged amino acid content ratio. **Reproduced from** [101], **permission pending**. B: Stokes radii of various FG nups and FG nup segments calculated by one-bead-per-amino-acid model (in Kirkwood approximation), compared with experimental data; see text for details. **Reproduced from** [62], **permission pending**. C: Experimental FG nups dimensions analyzed using mean field Flory type polymer model. Increasing the cohesiveness makes the coils more compact and decreases the scaling exponent (see text). Dots: experimental data (normalized). Solid black, red, green and blue lines are the theoretical model predictions for chains of different length appropriate for the corresponding FG nups. The cohesiveness is proportional to the hydrophobic content of the chains. **Reproduced from** [56], **permission pending**.

1
2
3
4 1
5 2 At low average cohesiveness (small χ_c), the steric repulsion between the monomers dominates,
6 3 and the polymer chain behaves like a self-avoiding random walk, adopting “relaxed coil”
7 4 conformations at equilibrium [39,131,132]. In this regime the chain dimensions - both the R_G and
8 5 R_E - scale with the chain length N as $R \sim N^\nu$, where $\nu = 0.59$. As the intra-chain attractive
9 6 interactions increase (or, in polymer physics parlance, as the solvent quality decreases) the chains
10 7 progressively become more compact and behave as Gaussian chains with $\nu = 0.5$ at the point
11 8 where repulsion and attraction are balanced. With a further increase in cohesiveness, the polymers
12 9 undergo a smooth chain-globule transition to collapsed chains, with ν progressively decreasing to
13 10 $1/3$, characterizing the compact globular state [127,131,132]. Such scaling concepts have been
14 11 extremely useful in the classification and analysis of IDR behavior. In the protein literature, more
15 12 compact conformations are also known as “collapsed coils”, “molten globules” and “compact
16 13 globules” [39,115,132].
17 14

15 3.2.2 Simulation approaches and methods

16 17 Investigated through computer simulations using Brownian and Langevin dynamics, as well as
17 18 through various mean field and self-consistent field theories, simple homopolymer models have
18 19 been a staple of the computational studies of the NPC and its components, and provided important
19 20 insights into FG nup behavior [54,56,57,60,61,75]. Although lacking in molecular details, their
20 21 significant advantages are flexibility, robustness of the predictions with respect to parameter
21 22 choice, and speed, enabling to probe large spatial and long temporal scales.
22 23

23 24 At the opposite limit to simple homopolymer models, atomistic molecular dynamics (MD)
24 25 simulations have the potential to give atomically resolved interaction profiles and conformational
25 26 ensembles of FG nups [53,55,133–136]. However, these approaches have several pitfalls. First,
26 27 current state-of-the-art atomistic simulations have difficulties probing timescales beyond several
27 28 hundred nanoseconds to a microsecond in large multi-chain assemblies. This is significantly
28 29 shorter than the millisecond transport events through the NPC, and much shorter than the
29 30 timescales probed by coarse-grained models [137]. Beyond this technical limitation, the force
30 31 fields used for atomistic MD simulations have been parametrized and optimized largely based on
31 32 comparison with folded proteins. For IDRs, the ensembles predicted by atomistic simulations
32 33 depend rather sensitively on the force fields and the water models used [138–141], and frequently
33 34 appear more collapsed than experimental measurements [134,135]. Although modifications of the
34 35 atomistic force fields have been proposed, this can lead to a certain degree of over-
35 36 parameterization, and an accepted universal atomistic force field for IDRs is yet to be established
36 37 [134,135,142,143].
37 38

38 39 Bridging between the completely “sequence-free” polymer models, and the atomistic models are
39 40 chain models of intermediate coarse-graining levels that include some aspects of the sequence such
40 41
41 42
42 43
43 44
44 45
45 46
46 47
47 48
48 49
49 50
50 51
51 52
52 53
53 54
54 55
55 56
56 57
57 58
58 59
59 60
60 61
61 62
62 63
63 64
64 65

1
2
3
4 1 as FG "patches" or hydrophobic or charged character of individual amino acids [59,62,63,144–
5 2 146]. Although the coarse-graining procedure has not been standardized among different models,
6 3 the salient predictions are commonly consistent between different computational realizations of
7 4 FG nups.
8
9

10 5 11 6 3.2.3 Analysis of experimental data using theoretical and computational models 12 7

13 8 Dimensions of various FG nups were first systematically investigated by size-exclusion
14 9 chromatography [101]. This provided estimates for the Stokes radii of various FG nup segments
15 10 from *Saccharomyces cerevisiae* (yeast), and enabled comparisons with predictions for extended
16 11 and collapsed polymer chains (Figure 5A). In brief, FG nup segments with more charged (and less
17 12 hydrophobic) content showed more extended configurations (a regime that would correspond to
18 13 $\nu > 0.5$), whereas segments with more hydrophobic (and less charged) content had a more
19 14 collapsed, cohesive character (regime that would correspond to $\nu < 0.5$). These results come with
20 15 the caveat that the interpretation of size-exclusion chromatography experiments is inherently
21 16 complicated by the uncertainty in ascertaining the hydrodynamic radii of intrinsically disordered
22 17 proteins moving through a gel. Analysis of these results using simple polymer models indicates
23 18 that the chain cohesiveness, as expressed in the Flory parameter χ_c , roughly correlates with the
24 19 ratio of the hydrophobic to charged content in the FG nup sequence [56]; see Figure 5C. In another
25 20 work, differences in FG nup extension could be also accounted for via the differences in total van-
26 21 der-Waals volumes (and hence excluded volumes) of the amino acids in these sequences [74].
27 22 These observations are consistent with the general classification of IDRs according to their
28 23 sequence composition [39,128]. A meta-analysis of a wider set of FG nups shows that on average,
29 24 the FG nup dimensions agree with predictions for "ideal" Gaussian chains with $\nu = 0.5$, where
30 25 repulsive and attractive interactions are balanced [74].
31 26

32 27 The nature of the individual FG nup chains has been further probed by density functional and
33 28 molecular dynamics models that more explicitly take into account the specific amino-acid
34 29 composition of the different FG nups. Ghavami *et al.* [62,147] described the FG nups as chains of
35 30 beads with one bead per amino acid, with explicit parametrization for electrostatic and
36 31 hydrophobic interactions as well as bond stretching, bond bending and bond torsion potentials
37 32 based on Ramachandran data of the coiled regions of protein structures. The parameters were
38 33 selected to match experimental hydrophobicity scales for the different amino acids and scaled to
39 34 match the dimensions of a low-charge and high-charged FG nup segment. These works calculated
40 35 the Stokes radii using hydrodynamic theory of interacting beads based on Kirkwood theory
41 36 [148,149]. The resulting model reproduced the experimentally obtained Stokes radii of a wide
42 37 range of FG nups and FG nup segments [40,101] with a maximal error of 20%, as shown in Figure
43 38 5B.
44 39

1
2
3
4 1 Another experimental assessment of FG Nup dimensions was performed by SAXS and FRET
5 2 experiments that directly probe the equilibrium conformations and the dimensions of the FG nups
6 3 [124,150]. While smFRET provides distance information between two distinct points in an IDP
7 4 chain which provides a measurement of R_E , the radius of gyration R_G can be measured by SAXS
8 5 and is an average manifestation of all interatomic distances and thus provides a measurement that
9 6 is complementary to smFRET [124,151,152]. Due this weighting, however, R_G is often dominated
10 7 by inter-residue distance at shorter length scales (<40 residues [124]), and can thus be less sensitive
11 8 towards collapse and scaling behaviour of FG nups specifically and IDPs in general. Furthermore,
12 9 interpretation and comparison of FRET and SAXS experiment commonly relies on homopolymer
13 10 theory, and it still remains to be established to what extent this can be used also for heteropolymers
14 11 such as FG nups [124]. Atomistic models have been a powerful tool in analyzing FRET and SAXS
15 12 experiments, despite some of their deficiencies mentioned above. The solvation problem of IDPs
16 13 in traditional force fields has been partially tackled by using force fields based on Kirkwood-Buff
17 14 solution theory. This approach has been successful in better matching experimental observations
18 15 from FRET, SAXS and NMR [135]. This approach has also been successful in recapitulating
19 16 small, yet experimentally (smFRET) resolvable changes in FG nup collapse upon minor
20 17 modifications such as removal of ~2 proline residues [153]. Another powerful approach involves
21 18 constraining MD simulation ensembles with experimental observables such as distance restraints
22 19 from FRET and R_G from SAXS [124]. More experimental and theoretical work is required for a
23 20 consistent interpretation of smFRET and SAXS data [124,154]

24 21
25 22 Due to the technical challenges of both methods, only limited amount of experimental data are
26 23 currently available for SAXS and smFRET, but overall the data obtained so far is consistent with
27 24 the above mentioned hydrodynamic radius measurements and their interpretations in terms of
28 25 polymer concepts. For different human and yeast FG nups, smFRET and SAXS yielded scaling
29 26 exponent ν 0.45 and 0.61, ranging between collapsed and relaxed coil configurations [124,150].
30 27 For instance, human Nup153 FG fragments may appear more relaxed, whereas human Nup98 is
31 28 more collapsed. Overall, these results are qualitatively similar to several other assays that aimed
32 29 to detect cohesiveness/propensity of self-interaction in FG nups [41,101]. The more collapsed
33 30 nature of human Nup98 is consistent with the observation that Nup98 from different species can
34 31 undergo a phase separation into hydrogels that recapitulate the transport selectivity of the pore
35 32 [104]. Atomistic simulations of artificial FG nup-like constructs have also observed the expected
36 33 scaling, although the results depended on the choice of water model [134].
37
38
39
40
41
42
43
44
45
46
47
48
49
50
51
52
53
54
55
56
57
58
59
60
61
62
63
64
65

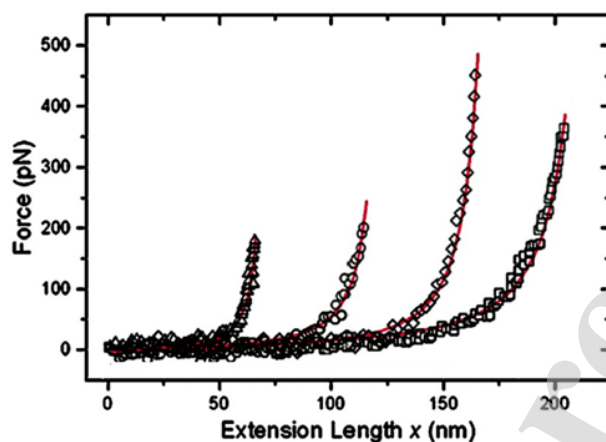


Figure 6. The nanomechanical behavior of FG nups is consistent with that of polymer models. Surface grafted FG nups were pulled by AFM at different locations. The force-extension curves (symbols) are well described by worm-like chain fits (red lines). Adapted from [73], permission pending.

Finally, the descriptions of FG nups based on the concepts of polymer physics have been validated in measurements of their resistance against mechanical extension using atomic force microscopy (AFM), as shown in Figure 6. In these experiments [73], a human FG nup (Nup153) was grafted at one end to a rigid surface. By pulling on the chain at different positions along its contour length with an AFM tip, the force-versus-extension was found to show classical worm-like chain behavior [155]. These experiments yielded a mean persistence length of 0.39 ± 0.14 nm for this FG nup, comparable to the size of an individual amino acid (~ 0.4 nm). At length scales beyond the persistence length, angular correlations become negligible and the polymer behaves as a flexible chain.

In summary, thanks to the combination of multiple experimental methods with multi-scale computational approaches, the structure and the dynamics of FG nups have been characterized at the single chain level. In many aspects, FG nups behave like long, flexible polymer molecules with some degree of cohesiveness. Much of their nano-mechanical behavior on the relevant time- and length-scales can therefore be described by simple polymer physics and expressed in mathematical models of differing degrees of complexity. This insight provides a basis for understanding the collective behavior of FG nups in more condensed phases such as in the NPC, as described in the following sections.

3.3. Collective effects in assemblies of FG nups

3.3.1. Bulk phases and phase transitions of FG nups

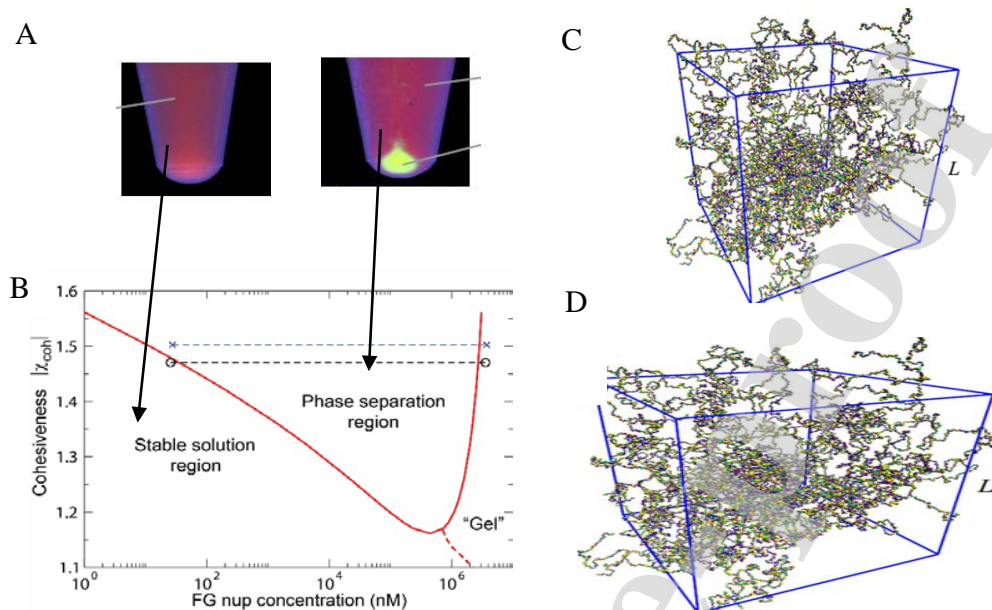


Figure 7. Phase separation and gelation in solutions of FG nups. A: Dense aggregates (yellow “droplet”) are formed by cohesive FG nups at sufficiently high concentrations. Adapted from [98], permission pending. B: Phase diagram of an FG nup solution obtained using Flory-Huggins type theory of Eq. (3). The red line indicates the theoretically predicted boundary of the phase separation region. Dashed line: schematic boundary of the formation of the percolating “gel”. Symbols: experimentally observed densities of the dilute and the dense phase. Reproduced from [156], permission pending. C: Gelation in FG nup solutions studied by a molecular dynamics model with one bead per amino acid. D: Critical concentration for gel formation c_{crit} as a function of the charge C , hydrophobicity H , and FG nup length N , as follows from applying percolation theory to the simulation results. The results show that hydrophobic interactions are the main driving force for gel formation in FG-nup solutions, reflected in the increase of the critical concentration for gel formation increases with the charge-to-hydrophobicity ratio. Adapted from [157], permission pending.

Within the NPC, approximately 200 FG nups of a typical molecular weight ~ 100 kDa, and containing ~ 150 -800 amino acids each in their intrinsically disordered regions, are end-grafted to the walls of the central channel that bears an inner diameter of ~ 40 nm and a length of several tens of nm ([5] and references therein). Hence, the concentration of FG nups inside the NPC is of the order of mM, or ~ 100 mg/mL [62] with an approximate volume packing fraction of $\sim 10\%$. Considering that a large fraction of the NPC passageway is occupied by transport factors and/or cargo in transit, the local FG nup and transport proteins density may even be considerably higher [7,57,62,83,104,158].

At such high concentrations, the interactions between individual FG nup chains come to play, potentially leading to collective effects. Given their intrinsic cohesiveness, there is a propensity for some FG nups (such as Nup98 or Nup100/116) to form dense multi-molecular assemblies or aggregates (Figure 7A). In early works, FG nup aggregation produced irreversible dense condensates that were reminiscent of polymer “gels”, but the experimental conditions were far from physiological [97,109]. More recent work has shown that dense non-surface grafted FG nups

1 can also self-aggregate under more physiological conditions [104]. The mechanism of initial
 2 formation of these droplet-like aggregates from a dilute solution of FG nups resembles a phase
 3 separation of self-associating polymers where a dense polymer phase co-exists with a dilute
 4 solution of chains as shown in Figure 7A,B [159,160].

5
 6 However, all FG nup aggregates have a high tendency to age into solid-like states, commonly
 7 enriched in amyloid fiber type structures, a process that in other phase separation proteins has been
 8 referred to as molecular aging [161–163]. A recent microfluidic platform was used to trigger phase
 9 separation of an FG nup quickly and to optically interrogate the properties of emerging droplets,
 10 which clearly showed that freshly formed FG nup droplets show liquid properties, such as
 11 coalescence and deformability [164]. The microfluidic device also enabled to test for permeability
 12 barrier properties of the liquid FG nup assemblies (see Section 3.4).

13
 14 Two main factors control the behavior of the solutions of interacting polymer chains: the entropy
 15 of the polymer molecules in space (and the corresponding solvent entropy) and the interactions
 16 between the chains. Interestingly, the intra-chain configurational entropy, which is so important in
 17 determining the properties of individual polymer chains, is not fundamental for polymer solutions
 18 [127]. In the classical mean field model, known as the Flory-Huggins theory, the free energy (per
 19 unit volume) of a polymer solution is

$$\frac{F}{k_B T} = \frac{\psi}{N} \ln(\psi) + (1 - \psi) \ln(1 - \psi) + \frac{1}{2} \chi_c \psi^2, \quad (3)$$

22
 23 where N is the number of monomers in the chain and $\psi = n v_0$ is the volume fraction occupied by
 24 the polymers, with v_0 the volume of a monomer and n the average monomer density as before
 25 [127]. Although the Flory-Huggins free energy is commonly derived on a lattice, it has a general
 26 applicability due its simple physical interpretation. The first term in equation (3) describes the
 27 translational entropy of the chains in space. The second term describes the reduction in the entropy
 28 of the polymer chain configuration due to steric repulsion (excluded volume) between them; it can
 29 be also interpreted as the entropy of the surrounding solvent [121]. The last term in this equation
 30 describes the attractive/cohesive interactions between the monomers of the polymers, similar to
 31 the expression for an individual polymer in Equation (2). This cohesiveness parameter χ_c
 32 subsumes all the intra- and inter-chain molecular interactions on the average level and is related to
 33 the second virial coefficient of the monomer-monomer interaction [127].

34
 35 For sufficiently strong cohesiveness, $\chi_c > 1 + 1/\sqrt{N}$, the system undergoes a phase separation,
 36 resulting in the formation of a dense phase in equilibrium with a dilute solution [56,127]. This
 37 minimal-complexity model incorporates only the key equilibrium properties of the FG nup
 38 molecules and their interactions, yet is in remarkable agreement with the experimental
 39 observations, as illustrated in Figure 7B. Note that the formation of the percolating “gel”-like

1 network of FG nups (sometimes known as a sol-gel transition) is not necessarily accompanied by
2 a phase separation, and can theoretically proceed in a continuous manner [165–168].

3
4 The insights of the minimal models are consistent with more detailed simulations that take into
5 account the amino acid sequence of the FG nups as described in Section 3.2 [59,62,63,169,170].
6 Using such simulations, the sol–gel transition was studied by considering the propensity of FG
7 nups to form (reversibly) cross-linked networks, defined by the formation of a percolating network
8 of residues of different FG nups approaching each other to below a critical distance [157], as shown
9 in Figure 7C. The computed critical concentrations for gel formation were found to increase with
10 charge content and decrease with hydrophobic amino acid content and chain length, consistent
11 with the predictions of the mean field theories. Notably, the computed critical concentrations are
12 lower than the typical FG nup concentrations found for yeast NPCs [62] and in selective
13 biomimetic nanopores [25], supporting the hypothesis that the FG nup gel-like state may form in
14 the confinement of the NPC transport channel. This observation comes with the caveat that, unlike
15 the bulk simulations of [157], the NPC contains multiple different FG nups which are anchored to
16 the pore scaffold. Furthermore, the current theoretical and computational model do not include
17 amyloid-promoting interactions such as hydrogen bonds that might result in more complex 3D
18 structures [104,161,162].

19
20 Finally, these collective FG nup morphologies are sensitive to interactions with the cellular milieu,
21 and are likely to be modified in the presence of the transport proteins and other proteins in the
22 dense environment of the cell, as discussed in the next section.

23 24 3.3.2. Assemblies of FG nups grafted to planar surfaces

25
26 To study the collective behavior of FG nups under conditions that more closely mimic their
27 assembly in the NPC, various model systems have been developed in which FG nups were grafted
28 to planar surfaces at the grafting densities resembling the NPC transport channel
29 [57,99,108,113,130,171–174]. This allows more systematic study of FG nup properties whilst
30 preserving a key physical attribute of the NPC, the grafted nature of the FG nups at physiological
31 densities.
32

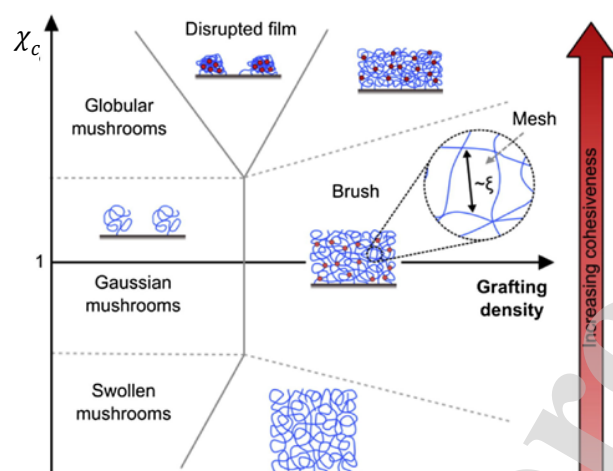
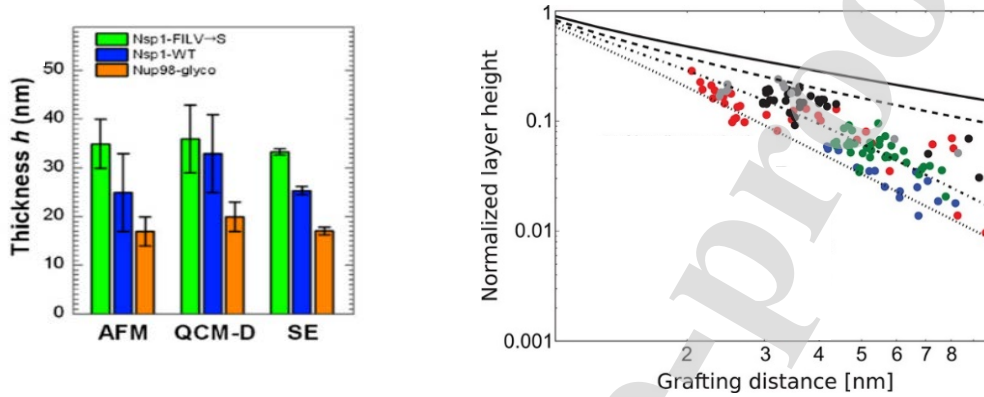


Figure 8. Schematic phase diagram, illustrating different types of behaviors of layers of end-grafted polymers as a function of the interaction parameter χ_c and the grafting density. Adapted from [108], permission pending.

In these experiments, FG nup molecules are typically attached to solid surfaces using diverse experimental techniques: cysteine-tagged FG nup constructs grafted to gold surfaces [99,173,174], histidine-tagged FG nup constructs to a supported lipid bilayer containing functionalized lipids [130], or directly to commercial PEG-functionalized silica substrates via divalent metal ions [171]. Collective morphologies and conformational states of the FG nups in the layer are reflected in the layer height that can be measured through a number of surface-science based methods. These include indentation by atomic force microscopy (AFM), quartz-crystal microbalance with dissipation monitoring (QCM-D), spectroscopic ellipsometry (SE), and surface plasmon resonance [57,99,108,113,130,171–174].

Surface grafted polymer layers have been studied extensively and are well understood in terms of concepts and key variables determining the collective polymer behavior [175–177]. These insights also translate to grafted layers of intrinsically disordered polypeptides [178]. A wide range of collective morphologies may be observed in surface grafted polymer layers, depending on the grafting distance and on the cohesiveness of the polymers, as illustrated in Figure 8. In the absence of polymer-surface interactions, a single surface-grafted polymer chain adopts a coil-like “mushroom” conformation, similar to its shape in solution, due to the thermal motions of the chain monomers. In sufficiently dense multi-polymer grafted layers, where the next-neighbor grafting distance is closer than the natural dimension of an individual mushroom, the layer adopts a structure known as the polymer “brush”. Here, each chain becomes more stretched in the perpendicular direction than in the lateral direction, being stabilized by the steric repulsion that results from the thermal motion of the adjacent chains, known as “entropic stabilization” [175]. Similar to individual polymer coils in solution, mushroom size and brush height can be modulated by inter- and intra-chain cohesion and solvent properties that favor more compact morphologies [56,179,180]. Nevertheless, despite significant stretching, each chain in a polymer brush is still

1 sufficiently coiled, and the resulting diffuse structure typically contains a large amount of free
 2 water. Accordingly, the average brush height as measured from the grafting surface is typically
 3 much shorter than the fully extended contour length of the polymer, and can be controlled by
 4 varying the grafting density [175].
 5



6
 7
 8 *Figure 9. Effects of chain cohesiveness and density on the morphology of FG nup surface layers. Left: FG nup layer heights*
 9 *measured for three different FG nups (orange is the most cohesive one (nup98), blue is the less cohesive one (Nsp1) and green is*
 10 *the even less cohesive mutant of blue). The measured height is consistent between atomic force microscopy (AFM), quartz-crystal*
 11 *microbalance with dissipation monitoring (QCM-D), and spectroscopic ellipsometry (SE). **Reproduced from** [108], **permission***
 12 *pending.* *Right: Increasing the grafting distance decreases the layer height, in accord with theoretical expectations. Dots are*
 13 *experimental data for different (human) FG nups measured using surface plasmon resonance (SPR). All measured FG nups*
 14 *layers behave as cohesive polymer brushes and lie between the theoretical predictions for the pure repulsive brush (solid line)*
 15 *and the fully compact brush (dotted line). Dots show experimental data. Different colors correspond to different FG nup types.*
 16 *Reproduced from* [173], *permission pending.*

17 Basic insight into the collective morphologies of surface grafted FG nups can be obtained within
 18 the same conceptual framework that describes the properties of individual FG nups in solution. In
 19 the simplest mean field model, also known as the Alexander-de Gennes model[179], for a layer of
 20 polymers with a length of N monomers, each grafted at a distance a from each other, the free
 21 energy per unit area is given by an expression that parallels the free energy of a single chain of
 22 Equation (2):
 23

$$\frac{F}{k_B T} = \frac{h^2 \sigma}{2N} + g(n)h,$$

24 where h is the layer height, $\sigma = \frac{1}{a^2}$ is the surface grafting density (number of polymers per unit
 25 area) and $g(n)$ is the interaction part of free energy density of the solution of monomers within
 26 the layer described in Section 3.3.1 [56,181]. The monomer density inside the layer is $n = \sigma/h$,
 27 and the equilibrium height is found via minimization of the free energy over h . This oversimplified
 28 model neglects a number of potentially important features, such as non-uniform monomer density
 29 inside the layer and the effects of the FG nup sequence heterogeneity. Nevertheless, the resulting
 30
 31

1 predictions are in agreement with more detailed models based on self-consistent field
2 approximation and other methods [181,182].

3
4 Increase in the intra- and inter-chain cohesiveness causes a decrease in the layer height. Analogous
5 to the coil-globule transition of single polymer coils in solution, this compaction is accompanied
6 by a qualitative change in the scaling of the layer height with the grafting distance a [56,176,183].
7 In the absence of cohesiveness, for a “pure” sterically stabilized brush, the layer height scales as
8 $h \sim a^{-2/3}$ [175]. As the cohesiveness increases, the scaling exponent increases to $h \sim a^{-2}$ for a
9 compact layer [56]. This is analogous to the transition from the Flory exponent $\nu = 3/5$ for
10 relaxed coils to $\nu = 1/3$ for compact globules of single chains described in the previous section.
11 In the polymer physics parlance, this transition is analogous to the change from a “good” to a “bad”
12 solvent.

13
14 The experimental results agree well with this theoretical picture, across many experimental
15 platforms and different FG nup types, as summarized in Figure 9. Similar good agreement was
16 obtained using other coarse- [57] and finer-grained [62] molecular models. Taken together, these
17 experimental results, combined with theoretical and computational modeling show that surface
18 layers of grafted FG nups are well described as moderately cohesive flexible polymeric brushes,
19 consistent with their behavior in bulk solutions [56,57,173]. Nevertheless, FG nup sequence detail
20 may play an important role. It has been shown that many FG nups possess “di-block polymer”
21 nature, where the cohesive FG repeat rich domains are segregated from FG poor, more charged
22 domains, which may play a role in their collective conformations [53,111]. Furthermore, atomistic
23 modeling indicates that FG nup in brushes may braid into multi-chain bundles that expose FG
24 repeats on their surface [55,133], which may be related to the experimentally inferred amyloid-
25 like structures within FG nup assemblies [104,161]. These atomistic and one-bead-per-amino-
26 acid simulations provide the molecular underpinning for the average mean field parameters such
27 as the chain cohesiveness χ_c that cross-verifies their estimates based on the single molecule and
28 brush measurements.

30 3.3.3. FG nups in NPC mimicking synthetic nanopores

31
32 To further approximate the spatial arrangement of FG nups in the confined geometry of the NPC,
33 several studies have employed FG nup layers grafted into artificial nanopores of dimensions
34 similar to those of the NPC channel (Figure 10). These include nanochannels in polycarbonate
35 membranes [23] and solid state nanopores [24–26,28]. NPC mimics allow quantitative
36 investigation of FG nup morphology and the translocation of transport proteins in a minimalistic,
37 well-controlled system focusing on specific FG nups. Hence, structural and functional
38 measurements on these systems are more readily interpreted in terms of FG nup properties
39 compared to measurements in biological setting. In particular, these mimics serve as testbeds for
40 the verification and calibration of the computational models [25,54,59–63,110,111,184,185].

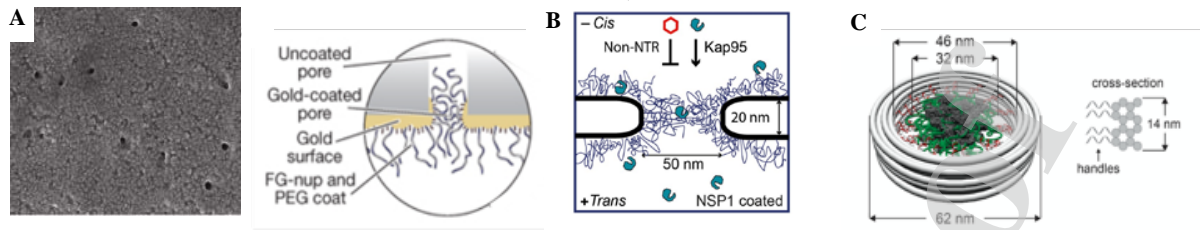


Figure 10. Nanopore mimics of the NPC. **A:** (Left) Polycarbonate membrane perforated by ~ 30 nm channels, coated on one face with a ~ 15 nm gold layer. (Right) FG nups are grafted to the gold layer by a single C-terminal cysteines. PEG is used to block unspecific binding to exposed gold. **Reproduced from** [23], **permission pending.** **B:** Schematics of a nanopore drilled in a silicon nitride (SiN) membrane by a focused electron beam. FG nups are grafted to the silicon nitride by a terminal thiol. **Reproduced from** [25], **permission pending.** **C:** DNA origami pore scaffold containing 48 single-stranded DNA handles, allowing specific attachment of FG nups that are conjugated with the matching single-stranded DNA sequence. **Reproduced from** [28], **permission pending.**

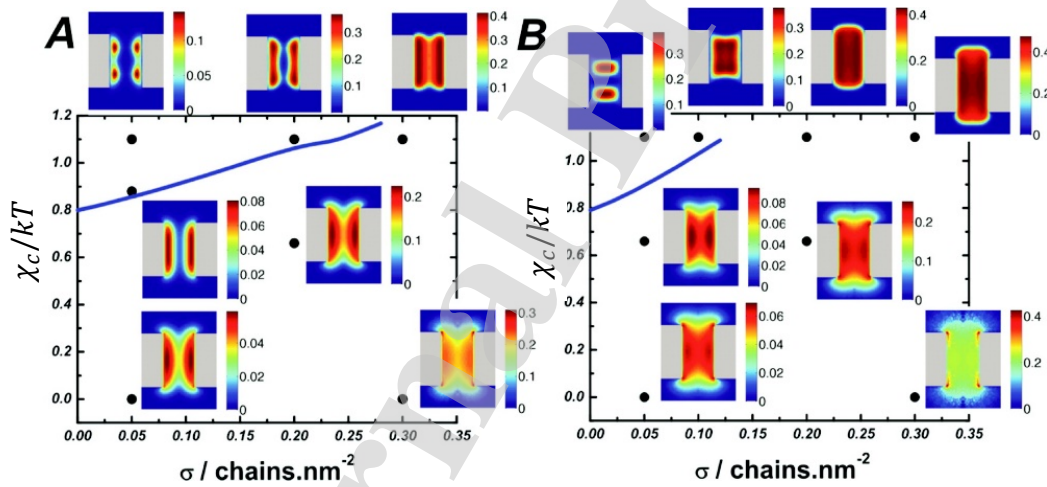
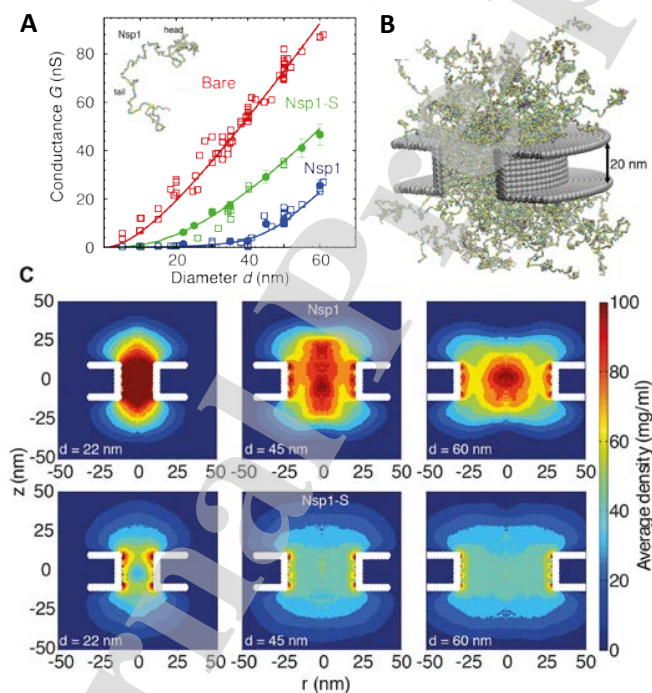


Figure 11. Phase diagram of possible morphologies of cohesive polymers grafted in nanochannels as a function of the grafting density σ and the chain cohesiveness χ_c . For short chains (left panel), increasing cohesiveness causes the chains to compact towards the walls, similar to the planar surfaces. Longer cohesive chains (right panel) can collapse towards the center instead. **Adapted from** [186], **permission pending.**

A downside of the earlier NPC mimics [23,25,26] was the lack of control over the grafting positions and grafting densities for FG nups in the nanopores. To address this problem, more recent approaches use DNA origami pore scaffolds that expose precise numbers of single-stranded DNA handles on the scaffold structure. Purified FG nups are chemically conjugated with single-stranded DNA linkers that match the sequence of the handles, and thus grafted to the DNA origami scaffold

1 at the handle positions [24,28]. However, for these DNA-origami based mimics, NPC-like
 2 transport functionality has yet to be demonstrated, which may be related to the substantial negative
 3 charge of the DNA, which is absent in the actual NPC scaffold. Another approach focusing on *de*
 4 *novo* reconstitution of NPCs uses self-assembly of NPC pore membrane proteins into ~20 nm-
 5 diameter nanopores in lipid bilayers [187].

6 The rudimentary NPC-like affinity-based selectivity is also observed in completely synthetic
 7 nanopores that use synthetic polymers [27], and provide a link to a wider field of design of polymer
 8 functionalized nanochannels for various nanotechnology applications such as protein sorting,
 9 DNA sequencing and “smart” materials [146,188–199]. Such artificial nanopores, although not
 10 the direct focus of this review, can also serve as experimental venues for testing the conceptual
 11 models of NPC transport.
 12
 13



14
 15
 16 *Figure 12. FG nups grafted in a nanopore. (A) Ionic conductance as a function of nanopore diameter for the bare pore (red), for*
 17 *a pore covered with the yeast FG nup Nsp1 (blue), and for a pore covered with the less cohesive mutant Nsp1-S (green). See text*
 18 *for discussion. Open symbols: experimental data. Closed symbols and lines: theoretical predictions. (B) Snapshot of simulations*
 19 *of the Nsp1 pore. (C) Time-averaged protein density distributions in Nsp1 and Nsp1-S pores; note that qualitatively similar*
 20 *dependencies of the polymer morphologies on the parameters are present in Figure 11. Adapted from [25], permission pending.*

21
 22 We return to the transport functionality of these NPC mimics in Section 4. In this section, we focus
 23 on the morphology of the FG nups in the nanopore geometry.
 24

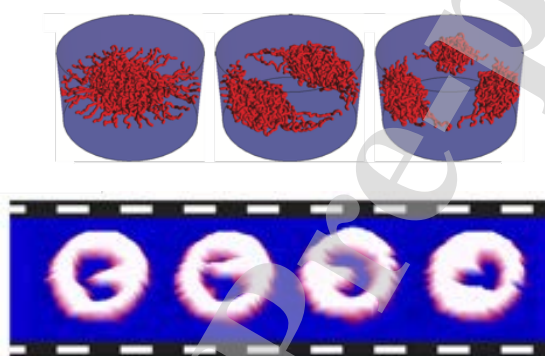
1
2
3
4 1 From a general perspective, the same factors that affect the morphology of polymer assemblies
5 2 grafted to flat surfaces also determine their behavior in cylindrical channels, with an additional
6 3 control parameter, the channel radius, that adds to the richness of the phase behavior [186,200–
7 4 202]. The different regimes and factors controlling the transitions between them are summarized
8 5 in Figure 11. In brief, paralleling the behavior of planar assemblies, the intra- and inter-chain
9 6 cohesiveness controls the transition from diffuse/extended to more condensed/collapsed states.
10 7 However, in the channel geometry the grafted layer can condense either towards the grafting walls
11 8 or towards the center of the channel, depending on the relative dimensions of the channel and of
12 9 the polymers [45,184,186,200].
13
14
15
16
17

18 11 There is good agreement between, on one hand, detailed molecular modeling that incorporates the
19 12 full amino acid sequence of the FG nups, and, on the other hand, the insights from the simple
20 13 polymer models, and both have been used to interpret experimental data in nanopores coated with
21 14 FG nups of different degree of cohesiveness. As illustrated in Figure 12 [25], molecular modelling
22 15 can capture the experimental ionic conductances showing that the FG nup chains partially block
23 16 the ionic flux through the pore with the flux being related to the FG nup density distribution using
24 17 certain assumptions about the dependence of the local ionic conductivity on the local molecular
25 18 density (see references in [25]). Consistent with the theoretical expectations, the more cohesive
26 19 FG nup Nsp1 shows higher density along the central axis of the channel (see Figure 12). In
27 20 contrast, simulations of the less cohesive Nsp1-S mutant, with the hydrophobic Phenylalanines
28 21 being mutated to hydrophilic Serines, predict lower densities and a more uniform distribution
29 22 within the pore. By increasing the channel radius, the density of the FG nup cloud in the pore
30 23 decreases, opening conduction pathways, accompanied by the increase in the ionic conductivity,
31 24 as observed experimentally. Whether these low-density pathways are located next to the channel
32 25 walls or along the central axis may depend on the channel radius and the FG nup type [25,26].
33 26 Notably, this behavior is largely consistent with the general theoretical expectations of Figure 11,
34 27 based on homopolymer models [45,53,60,114,184,186,203].
35
36
37
38
39
40
41
42
43

44 29 The different spatially condensed states (or phases) shown in Figure 11 and Figure 12, raise a
45 30 possibility of bi-stable behavior of the polymer layer, switching between “open” and “closed”
46 31 states in some parameter range. [58,184] (Figure 13, top). These predictions may be related to the
47 32 collective dynamic rearrangements of FG nups in nanopores observed by fast AFM [28,204], with
48 33 FG nups alternating from one clumped/condensed configuration to the other (Figure 13, bottom),
49 34 and possibly switching between more open and more closed configurations. (The technique comes
50 35 with the caveat that the AFM tip might have an effect on the observed behavior.) Further Brownian
51 36 dynamics simulations suggest that the FG nup assembly might alternate between these open and
52 37 closing configurations during cargo translocation [170].
53
54
55
56
57

58 39 In summary, NPC-mimicking nanopores have provided fundamental insights into the potential
59 40 collective conformations of the FG nups in nano-confinement geometries resembling the NPC.
60
61
62
63
64
65

1 They also enabled calibration and testing of the computational models of FG nups in
 2 physiologically relevant geometries. Overall, experimental and computational approaches are
 3 converging in our understanding of the biophysics of the FG nups in pore geometries. Notably,
 4 many of the features of the FG nup distribution in the nanopores are recapitulated both in
 5 simulations that take into account the full amino acid sequences, and in ultra-coarse grained,
 6 homopolymer models with averaged interaction parameters. Nevertheless, the full experimental
 7 characterization and theoretical understanding of the structure of the FG assemblies still remains
 8 for the future. In Sections 3.4.5 and 4.1.4, we discuss how this understanding extends to the
 9 collective behavior of FG nup morphologies in the presence of transport proteins, as well as to
 10 their dynamics during transport.



13
 14
 15 *Figure 13. Collective re-arrangements of polymers in the pore. Top: as shown by Monte Carlo simulations of polymers in a*
 16 *cylinder. Bottom: sequential AFM images of FG nups in DNA-origami ring scaffolds, recorded at 1.6 sec/frame. Reproduced from*
 17 *[58] and [28], permission pending.*

18 19 3.4. Interactions of FG nups with transport proteins

20
 21 Specific, transport-protein driven transport through the NPC crucially relies on the binding of the
 22 transport proteins to the FG nups in order to at least partially offset the free energy costs of
 23 penetrating the FG nup assembly in the NPC [5,6]. Accordingly, this interaction is a consensus
 24 component of all models of NPC function. The interactions of the transport proteins with the FG
 25 nups have been intensively studied during the past two decades with the goal of identifying the
 26 main physical variables and molecular features that facilitate penetration of transport proteins into
 27 FG nup assemblies [56,57,99,106,119,130,150,152,173,174,205–211]. Yet, the quantitative
 28 characterization of such interactions is challenging. The main obstacles are chain flexibility,
 29 multivalency of the interactions, FG nup sequence heterogeneity, and collective effects of the
 30 environment that complicate the relations between the macroscopic measurements and
 31 microscopic interactions.

1
2
3
4 1 Moreover, the knowledge of the exact molecular nature of the interactions between the transport
5 2 proteins and the FG nups is still incomplete. Previously, the hydrophobic interaction between the
6 3 hydrophobic Phenylalanines (F's) and the hydrophobic grooves on the transport proteins was
7 4 considered to be the primary driver of the transport protein binding to the FG nups. However, the
8 5 actual number of the binding sites on the transport proteins in general is not fully known, and
9 6 structural studies have been able to confirm only a few definite binding sites [106,107,205] out of
10 7 the up to 14 potential binding sites on the larger transport proteins (such as Importin β) that were
11 8 suggested by computational studies [210–212]. Other computational studies have highlighted the
12 9 potential role of electrostatic interactions in the transport protein/FG-nup binding [63,105]. This
13 10 goes in line with recent experimental work which established that the permeability of the NPC
14 11 with respect to various cargoes is determined not only by the hydrophobic binding sites on their
15 12 surface but also by charged, cation- π , and $\pi - \pi$ forming residues [96,213,214].
16 13

14 3.4.1. Quantification of interactions between FG nups and transport proteins: thermodynamics

15
16 16 Measurements of the affinity of interaction between transport proteins and FG nups have been
17 17 performed on FG constructs ranging from the “elementary interaction unit” (one FG ‘patch’) to
18 18 the full-length proteins using a range of transport proteins.
19 19

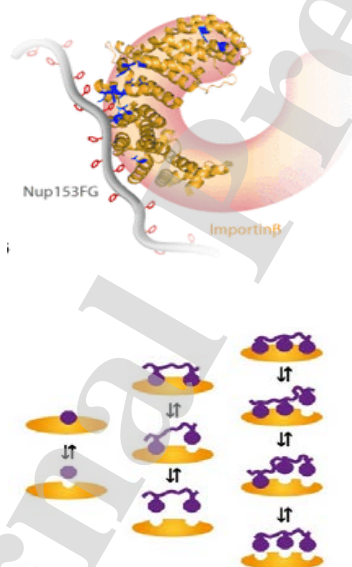
20 20 The interaction between a transport protein (NTF2), which contains only two known FG binding
21 21 sites, and a polypeptide construct incorporating a single FG “patch” been measured in solution by
22 22 NMR and isothermal calorimetry and yielded a dissociation constant of $K_d \approx 3 - 4$ mM, which
23 23 corresponds to an effective binding energy of approximately $E = 5 k_B T$ assuming mostly
24 24 monovalent binding with $K_d = 1M \cdot e^{-E/k_B T}$ [209]. Similar values were found for various native
25 25 and artificial FG nup constructs and transport proteins in solution, with dissociation constants in
26 26 the range of hundreds of μM to several mM, depending on the number of FG motifs in the
27 27 sequence and the distance between them [103,119,209]. Nevertheless, binding of some FG nups
28 28 to transport proteins can be significantly stronger.
29 29

30 30 By contrast, the dissociation constants of transport proteins (Importin- β) and surface-grafted full-
31 31 length FG nup segments (containing multiple FG motifs) were measured using surface plasmon
32 32 resonance (SPR), and found to be in the μM range in sparse grafting “mushroom” regime [173],
33 33 where one might assume 1:1 stoichiometry between FG nups and transport proteins (though not
34 34 between FG motifs and transport proteins, which can compound the interpretation). In the “brush”
35 35 regime, the dissociation constants were found to be in the range of hundreds of nM to several μM
36 36 (depending on the FG nup and transport protein type) [8,57,130,173,174]. However, the
37 37 interpretation of the “brush” results is complicated by the possible non 1:1 stoichiometries, by high
38 38 density effects and by spatial heterogeneity: hence not surprisingly, the binding curves do not obey
39 39 a Langmuir shape for simple one-to-one binding, as discussed below. Other studies using micro-
40
41
42
43
44
45
46
47
48
49
50
51
52
53
54
55
56
57
58
59
60
61
62
63
64
65

1 bead assays found, in some cases, dissociation constants in the nanomolar range, although it was
 2 realized that these nanomolar affinities are probably not physiologically relevant [206,208,215].

3
 4 Some of these discrepancies might be attributed to the differences in experimental conditions, e.g.
 5 Importin- β with multiple binding sites vs smaller NTF2 with smaller number of binding sites, or
 6 the different FG nup segments used. However, more generally, the interpretation of the effective
 7 dissociation constants in terms of local interaction strengths between the FG nups and NTRs
 8 remains elusive due to several complicating factors.

9
 10 The first factor is the multivalency (commonly known as “avidity”) of the interactions between
 11 transport proteins and FG nups: while the affinity between a transport protein and a single FG
 12 “patch” may be low, much stronger binding may be observed when multiple FG repeats are
 13 accessible on the same chain or – in FG nup assemblies – on multiple chains.



16
 17 *Figure 14. Multivalency of transport protein binding to FG nups. Top: Schematic illustration of the multivalent binding of a*
 18 *transport protein (Importin- β) to an FG nup (Nup153). In the classical picture the interaction predominantly arises from the*
 19 *binding of the hydrophobic side chains of the phenylalanines (shown in red rings) to the hydrophobic grooves on the transport*
 20 *protein (shown in blue). Bottom: schematic illustration of the multivalent binding-unbinding process Adapted from [216] and*
 21 *[119], permission pending.*

22 Some of the effects of avidity/multi-valency can be understood within a simple toy model (see
 23 also [145]). Consider a polymer with M cohesive “patches” and a particle with N binding sites
 24 within a box of volume V . Assuming the polymer is “bound” to the particle if it is located within
 25 a certain volume $v_p \ll V$ around the particle and at least one of the “patches” is bound to a
 26 binding site on the particle, the bound probability is given by

$$P_b = \frac{v_p/V \sum_{k=1}^N \binom{N}{k} \binom{M}{k} e^{-\epsilon k}}{1 + v_p/V \sum_{k=1}^N \binom{N}{k} \binom{M}{k} e^{-\epsilon k}},$$

where $\epsilon < 0$ is the binding energy between a “patch” and a binding site measured in units of $k_B T$. For the sake of the example, we have neglected the entropic contributions of the inter-patch likers and the associated correlations between different patches. These correlations can substantially modify the results via the mechanism known as local density enhancement [209,217]. The degree of this enhancement depend in part on the entropy of the flexible inter-FG spacers, which is difficult to compute [114,209,217].

The dissociation constant is given by [218]

$$K_D = \frac{(1-P_b)^{\frac{1}{v_p}} 1/V}{P_b/V} \approx \frac{1}{v_p} \left(\sum_{n=1}^N \binom{N}{n} \binom{M}{n} e^{-\epsilon n} \right)^{-1} \quad (4)$$

For $N = 1, M = 1$ this expression reduces to the familiar formula for the dissociation constant of simple monovalent binding $K_D \approx \frac{1}{v_p} e^\epsilon$ so that affinity is high (K_D small) for strong binding (strongly negative $\epsilon < 0$) [219]. For particles with only one binding site and multi-patch polymers, $N = 1, K_D \approx v_0^{-1} M^{-1} e^\epsilon$; as expected, the prefactor M^{-1} reflects the increase in the association rate due to the multiple available binding sites on the polymer.

Second, in multi-chain settings, multivalency makes the apparent binding affinity of the transport proteins to FG nup assemblies dependent on the spatial density of the FG repeats [173,220]. From the analysis of assays using surface grafted FG nup layers, it emerged that the estimated dissociation constants strongly depend on the grafting density of the FG nups on the surface [173]. The interpretation of the experiments is further complicated by the fact that the binding curves can substantially differ from classical one-to-one (Langmuir) binding models with a single value of binding affinity [56,57,130,173,182,221]. This context-dependence also manifests itself in the sensitivity of the measured affinities to the presence of soluble competitors, such as other transport proteins or macromolecules [174]. For instance, the presence of cell lysate was shown to weaken the observed equilibrium binding affinity by orders of magnitude [103,206,222].

The context-dependent nature of the transport protein affinity to the FG nups can be illustrated in another toy model as follows. Consider a transport protein as a particle with N binding “patches”, which resides in a milieu of polymeric chains with M binding sites each. The polymer concentration is defined as C/M , so that the average concentration of the binding sites around the particle is C (measured in units of v_0^{-1} , where v_0 is a typical molecular volume). For the sake of the example, we neglect correlations between the binding sites that lie on the same chain,

appropriate in the high-density regime because the particle is typically bound to many chains simultaneously.

The fraction of the particles bound at least at one site is $\frac{\sum_{n=1}^N \binom{N}{n} C^n e^{-\epsilon n}}{Z} = (Z - 1)/Z$ [217,223] where $\epsilon < 0$ is the binding energy of each individual contact measured in units of $k_B T$, and $Z = \sum_{n=0}^N \binom{N}{n} C^n e^{-\epsilon n} = (1 + C e^{-\epsilon})^N$ is the partition function. Accordingly, the fraction of the particles that are not bound to any polymer is $1/Z$. Thus, an effective dissociation constant can be defined as [219]

$$K_D = v_0^{-1} \frac{C/M \cdot (1/Z)}{(\sum_{n=1}^N \binom{N}{n} C^n e^{-\epsilon n})/Z} = v_0^{-1} \left(\frac{M}{C} (Z - 1) \right)^{-1} = v_0^{-1} \frac{1}{M} \frac{C}{(1 + C e^{-\epsilon})^{N-1}}.$$

At a high concentration of the polymers, when $C e^{-\epsilon} \gg 1$, the effective dissociation constant is $K_D \approx M^{-1} e^{\epsilon} C (C e^{-\epsilon})^{-N}$. As a consequence, the effective affinity is strongly density dependent, and particles can experience much higher effective affinity in high-density FG nup assemblies.

To summarize, in general care should be exercised when inferring microscopic interaction parameters from macroscopic measurements of the binding affinities (which are significantly context-dependent) and translating from *in vitro* measurements to *in vivo* interactions in crowded cell environments. The dense assemblies of transport proteins and FG nups are further discussed in Sections 3.4.3-3.4.4. The relation between the FG nup-transport protein equilibrium interactions, kinetics and transport is described in Section 3.4.2 and Section 4.

3.4.2 Kinetics of the FG nup- transport protein interaction

One of the big questions about NPC operation is the contrast between its strict thermodynamic selectivity and the rapidity of transport. In particular, given the effective binding affinities of $1 \mu M$ and a typical protein association rate of $k_{on} \sim 10^5 - 10^6 \text{ M}^{-1} \text{ s}^{-1}$, the expected dissociation rate is $k_{off} = k_{on} K_d \sim 0.1 - 1 \text{ s}^{-1}$, which is incompatible with the millisecond transport times observed in the NPC.

This paradox might be partially explained by the high observed association rates (k_{on}) of transport proteins and FG nups [103,119,224] that arise from the combination of the multivalent interactions and the high conformational flexibility of the FG nups. Measured for the binding of several pairs of FG nups and transport proteins using stopped flow spectroscopy, the resulting association rates (k_{on}) were found as high as $10^9 \text{ M}^{-1} \text{ s}^{-1}$, close to the theoretically maximal diffusion limit [119]. In particular, it was found that the FRET efficiency between dyes on an FG nup does not change appreciably upon transport protein binding [119]. This indicates that FG nups bind transport proteins not in one specific configuration, but across a wide range of conformational states, with

1 rapid conformational exchange between different states – a feature also confirmed by NMR
 2 [103,119,209]. Similar concepts have been invoked in the analysis of a classical “fuzzy complex”
 3 observed for other multivalent protein interactions [225]. Combined with experimental
 4 dissociation constants in the range of $K_d \sim 100 \text{ nM} - 100 \text{ }\mu\text{M}$ these association rates predict
 5 mean dissociation time of FG nup-transport protein complexes of $\tau_{off} = (k_{on}K_d)^{-1} \sim 0.01\text{-}10$
 6 ms, shorter or comparable with the typical transit time (1-10 ms) of transport proteins traversing
 7 the NPC.

3.4.3. Morphologies of multi-chain assemblies of FG nups and transport proteins in solution

11 Due to the multivalent and promiscuous nature of the interactions between FG nups themselves
 12 and between FG nups and transport proteins, their collective morphologies can be highly sensitive
 13 to the environment. *In vitro* experiments have shown that addition of the transport proteins to the
 14 solutions of FG nups promotes aggregation [43,162]. On the other hand, under cytoplasmic
 15 conditions (either in cells or lysate), cohesive FG nups have been shown to remain flexible and
 16 dynamic which otherwise form aggregates in solutions [103]. The FG nup assemblies and phases
 17 in solution serve as rudimentary mimics of the permeability barrier of the NPC, in the sense that
 18 they generally exclude inert proteins but are permeable for the NTRs, similar to the selective
 19 permeability of the NPC [98,104,164]. The properties of the assemblies of FG nups with the
 20 transport proteins were systematically investigated in bulk solutions in [98] and in microfluidic
 21 devices in [164], using FG nup aggregates of the type described in Section 3.3.1. Larger cargoes
 22 showed reduced penetration of transport protein/cargo complexes into these dense FG nup phases,
 23 similar to what is observed in NPC transport [67,77,86,104]. Remarkably, even larger cargoes can
 24 permeate dense FG nup assemblies if they are attached to a sufficiently large number of transport
 25 proteins [56,104] (Figure 15).

27 Despite the complexity of the FG nup-transport protein interactions on the molecular level, the
 28 behavior of these composite dense phases can be understood within the same conceptual
 29 framework that has been used above to describe the behavior of FG nup chains and their
 30 assemblies. Because the composition and morphology of an FG nup assembly changes with the
 31 penetration of multiple transport protein-cargo complexes, this process can be viewed as a
 32 formation of a mixed dense phase through a phase separation mechanism in the ternary FG
 33 nup/transport protein/solvent solution. Accordingly, the free energy of Equation (3) can be adapted
 34 to account for the entropy of mixing and exclusion of the transport proteins and the FG nups, as
 35 well as the attractive interactions between the FG nups and the transport proteins
 36 [56,57,60,114,182]. On the mean field level, the latter can be characterized by an average
 37 interaction Flory type parameter χ and the appropriate additional term in the free energy, $\chi\psi\phi$,
 38 where ψ is the monomer density/volume fraction and ϕ is the density/volume fraction of the
 39 transport proteins [56]. Microscopically, χ is roughly proportional to the second virial coefficient
 40 of the interaction between the transport proteins and the FG nups, $\chi \sim \int d\vec{r} \left[1 - \right.$

1
2
3
4
5 1 $\exp(U(\vec{r})/kT)$ where $U(\vec{r})$ is the microscopic interaction potential that can include both direct
6
7 2 and water-mediated interactions [114,120]. This coarse-grained parameter is able to describe a
8
9 3 wide variety of (short-ranged) microscopic interaction potentials: e.g., a slightly weaker potential
10
11 4 uniformly distributed over the whole surface of the particle may result in the same value of χ as a
12
13 5 stronger but anisotropic potential confined only to discrete binding “patches” on the surface.
14
15 6

16
17 7 The overall theoretical phase diagram of such ternary (FG nup/protein/ implicit solvent) mixtures
18
19 8 is shown in Figure 15 (bottom). The phase diagram comprises a single-phase region, where the FG
20
21 9 nup/transport-protein solutions are stable, and a phase separation region, where the system phase
22
23 10 separates into a dense phase in equilibrium with the dilute one [56]. The dashed tie-lines show the
24
25 11 pairs of the co-existing phases at different concentrations. Remarkably, the permeability of the
26
27 12 dense phase with respect to the transport proteins, as reflected in their density inside the dense
28
29 13 phase relative to the outside solution, is largely captured by one parameter $\xi = v/\chi$, which is equal
30
31 14 to the ratio of the transport-protein/cargo complex volume v to the transport protein-FG nup
32
33 15 attractive interaction/binding strength χ . For small v (small cargoes and/or strong transport
34
35 16 protein-FG nup binding), the concentration of the transport proteins in the high-density phase is
36
37 17 higher than in the low-density phase, indicating penetration. For large ξ (large cargoes or weak
38
39 18 transport protein-FG nup attraction), the tie-lines flip, and the transport protein concentration in
40
41 19 the dense phase is lower than in the low-density phase, indicating exclusion, shown in the red lines
42
43 20 in the inset. At very high concentrations of the transport proteins and the polymers, there is
44
45 21 additional phase separation/de-mixing region [114], which is not discussed here. Interestingly, at
46
47 22 low concentrations, phase separation is promoted by the addition of transport proteins to an FG
48
49 23 nup solution even when the pure FG nup solution is stable, while at high concentrations the
50
51 24 addition of transport proteins inhibits the phase separation. This might resolve the apparent
52
53 25 discrepancies in the literature regarding the effect of transport proteins on the stability of FG nup
54
55 26 solutions and aggregates [43,103,162].
56
57 27
58
59
60
61
62
63
64
65

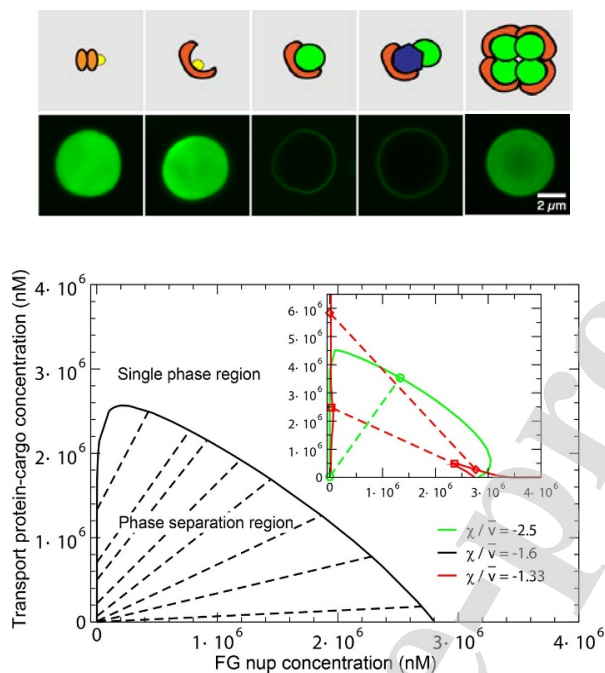


Figure 15. Phase separation in FG nup/transport protein solutions. Top: (Upper row) Schematic illustration of the transport proteins (brown) with and without bound proteins (green and blue). (Lower row) Fluorescently labeled transport proteins penetrate the dense FG nup “droplet” aggregates as indicated by green fluorescence within the droplets. From left to right, schematically: NTF2 ($\sim 40 \text{ nm}^3$ volume); Importin- β ($\sim 100 - 120 \text{ nm}^3$); Importin- β with GFP-cargo; Importin- β with GFP-MBP cargo; ternary complex of four Importin- β with GFP cargo. Larger particles, comprising transport proteins with bound cargo (green and blue) are excluded from the FG nup “droplets”. Penetration is recovered for large particles bound to sufficient number of the transport proteins. Adapted from [98], permission pending. Bottom: Theoretical phase diagram of the phase separation. The dashed tie-lines connect the co-existing dense and dilute phases located on the boundary of the phase separation region, shown in black line. The permeability of the dense FG nup phase to transport proteins is controlled by the parameter $\xi = v/\chi$; see text. Adapted from [56], permission pending.

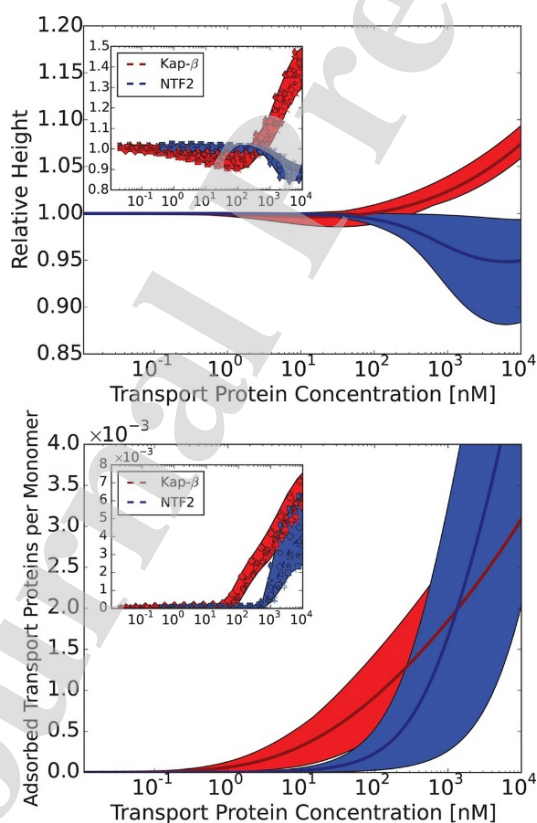
Overall, selective permeability of dense FG nup assemblies arises from the balance between the free energy cost of penetration of a transport protein-cargo complex into the dense phase, and the free energy gain due to the attractive interactions between the transport proteins and the FG nups. The penetration cost arises from the work against the osmotic pressure in the dense phase and the entropic costs of polymer re-arrangement, as well as the cost of breaking the cohesive contacts between the FG nups [52,56,57,104,114,198,226]. For large particles and/or weak interaction between them and the FG nups, the penetration cost is higher than the free energy gain, resulting in their exclusion from the FG nup aggregates as shown in Figure 15 [56,104].

This minimal phase separation model explains well the observed densities and composition of both the dilute and of the dense phases of transport-protein/FG nup solutions, as well as their selective permeability patterns, as explained in Figure 15 [56]. These results come with the caveat that the long-term behavior of the FG nup and FG nup/transport protein aggregates is not described anymore by equilibrium physics, as they undergo aging, amyloidization and potentially

1 irreversible chemical cross-linking taking them out of the physiologically relevant realm. Although
 2 the precise state of the FG nup assembly within actual NPCs remains unknown, recent experiments
 3 in microfluidic devices that enable examination of the liquid state of the FG nup droplets before
 4 they mature into less fluid states. In particular, it showed that attachment to transport proteins
 5 enables entry into FG nups assemblies for otherwise excluded cargoes, and even very large cargoes
 6 based on phage capsids (27 nm in diameter) can enter into a droplet when attached to a sufficient
 7 number of transport proteins (up to ~100), in accord with the results of [56,104] and Figure 15.
 8 Specific details may vary depending on the density of the FG nups in a droplet.

9
 10 Thus, although likely incomplete, the equilibrium phase separation model pinpoints the key
 11 pertinent variables that control the spatial organization of the transport proteins and FG nup
 12 assemblies and provides the foundation for future work towards understanding the internal
 13 morphology and dynamics of the NPC.

14 3.4.4. Assemblies of transport proteins and surface grafted FG nups



17
 18 *Figure 16. Changes in FG nup layer height induced by the penetration of the transport proteins. Top: relative layer height as a*
 19 *function of the transport protein concentration in solution. Bottom: corresponding number of the transport proteins in the layer.*
 20 *Blue band: theoretical prediction and confidence interval for a large, strongly binding transport protein (Importin- β). Red band:*
 21 *theoretical predictions and their confidence interval for a small, weakly binding transport protein (NTF2). Insets: corresponding*
 22 *experimental data. Adapted from [56], permission pending.*

1
2
3
4 1
5 2 As described in Section 3.3.2, assemblies of surface-grafted FG nups resemble the confined
6 3 geometry of the NPC. Accordingly, they have been used to characterize the interactions between
7 4 transport proteins and FG nups and the selective permeability of FG nup assemblies. Although the
8 5 effects of transport proteins on the layer morphology have been a matter of controversy, a
9 6 consensus picture has emerged [56,57,99,130,171,173]. Similar to the bulk FG nup aggregates,
10 7 layers of grafted FG nups repel inert proteins such as bovine serum albumin (BSA), while transport
11 8 proteins and transport protein-cargo complexes can penetrate the layers due to their attractive
12 9 interactions with the FG nup chains.

13 10 At low concentration of the transport proteins in solution, their penetration into the layer does not
14 11 cause significant changes in the layer height or its overall internal morphology, and they mostly
15 12 occupy the available space within the layer [56,57,130,182]. However, increasing concentration
16 13 can result in collective effects resulting in the conformational changes of the layer. At a critical
17 14 concentration of transport proteins, collective interactions between the transport proteins and the
18 15 FG nups may cause some overall compaction (also known as “collapse”) of the layer, as indicated
19 16 by a reduction in assembly height by up to ~10% [56,173,174,182]. The degree of this layer
20 17 compaction depends on the experimental conditions, such as the grafting density and the type/size
21 18 of transport proteins and FG nup segments used [56,57]. NTF2, smaller and with less FG binding
22 19 sites compared to Importin β , causes a higher degree of condensation in FG nup assemblies
23 20 [56,174]. In general, for the relatively large objects such as the transport proteins, these effects are
24 21 only moderate. Further addition of transport proteins, after the maximal compaction has been
25 22 attained, results in the layer swelling [56,57,99,130,172]. These collective morphological changes
26 23 can also result in a non-Langmuir adsorption curves [56,57,99,130,172]. The potential functional
27 24 significance of these morphological transitions for *in vivo* transport is still being debated.

28 25
29 26 These observations are well described by the minimal polymer models used in Section 3.4.3 for
30 27 bulk solutions, once adapted to the surface geometry, and treated in a variety of approximations
31 28 including mean-field approximation, density functional theory, and coarse-grained simulations
32 29 [56,57,182,227]. The comparison between the theory and experiment is summarized in Figure 16
33 30 and Figure 17. Similar to the bulk aggregates, the degree of transport protein penetration is
34 31 determined by the balance between the free energy cost of insertion and the free energy gain from
35 32 transport protein/FG nup binding.

36 33 The permeability of the surface-grafted assemblies to transport proteins can be regulated by the
37 34 grafting distance, the size of the transport protein and the interaction strength between FG nups
38 35 and transport proteins [38,39]. For large proteins, the penetration cost largely arises from the work
39 36 against the osmotic pressure in the polymer layer and is thus proportional to the volume of the
40 37 protein; it can be modulated by additional costs of polymer re-arrangement around the transport
41 38 protein, and the cost of disrupting cohesive inter FG contacts [57,114,226].
42 39

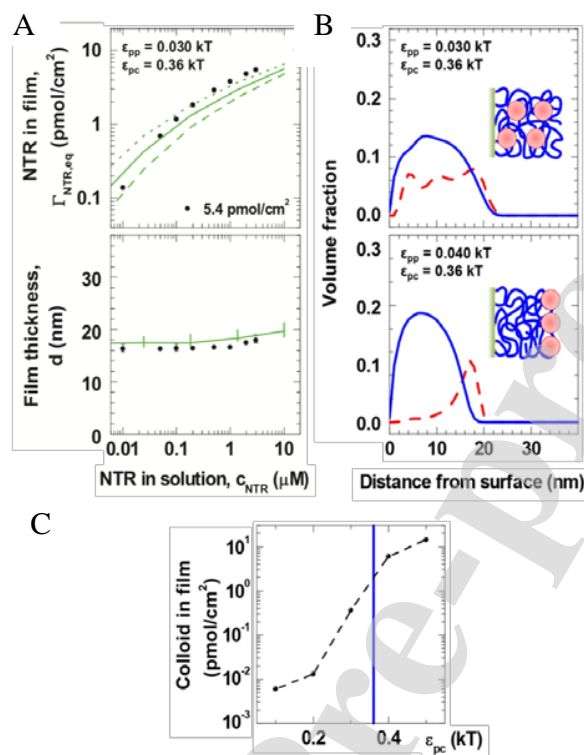


Figure 17. Distribution of transport proteins within FG nups layers. **A:** Polymer models (lines) accurately describe the experimental results (symbols) on transport protein (NTR) uptake in grafted FG nup assemblies. **B:** Moderate changes in FG nup cohesiveness (ϵ_{pp}) can lead to qualitatively different distributions of transport proteins (red) in the FG assemblies (blue). **C:** these models predict a sharp decline in transport protein uptake when the attractive interaction (ϵ_{pc}) between FGs and transport proteins drops below experimentally relevant values (blue line). Adapted from [57], permission pending.

The collective effects in the uptake of transport proteins into the layer of grafted FG nups may result in the spatial stratification and formation of a dense region of intercalated FG nups and transport proteins near the grafting surface, reminiscent of the dense phase appearing in bulk solution [182]. However, unlike in bulk solution experiments, surface grafting prevents the system from undergoing a true phase separation, and the resulting spatial inhomogeneity is reminiscent of a “micro-phase separation” of block copolymers [228]. Formation of this dense region correlates with the compaction of the FG nup film (see Figure 16). With further increase of the transport protein concentration, more protein can enter the FG nup film therefore leading to a moderate layer swelling as predicted theoretically and observed experimentally. The effect of concentration dependent protein uptake and layer swelling, although very moderate for large particles such as the transport proteins, is much more pronounced for small particles or mixed solvents, and are related to a phenomenon known in polymer science as “co-non-solvency” [229,230]. The morphologies of FG nup and transport proteins assemblies in channel-like geometry of the NPC are discussed in Section 3.4.5 and Section 3.5.

1
2
3
4 1 Although difficult to measure experimentally, the predicted stratification of the FG nup assembly
5 2 into compact and dilute regions is consistent with the observation that transport proteins in dense
6 3 grafted FG nup layers may be separated into two different populations of transport proteins - one
7 4 strongly bound with sub- μM dissociation constant and another population with a weaker μM
8 5 binding, but the validity of these interpretations is still unclear [173] (See also Section 3.2.3).
9 6

10 7 Furthermore, computational models provide additional insights on how FG nup assembly
11 8 permeability is influenced by inter-FG cohesiveness, a question that has been a subject of a long-
12 9 standing controversy in the field [41,56,57,97,114,163,231–233]. In particular, for larger transport
13 10 proteins, some models predict that moderate increases in FG nup cohesiveness may lead to
14 11 qualitatively different distributions of transport proteins (see Figure 17), favoring transport protein
15 12 accumulation on top of instead of inside the FG nup films [57]. Accordingly, transport protein
16 13 uptake can be highly sensitive to the strength of attractive interactions with the FG nups, as
17 14 illustrated in Figure 17B,C. While transport proteins readily accumulate within the layer, the
18 15 uptake drops by several orders of magnitude for similar sized proteins with only moderately lower
19 16 binding strength to FG nups [57]. These findings are consistent with the “selective phase” model,
20 17 which postulates that the cohesive FG-FG contacts are important contributors to the permeability
21 18 barrier of FG nup assemblies [97]. In contrast, at low FG nup densities, the effect of the
22 19 cohesiveness can be the opposite and facilitates the penetration of transport protein in the film, by
23 20 enhancing the local concentration of FG repeats (i.e., binding sites for transport protein) in the film
24 21 [114]. Furthermore, in mixtures of different transport proteins, the conformational transitions and
25 22 selectivity can be more complicated and still await theoretical explanation [174].
26
27
28
29
30
31
32
33
34
35

36 23 To summarize, relatively simple polymer models capture the morphological behavior of surface-
37 24 grafted FG nup assemblies, and predict a vastly preferred uptake of transport proteins over inert
38 25 macromolecules, analogous to NPC transport selectivity. Earlier finer-grained and atomistic
39 26 models lend additional support to general principles of selectivity transpiring from the simple
40 27 polymer models, such as its reliance on weak, multivalent interactions of transport proteins with
41 28 flexible, and moderately cohesive FG-nup assemblies. They also provide molecular underpinning
42 29 for the coarse-grained parameterization [55,133,234].
43
44
45
46
47
48
49
50
51
52
53
54
55
56
57
58
59
60
61
62
63
64
65

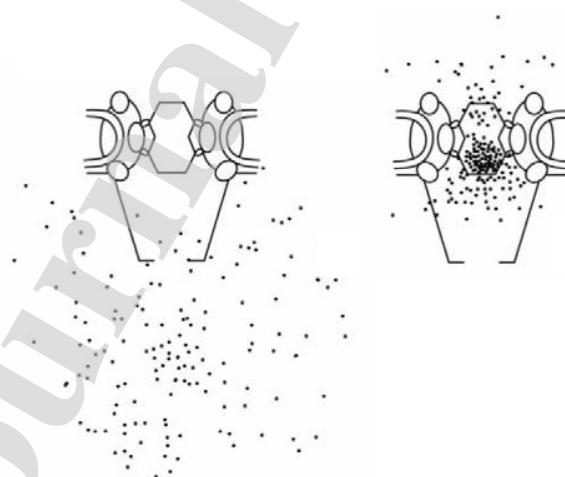
31 3.4.5. Transport proteins in FG nups assemblies in nanopores

50 33 As pointed out in Section 3.3.3, confinement within the nanopore geometry of the NPC can enrich
51 34 the range of morphologies of FG nup assemblies, with potentially important implications for the
52 35 penetration and translocation of transport proteins through NPC. However, there has been only
53 36 limited direct experimental information on the uptake and distribution of transport proteins in
54 37 nanopore-confined FG-nup assemblies. Likewise, most computational work on the NPC has
55 38 focused on the FG nups, ignoring possible effects of incorporated transport proteins on the overall
56 39 morphology and transport properties.
60 40

1 Computational models predict that polymer-coated nanopores infiltrated by transport protein
 2 particles exhibit many of the behaviors observed in planar assemblies. In particular, for relatively
 3 short polymers that do not fill the entire pore, addition of nano-sized particles causes collapse
 4 followed by expansion. Changing the particle concentration or solvent composition can be used to
 5 “gate” the channel between open and closed states [60,185,203].

6
 7 For longer polymers such as the full FG nups, multiple possible physical behaviors were predicted
 8 [60]. Besides the condensation of polymers in the pore center as discussed in Section 3.3.3, these
 9 simulations predict distinct morphologies for transport protein particles. Notably, transport
 10 proteins could accumulate at the interface of the condensed FG nup assemblies and the solution;
 11 or they could penetrate the assemblies and even form lattice-like structures in the pore under
 12 excessive large polymer-colloid attraction. It remains to be determined to what extent the insights
 13 obtained from these different equilibrium regimes are most appropriate for the dynamic non-
 14 equilibrium environment of the for the NPC. Overall, given the range of qualitatively different
 15 behaviors and the large numbers of transport proteins that have been reported in the NPC [7,43],
 16 it is likely that the transport proteins are a defining factor for the FG-nup morphologies adopted in
 17 the NPC [83,100], as discussed in the next section and in Section 4.2.4. However, it is important
 18 to bear in mind that this section only deals with the thermodynamic aspects of NPC specificity.
 19 Full understanding of the selectivity of the NPC transport mechanism requires kinetic and
 20 dynamical considerations discussed in Section 4.

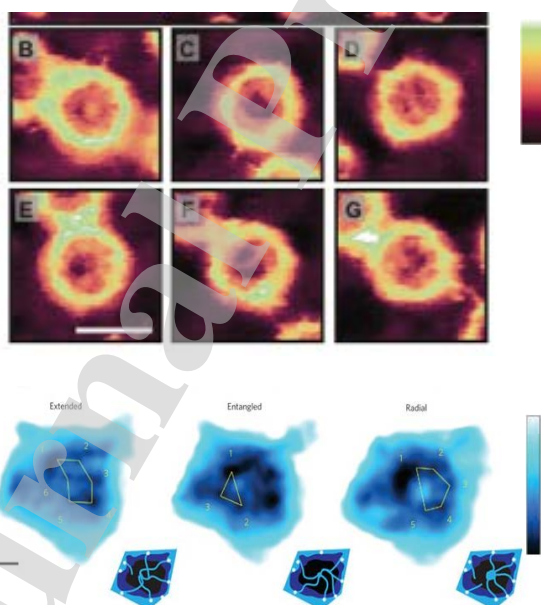
21 22 3.5. Biophysical insights into the morphology of transport channel of intact NPCs



24
 25
 26 *Figure 18. Barrier function of the FG nups in the NPC. Left: distribution of large gold particles around the NPC. Right:*
 27 *distribution of the same size particles covered with NLS, which enables their binding to the transport proteins and thus to FG*
 28 *nups in the pore. Adapted from [235], permission pending.*

1 As described in the previous sections, *in vitro* studies have, to a large degree, identified the key
 2 physical principles and molecular features that underpin FG nup assemblies and their interactions
 3 with transport proteins. Yet, it remains challenging to extrapolate these insights to gain detailed
 4 information about the organization the FG nups and the transport proteins inside the channel of
 5 the NPC, and to the nature and the mechanism of the NPC transport. Recent technological
 6 advances have made the challenge of probing the internal morphology of intact NPCs more
 7 tangible [42–45,119,236,237], albeit still daunting given the large amount of different transport
 8 proteins and cargo that can be found even in isolated NPCs [7].

9
 10 Early experiments used immuno-histochemistry and electron microscopy to image micro-injected
 11 gold nanoparticles of different sizes and surface properties in and around the NPC, and provided
 12 the first indication of the NPC transport barrier [235]. The results are illustrated in Figure 18, which
 13 shows that 30 nm gold particles are essentially excluded from a wide region around the NPC. This
 14 exclusion zone indicates the extent of the FG nup “cloud” around the pore. By contrast, particles
 15 accumulate in the NPC passageway if they are covered with NLSs (which allows the binding of
 16 transport proteins), especially in the regions that are now known to contain FG nups at high
 17 densities.



19
 20
 21 *Figure 19. AFM imaging of the NPC. Top: High-resolution AFM images of the cytoplasmic side of different NPCs in the same*
 22 *nuclear envelope. Adapted from [46], permission pending. Bottom: Different AFM images of the central channel of a single*
 23 *NPC, indicating dynamic FG nup behavior. Adapted from [42], permission pending. Scale bars: 100 nm*
 24 *(bottom). Color scales indicating heights: 0-60 nm (top); 0-4 nm (bottom).*

25 In recent years, atomic force microscopy (AFM) and fluorescence microscopy techniques have
 26 started to provide information about the internal organization of the FG nup/transport protein

1
2
3
4 1 assembly within the NPC. AFM is unique in resolving the surface topography of individual
5 2 molecules and molecular complexes at nanometer resolution, without the need for drying, staining,
6 3 labelling or ensemble averaging. It has been extensively applied to NPCs, often using isolated
7 4 nuclear envelopes that, in most cases, were mechanically extracted from *Xenopus laevis* (frog)
8 5 oocytes [42,45,46,204,238–245].
9 6

10 7 By indentation of NPCs with sharp tips, AFM probed the NPC surface structure and subsurface
11 8 nanomechanical features [45,46], and the ensemble-averaged results were consistent with cryo
12 9 electron microscopy data [241,246]. In addition, the nanomechanical stiffness of the NPC transport
13 10 channel was consistent with model predictions for a marginally stable FG nup condensate
14 11 [45,46,247]. However, it remains hard to define if such measurements probe the behavior of FG
15 12 nups alone or (more likely) the behavior of a mixture of FG nups and transport proteins. At the
16 13 level of individual NPCs, the surface structures of the transport channel show significant
17 14 variability from one NPC to the other (Figure 19, top) and remain static over many minutes (in
18 15 isolated nuclear envelopes, in solution) [35]. This suggests that during the isolation process, the
19 16 NPCs may have been trapped in a large number of possible arrangements of FG nups, including
20 17 transport receptors and cargoes inside the transport channel [7].
21 18

22 19 Recent technological advances have improved the temporal resolution of AFM from minutes down
23 20 to ~0.1 seconds per frame under favorable conditions. This so-called “high-speed” AFM (HS-
24 21 AFM) has enabled the rapid imaging of NPC substructures such as the cytoplasmic lumen and the
25 22 nuclear basket [42], which were resolved at nanometer spatial resolution. Its temporal resolution
26 23 may be sufficient to capture “coarse-grained” views of the NPC morphology and its dynamics
27 24 [42,204,238]. Indeed, HS-AFM imaging at ~200 ms per frame resolved dynamic behavior within
28 25 the central channel, attributed to FG nups (Figure 19, bottom) [42]. This observation comes with
29 26 the technical caveat [204] that it is unclear if and how intrinsic mobility of the nuclear envelope
30 27 might influence dynamic measurements at specific locations in the NPC lumen.
31 28

32 29 Interestingly, averaging over successive HS-AFM images resulted in the impression of a dense
33 30 clump in the pore center [42], which is in good agreement with static AFM measurements of NPCs
34 31 obtained at lower temporal resolution [45]. This resembles a structure reported by averaging
35 32 techniques as a “central plug” or “transporter module” [7,101,241,246,248], and is consistent with
36 33 the hypothesis that dynamic interactions between FG nups might appear as condensates in the pore
37 34 center at longer time scales [42,45] (see section 3.3).
38 35

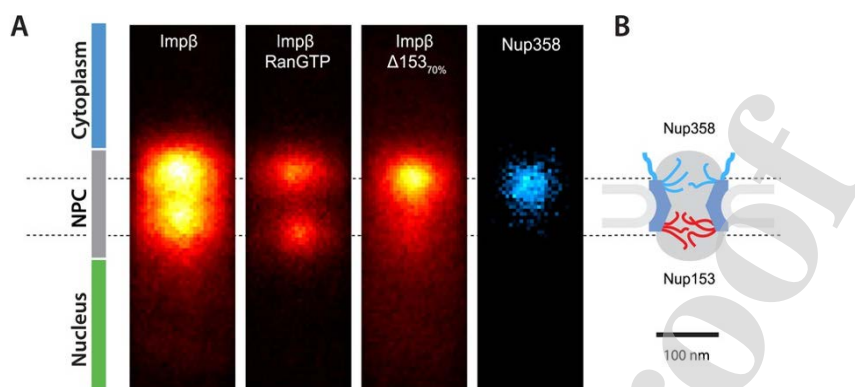


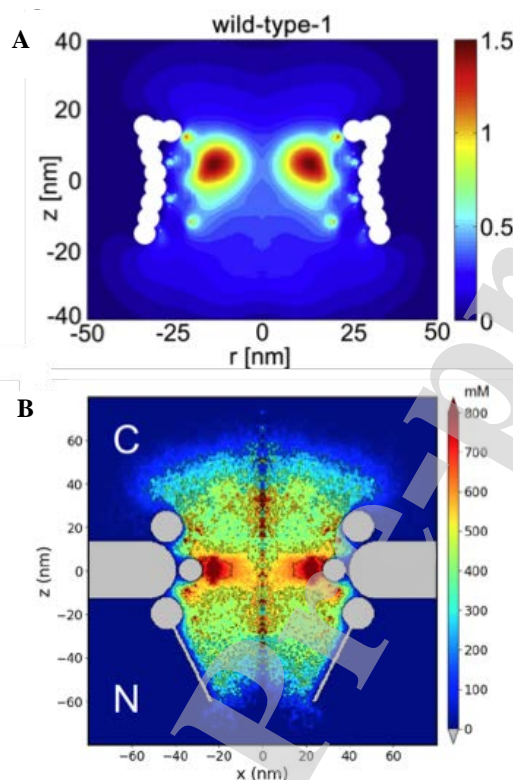
Figure 20. Distribution of fluorescently labelled transport receptors ($Imp\beta$) in the human NPC measured in permeabilized cells. Transport protein binding is associated with specific FG nups ($Nup153$ and $Nup358$) at the opposite sides of the transport barrier. In a mutant cell lacking $Nup153$, transport protein accumulation is severely diminished, especially in the nuclear basket. $RanGTP$ modulates NPC occupancy. **Reproduced from** [43], *permission pending*.

Complementary to AFM, fluorescence microscopy, including super-resolution microscopy, are tools that identify and localize fluorescently-labeled FG nups and transport proteins inside the NPC [249–251]. In particular, FG nup binding transport proteins were found to preferentially localize at either side of the NPC channel in permeabilized cells, showing a two-lobed distribution along the NPC channel axis, indicating that the FG nups might be distributed non-uniformly along the channel axis [43] (see Figure 20). Such spatial heterogeneity of the FG nups might play an important role in defining distinct, cargo-specific spatial pathways through the NPC [44,252,253]. We return to this question in Section 4.2. That section will also discuss the application of single molecule fluorescence microscopy as a means to study the kinetics of transport through the NPC.

Likewise, computer simulations support the picture of the heterogeneous distribution of the FG and its importance for NPC barrier and specificity function [59,62,63,169,170] (Figure 21). In particular, one-bead-per-amino acid models predict averaged amino-acid distributions that show signatures of FG-repeats condensed in a donut-like shape [62,63,169]. Such local variations in FG nup density distribution support the possibility of spatially distinct transport pathways for, e.g., ions and small proteins on one hand and larger proteins on the other [62]. Notably, although some of the detailed simulation models show potential importance of charge and electrostatic interaction in shaping the local FG nup distribution [62,63,110,111], the overall density distribution of the FG nups is consistent with simple homopolymer and patchy polymer models [60,144,184–186].

When interpreting the results of these computational studies, one should bear in mind that FG nup morphology is very likely modified by transport proteins present in the NPC [43,60,83,203]. Hence, future computational evaluations need to consider potential effects the various embedded

1 resident and/or translocating transport proteins on FG nup behavior, keeping in mind the richness
 2 of the possible phase diagram and its sensitivity to parameter settings [60].
 3



4
 5
 6 *Figure 21. Computational models of the FG nup distribution in the yeast NPC using one-bead-per-amino-acid models. Both models*
 7 *(although with different scaffold geometry and force field parametrization) predict a donut-shaped density profile of FG nups in*
 8 *the pore (in the absence of transport proteins). (Legends) A: Time-averaged FG-nup number density (in nm^{-3}); adapted from [62],*
 9 *B: Amino-acid density distribution (in mM); adapted from [169], permission pending.*

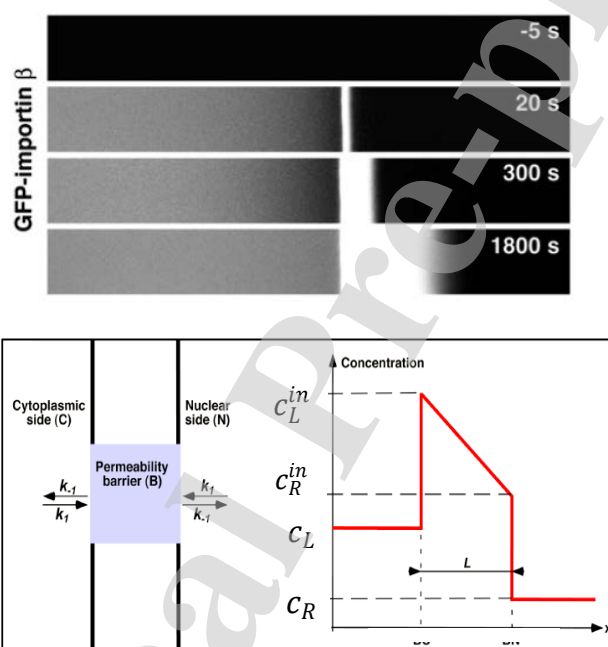
11 4. From structure to transport

12
 13 One fundamental question that surrounds the NPC problem is how the FG nups and transport
 14 proteins enable such efficient transport while combining several seemingly contradictory features.
 15 On the one hand, its high selectivity relies on the thermodynamically strong and specific
 16 interactions between the transport proteins and the FG nups. On the other hand, while transport
 17 proteins are enriched within the FG nup assembly, they do not clog the NPC, and individual
 18 transport proteins rapidly translocate through its passageway within milliseconds. Finally, NPC
 19 transport is robust with respect to structural perturbations and molecular noise, as mentioned
 20 earlier.
 21

1 Similar to the morphological properties of the NPC described in the previous chapter, the
 2 foundations of NPC transport dynamics may be understood via *in vitro* studies interpreted through
 3 the lens of theoretical and computational models. In this chapter we summarize the current
 4 consensus regarding the physics and the key principles of NPC transport.

6 4.1. Transport dynamics of the transport proteins within NPC-like FG nup assemblies *in* 7 *vitro*.

9 4.1.3. Diffusion of transport proteins within FG nup assemblies.



12
13
14 Figure 22. Penetration of transport proteins into FG nup “gels”. Top: experimental data, showing penetration of a fluorescently
 15 labeled transport protein into a hydrogel (right) as a function of time. Bottom: simple kinetic model of transport protein
 16 penetration into and diffusion through a slab of a “gel”. See text for discussion. Adapted from [97], permission pending.

17
18 Initial studies of transport protein kinetics within macroscopic FG nup environment were
 19 performed in hydrogel-like aggregates obtained by irreversible cross-linking of the FG nup chains
 20 [94,97,109,161,163,254]. It remains uncertain to what extent the insights from these studies
 21 translate to the actual FG nup assembly in the NPC due to differences in internal morphology,
 22 confinement and chemical environment [98,161,162]. Nevertheless, micron-sized FG-nup “gels”
 23 exhibit rudimentary selective NPC-like sieving properties [96–98,104]. Taken together, these bulk
 24 assemblies have provided important insights into the permeability and diffusion of transport
 25 proteins within the FG nups.

1 Protein uptake and transport in FG nup gels can be modeled using a simple kinetic model of entry,
 2 diffusion and exit from the FG nup assembly [97], as illustrated in Figure 22. Assuming that the
 3 proteins undergo simple diffusion inside the “gel” with a diffusion coefficient D , the steady state
 4 flux (per unit area) through a slab of material of width L is $J = \frac{D}{L}(c_L^{in} - c_R^{in})$, where L is the length
 5 of the slab and c_L^{in} and c_R^{in} are the (one dimensional) concentrations of the transport proteins at the
 6 left and the right edges of the slab, respectively. At steady state, they are related to the outside
 7 concentrations of the transport proteins, c_L and c_R , respectively, as $k_{-1}c_L^{in} = k_1c_L - J$ and
 8 $k_{-1}c_R = J - k_1c_R$, where k_1 and k_{-1} are the phenomenological rates of entry into and exit from
 9 the gel, respectively [97]. Solving for the flux gives

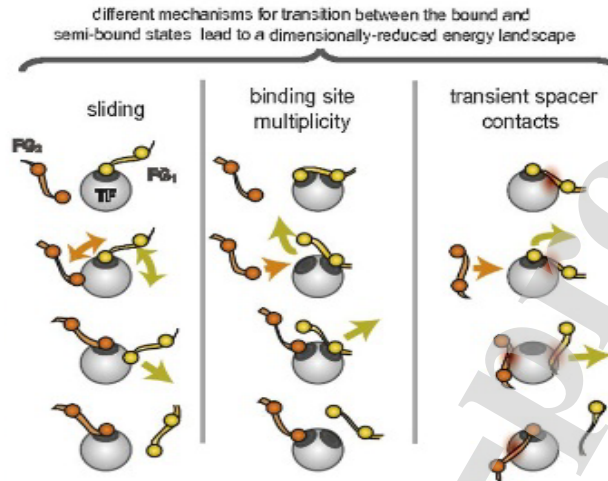
$$J = k_1 \Delta c \frac{1}{2 + k_{-1}L/D}, \quad (5)$$

13 where $\Delta c = c_L - c_R$ is the difference in the (one dimensional) concentration of the transport
 14 proteins on the different sides of the slab. For an inert protein, the entry rate is low and the exit
 15 rate is high, resulting in low flux. For the transport proteins, conversely, the entry rate is high, and
 16 the exit rate is low, resulting in high flux. The entry and exit rates depend on the free energy of
 17 entry of the particle into the gel: inert particles experience a high free energy barrier, while
 18 transport proteins experience a free energy well. The free energy barrier was initially assumed to
 19 arise from the cross-linking of the FG nups at the hydrophobic FG motifs [97,109]. However, as
 20 discussed in the previous section, the free energy of a particle inside an FG nup assembly likely
 21 combines the interplay of both enthalpic and entropic effects [56,57,108].

23 Consistent with the discussion in Section 3.3, permeability of FG nup assemblies with respect to
 24 transport proteins depends on the density of FG nup assemblies. At lower density, FG nup
 25 hydrogels do not provide a sufficient barrier and allow facile entry of both inert and transport
 26 proteins (i.e., they are non-selective) [97]. Accordingly, the measured diffusion coefficients of
 27 proteins inside these low-density gels are close to their diffusion coefficients in water. At higher
 28 density, FG nup gels permit the entry of transport proteins but severely restrict the entry of inert
 29 proteins. When inside high-density gels, it is noteworthy that both inert proteins and transport
 30 proteins exhibit similar diffusion coefficients D being on the order of $D \approx 0.1 \mu\text{m}^2/\text{s}$. This is two
 31 to three orders of magnitude lower than in a low-density gel, but is consistent with the typical
 32 diffusion coefficients in cellular environment [255,256]. It might appear puzzling at the first glance
 33 that the transport protein diffusion is slowed down in the FG nup assembly. However, their high
 34 thermodynamic partitioning leads to higher concentrations within the FG nup assembly, and
 35 therefore facilitates translocation through the assembly.

37 Further complicating things, the diffusion coefficient – which is treated as a phenomenological
 38 constant in this simple description – in general depends on the FG nup density, structure and the

1 interaction strength. How interacting particles diffuse within the interior of such a complex
 2 polymeric material still remains an open problem [52,257–270].



25 4
 26 5 Figure 23. Illustration of the “slide and exchange” mechanism; see text for details. Adapted from [134], permission pending.
 27
 28

29 6
 30 7 Previous theoretical works on diffusion of a patchy polymer through polymer solutions provided
 31 8 the basis for the earlier estimates of the diffusion coefficient of a patchy particle in a polymer
 32 9 solution, which was expected to vary as $D \sim e^{\epsilon|N|}$, where $\epsilon < 0$ is the binding energy of an
 33 10 individual patch [52,271]. However, already for a particle with several interaction patches and
 34 11 moderate binding energies of several $k_B T$, this prediction results in unrealistically low diffusion
 35 12 coefficients incompatible with *in vitro* measurements and *in vivo* translocation times.
 36
 37

38 13
 39 14 Although still not fully understood, multivalency likely helps to reconcile strong thermodynamic
 40 15 binding with the fast mobility of transport proteins in an FG nup milieu. At higher FG nup
 41 16 densities, single particles start to interact with multiple FG nups, allowing the transport proteins to
 42 17 slide in a “millipede-type” motion from one chain to another while breaking only a small number
 43 18 of bonds and remaining tightly bound to the FG nup assembly. Molecular dynamics simulations
 44 19 have provided insights and visualizations of this “slide-and-exchange” mechanism for transport
 45 20 protein motion within an FG nup assembly. In this model, only one binding site is released at each
 46 21 step, enabling the transport protein to progress forward due to the thermal fluctuations of the FG
 47 22 nups, finishing the step with the rebinding at the next available binding site [134]. This way, the
 48 23 transport proteins can have high thermodynamic affinity for the FG nups while maintaining fast
 49 24 kinetics [134].
 50
 51
 52
 53
 54
 55

56 25
 57 26 Using a simplified model of FG nup flexibility and transport protein transfer between FG nups, an
 58 27 analytical expression was obtained for the diffusion coefficient in the bound state in the case of a
 59
 60
 61
 62
 63
 64
 65

1
2
3
4 1 transport protein with two binding sites (NTF2) [268,272]. Similar ideas were used in [270] for
5 2 particles with multiple binding sites.
6 3

7 3
8 4 Furthermore, it was theoretically and computationally shown [258] that in solutions of cohesive
9 5 polymers, increased attraction between the diffusing particle and the polymers can actually
10 6 increase the diffusion coefficient compared to a neutral particle. This effect occurs because the
11 7 particle binding to the polymer chains facilitates the dissociation of the transient inter-chain cross-
12 8 links that otherwise impede the motion of a neutral particle.
13 9

14 9
15 10 These ideas provide a potential physical explanation for both the importance of high valency of
16 11 transport factors that allows inter-chain transfers without unbinding, and the flexibility of the FG
17 12 nups that allows for residual motion even when bound. Chain cohesiveness might enhance the
18 13 difference in the diffusivity between transport proteins and neutral cargoes. Further synthesis of
19 14 these ideas is necessary to provide a complete picture of the transport protein translocation through
20 15 the NPC.
21 16

22 16
23 17 However, diffusion rate is only one ingredient that determines the flux of transport proteins
24 18 through FG nup coated channels, the other being the rate of release at the channel ends, which is
25 19 closely related to the thermodynamic permeability discussed in the previous section. In the next
26 20 section we discuss how these two factors combine to determine the flux through FG nup coated
27 21 nanochannels.
28 22

29 22 30 23 4.1.4. Nanochannel mimics of the NPC. 31 24

32 24
33 25 Further understanding of NPC transport mechanism can be obtained by exploring nanochannel
34 26 NPC mimics functionalized with FG nups, which more closely approximate the FG nup
35 27 morphology and transport kinetics within a pore [23–26,273]. The equilibrium structural properties
36 28 of the FG nup assemblies in these nanochannel mimics have been discussed in Section 3.3.3.
37 29

38 29
39 30 Depending on the experimental design, these NPC mimics allow measurements of either bulk
40 31 molecular flux [23], or individual translocations [25,26]. An advantage of measuring bulk flux is
41 32 the ability to access the high concentration regime where channel crowding may become
42 33 important. However, in this regime it is harder to obtain information about the dynamics of
43 34 individual translocation events. Accordingly, experiments that detect single molecule translocation
44 35 events are able to assess individual event frequencies and translocation (dwell) times but are
45 36 challenging at very high transport protein concentrations. Moreover, it is often difficult to detect
46 37 short transport events and to distinguish between successful translocations and abortive events in
47 38 these experiments [274].
48 39

4.1.4.1. *Theoretical background: diffusion through nanochannels.*

As mentioned in Section 4.1.3, description of the motion of an interacting particle through a polymer assembly on the nanoscale is a non-trivial problem [51,52,257,263–265,267,275,276]. However, as a first approximation, such transport can be thought of as diffusion in an effective free energy potential. The depth, spatial shape of the potential, and effective diffusion coefficient are determined by the interactions between the protein/particle and the FG nups/polymers inside the channel, and the distribution of the latter within the channel. For small particles with relatively weak interactions, the effective potential is roughly proportional to $U(x) \sim B\psi(\vec{x})$ where ψ is the density of the monomers that make up the polymers and B is the second virial coefficient of the interaction between the particle and the polymer [276], in the spirit of Edwards's theory [95]. For larger particles, this potential can be related to the free energy of penetration discussed in the context of bulk and surface FG nup assemblies in Section 3, and to the potential of mean force discussed in Section 4.1.2.3.

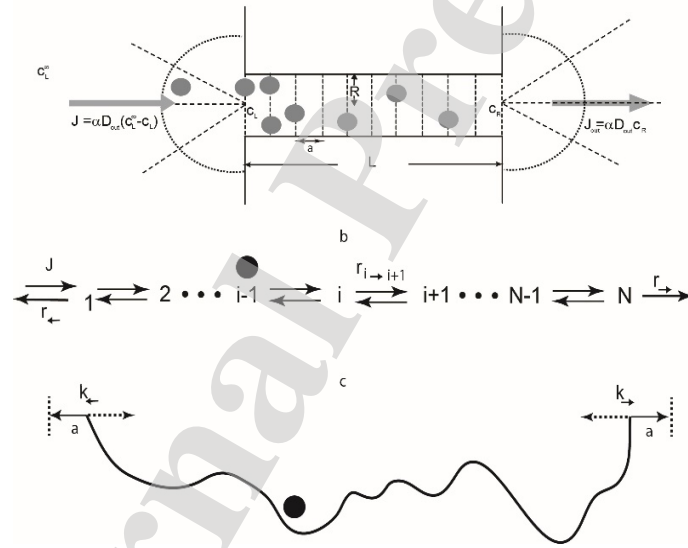


Figure 24. Schematic illustration of diffusion and hopping models that describe particle translocation through a channel. See text for discussion. Adapted from [277], permission pending.

In a one-dimensional approximation (see Figure 24), the probability of a particle to be at a position x along the channel axis at time t obeys the Smoluchowski equation [49,278]

$$\frac{\partial P(x,t)}{\partial t} = -\nabla J(x,t) \quad \text{with} \quad J(x,t) = -\frac{D}{k_B T} \frac{\partial U(x)}{\partial x} P(x,t) - D \frac{\partial P(x,t)}{\partial x},$$

1 where $U(x)$ is the effective potential and D is the effective diffusion coefficient. As discussed in
 2 Section 4.1.3, the diffusion coefficient may itself depend on the binding strength; we return to this
 3 question in Section 4.2.3. The same equation describes the density of particles in the channel in
 4 the non-interacting particles approximation. The time evolution of this probability distribution can
 5 be equivalently described by as hopping between discrete sites with transition rates $r_{i \rightarrow i \pm 1}$ obeying
 6 the detailed balance condition $\frac{r_{i \rightarrow i+1}}{r_{i+1 \rightarrow i}} = \exp\left(\frac{U_i - U_{i+1}}{k_B T}\right)$, using the Master equation approach [278–
 7 281] (see Figure 24). These models can be extended to explicitly include the binding-unbinding
 8 kinetics of the proteins by considering the protein diffusion in the bound and the unbound states
 9 [49,268,270,272,282].

10 These models of in-channel diffusion, illustrated in Figure 24 can be coupled to the particle
 11 diffusion outside the channel, and allow one to calculate the transport properties such as the
 12 translocation probability, translocation time and particle flux, under various assumptions
 13 mimicking different experimental conditions [49,277,283,284]. The translocation probability (the
 14 probability of a particle to successfully traverse the channel to the other end rather than returning
 15 back in an abortive attempt) is approximately

$$P_{\rightarrow} = \frac{1}{2 + \alpha \frac{D_{out}}{R D_{in}} \int dx e^{U(x)/k_B T}}, \quad (6)$$

19 where R is the channel radius, and D_{in} and D_{out} are the diffusion coefficient inside and outside
 20 the channel, respectively; α is a numerical prefactor that depends on the geometry of the channel
 21 entrance and the particle shape. This equation is the direct analogue of the one-dimensional flux
 22 equation in slab. Notably, the expression for the translocation probability is relatively insensitive
 23 to the exact shape of the potential $U(x)$. In order to account for the enhanced release of transport
 24 protein from the potential well facilitated by RanGTP in the nucleus equation (6) can be modified
 25 by modifying the corresponding exit rates or potential shapes [49,220]. The limitations of this
 26 single particle expression can be recognized by noting that the maximum translocation probability
 27 would – unrealistically – occur for an infinitely negative potential well $U(x)$. In reality, for very
 28 strong interactions the channel becomes jammed, either due to “freezing” of the particle motion
 29 due to low diffusion coefficients, or due to crowding present in deep wells [49,268,276,277,285].

30 The single-molecule translocation probability can be related to the bulk flux through the channel
 31 by noting that equation (6) also describes the particle density in the channel in the non-interacting
 32 particle approximation. At steady state, for particles that do not interact with each other, the flux
 33 through the channel is

$$J = J_{in} P_{\rightarrow},$$

1 where $J_{in} = k_{in}c$ is the flux impinging onto the channel entrance from a solution containing
 2 particles at a concentration c (assuming zero concentration at the other side). This flux equation
 3 becomes similar to Equation (5) in the slab geometry with the identification $k_{in} = k_1 \cdot \pi R^2$ and
 4 $k_{-1} = \alpha \frac{D_{out}}{LR} \int dx e^{\frac{U(x)}{k_B T}}$. For simple diffusion-limited entry, k_{in} can be approximated as $k_{in} =$
 5 $\beta D_{out} R$, where β reflects the shape of the channel opening [286–288]; if the interaction potential
 6 stretches outside the channel, that enhances the effective capture radius is enhanced by a factor
 7 approximately equal to $\sim \left(R \int_R^\infty \frac{dr}{r^2} e^{-\frac{U(r)}{k_B T}} \right)^{-1}$ [289,290].

8
 9 The general expression for the translocation time is more cumbersome [277,280,291]. For the
 10 simple case of a uniform trapping potential inside the channel, $U(x) = -E < 0$, the translocation
 11 time is approximately $T_{\rightarrow} \simeq \frac{RL}{D_{out}} e^{\frac{E}{k_B T}}$. Under these circumstances, the translocation time increases
 12 exponentially with the interaction strength E , as the probability of a fluctuation that takes the
 13 particle out of the potential well becomes exponentially small [289]. In the opposite situation of a
 14 repulsive barrier inside the channel, the translocation time (for those particles that do translocate)
 15 is approximately $T_{\rightarrow} \simeq \frac{L^2}{D_{in}}$. In this regime, although the successful translocations are rare, those
 16 that do occur are independent of the height of the free energy barrier in the pore. For simple
 17 diffusion models, the distribution of both the successful and abortive translocation times typically
 18 has exponential tails [280,289,292].

19
 20 Because the translocating particles remain longer in a deeper potential well, it is no surprise that
 21 the translocation time increases with the potential depth. Less intuitively, the translocation
 22 *probability* (and therefore flux) also increases with the potential depth. This effect, sometimes
 23 known as facilitated diffusion, has been noted in a variety of contexts [282,293,294]. It occurs
 24 because a deeper potential well leads to a local non-equilibrium enhancement of particle
 25 concentration in the channel and therewith to an enhanced flux through the channel. In other words,
 26 a deeper potential increases the translocation probability because it reduces the chance of abortive
 27 exit after the channel entry. More intuitively, a decrease in the diffusion coefficient inside the
 28 channel D_{in} decreases the translocation probability. Although the exact dependence of D_{in} on the
 29 interaction strength is still unknown, a number of models predict that it is decreased by the binding
 30 to the polymers (see Section 4.1.3). In this case, this effect can balance the increase in the
 31 translocation probability due to binding, resulting in the maximization of transport at an optimal
 32 interaction strength [268,272]. This may provide the foundation for the transport selectivity of the
 33 NPC, whereby translocation through the NPC is only favored for transport protein-cargo complexes
 34 with an effective affinity in a certain range (Figure 25).

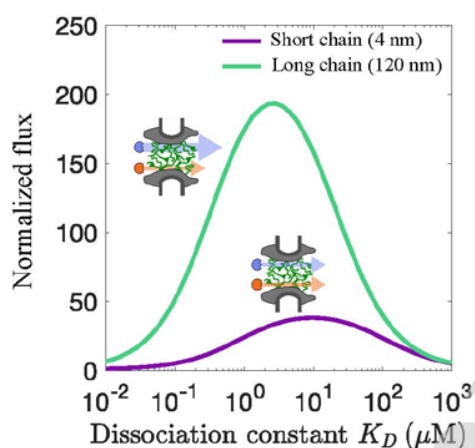


Figure 25. The ratio of the predicted steady-state flux of a transport protein (illustrated as blue arrow) to that of a non-binding protein of the same size (illustrated as orange arrow). The effective diffusion coefficient in the bound state inside the channel decreases with the binding affinity of the transport protein to the FG nups/polymers, resulting in a non-monotonic dependence of the flux through the NPC-like channel on the interaction strength. See text. Adapted from [268], permission pending.

These theoretical principles have been validated in micro-channel/micro-particle experiments with optically generated potentials [295,296].

4.1.4.2. Specificity of NPC mimics at the single molecule level

These simple concepts have been useful in analyzing the transport through NPC mimics. Results obtained from FG nup-functionalized solid state nanopores are illustrated in Figure 26 [26]. Electrochemical scanning techniques, which detect temporal decreases in ionic flux due to a “blockade” caused by a translocating particle, were used to detect single molecules passing through the nanopore. The main caveats of these techniques are that both successful and abortive translocation events cause a (transient) blockade, and that the electric driving force may cause an additional bias to the transport [25,196,274]. Nonetheless, these systems have provided powerful tools to test the theoretical concepts that describe selective transport in nanochannels and their application to the NPC.

These experiments showed that the dwell time distributions of the transport protein Importin- β and the control protein BSA were essentially the same in bare pores, as expected for proteins of similar size and charge. The presence of FG nups, however, led to a significant reduction in the number of entry events for BSA, thereby reinforcing the notion that the FG nups serve as a barrier for inert proteins. By contrast, the number of transport protein translocation events through an FG-nup coated pore was similar to the bare pore, although on average, each translocation event was longer. These observations support the overall conceptual picture of NPC transport whereby the FG nup assembly serves as a barrier for neutral proteins, while enhancing transport of the transport proteins [25,26].

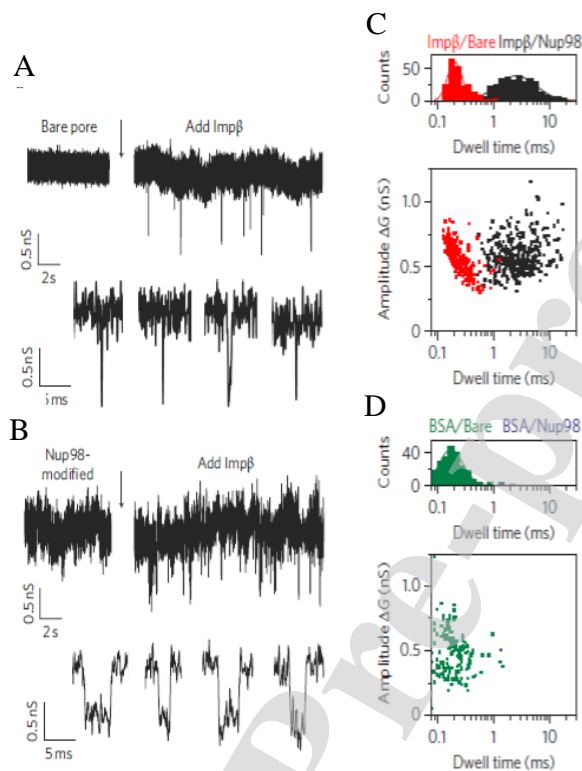
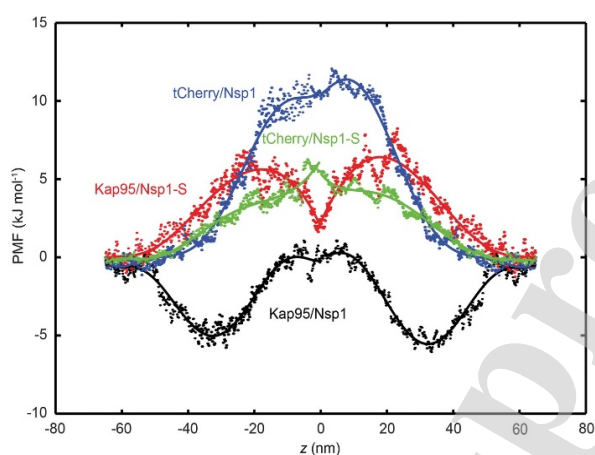


Figure 26. Translocation of transport proteins through nanochannels detected on the single molecule level. **A, B**: time traces of the ionic flux. The translocation of the transport protein Importin- β through the channel temporarily blocks the current. **C**: For the transport protein (Importin- β), the blockade times (dwell times) are longer in an FG nup (Nup98) modified pore than in a bare pore. The translocation frequency, however, is similar to that of the bare pore, indicating that the FG nup covered pore is permeable to the transport proteins. **D**: For the control protein (BSA) which does not interact with the FG nups, the translocation frequency is severely diminished compared to the bare pore and compared to the transport protein, indicating a selective permeability barrier. Adapted from [26], permission pending.

4.1.4.3. Effective potential in FG nup functionalized nanopores

The effective potential for translocating cargoes within NPC mimics is determined by the spatial distribution of the FG nups within the nanochannel. Although hard to directly determine experimentally, this effective potential can be estimated from simulations of particle translocations through FG nup covered channels by calculating the ‘potential of mean force’ (pmf) of a translocating particle [25,63,297]. The pmf at a position x within the channel is defined as the amount of work required to (adiabatically slowly) bring a particle from infinity to x , and can be calculated from the steady state distribution function $P(x)$ of the particle in the channel, $pmf(x) \simeq k_B T \ln(P(x))$; it is also related to the free energy of insertion ΔF , discussed in Section 3.4 [226]. The pmf can serve as a proxy for the effective potential with the caveats that: 1) for fast transport the force profile experienced by the particle might deviate from that dictated by the equilibrium pmf , as the FG nups and the particle might sample only a restricted set of their

1 configurations during the transport time; and 2) the effective potential can also be modified by the
 2 presence of multiple transport proteins in the pore.



4
 5 *Figure 27. Effective potential (potential of mean force, (pmf)) calculated for different cargo types translocating through*
 6 *nanopores functionalized with FG nups. Inert particles (tCherry protein) experience a high free energy barrier in FG-nup (Nsp1)*
 7 *coated pores (blue line), whereas the transport proteins (Kap95) experience a lower barrier (black line). No such contrast is*
 8 *observed when the pore is coated with a less cohesive mutant (Nsp1-S) (red and green). Reproduced from [25], permission*
 9 *pending.*

10
 11 In particular, ref. [25] used the one-bead-per-amino-acid model of the FG nups, described in
 12 Section 3.3.3, to compute *pmf* profiles for the transport protein (Kap95) and a control protein
 13 (mCherry) along the central axis of a 45 nm nanopore, coated with either a cohesive FG nup (Nsp1)
 14 or a less cohesive mutant (Nsp1-S) that also interacts more weakly with the transport protein, as
 15 shown in Figure 27. Inside a pore coated with the wild type FG nup (Nsp1), a pronounced free
 16 energy barrier was found for the control protein (blue line), while the transport protein experienced
 17 an attractive energy profile (black line). By contrast, the *pmf* curves for the control (green curve)
 18 and transport protein (red curve) for the mutant Nsp1-S pores were found to be similar, consistent
 19 with the non-selective nature of the mutant pore. The detailed shape of the effective potential
 20 depends on the force field that parametrizes the hydrophobic, electrostatic and steric interactions
 21 between the FG nups and the assumed properties of the particles that model the transport proteins
 22 [25,53,54,63,110,297]. However, the overall shapes and strengths of the effective *pmf* potentials
 23 are consistent across different models of varying degree of coarse-graining and parameterization
 24 choices.

25
 26 General principles of transport selectivity are emerging from the combined analysis of the
 27 equilibrium selectivity and permeability of the *in vitro* assemblies discussed in Section 3.4, and
 28 the analysis of the kinetics and energetics of translocation described in Section 4.1.4.1. In the main,
 29 permeability of an FG nup covered channel is determined by the effective cost of penetration of a
 30 particle into the FG nup assembly inside the channel. The probability of its subsequent
 31 translocation and therefore the flux through the channel can be understood using kinetic models

1
2
3
4 1 for diffusive transport through effective potential barriers/wells, informed by the *pmf* of the particle
5 2 in the channel. Attractive interaction with the FG nups in the channel, resulting in a deeper
6 3 potential well, enhances the transport through the channel at the expense of increased individual
7 4 translocation times, as illustrated in Figure 26 and Figure 27.
8
9

10 5
11 6 Overall, these general principles of transport specificity apply also to less explicit NPC mimics
12 7 [27] and other synthetic nanochannels, even quite removed from the NPC in terms of their
13 8 molecular components [146,298], as well as biological channels such as bacterial porins [299–
14 9 302]. For instance, NPC mimicking nanochannels functionalized with synthetic polymers are
15 10 selective with respect to the cargo interaction with the polymers in the channel, confirming the
16 11 basic principles of NPC operation [27].
17
18
19
20

21 13 4.1.4.4. *Transport protein crowding inside the channel*

22 14
23 15 Given that the NPC transports multiple molecules simultaneously [88,303,304] and is
24 16 continuously occupied by multiple transport proteins [43,83,305], the single-molecule analyses in
25 17 the previous section may not adequately account for the crowded conditions that apply in the NPC.
26 18 The question of crowding features prominently when considering the specificity of the NPC.
27 19 Diverse species such as export, import and mRNA transport complexes interact with the NPC,
28 20 presumably in different ways. On the other hand, there are many other proteins in the dense
29 21 environment of the cell, present at concentrations that may be several orders of magnitude higher
30 22 than those of transport proteins, and that can interact with the NPC non-specifically [103,206,222].
31 23 Yet these are efficiently filtered out, without clogging the NPC. In the more general context, the
32 24 question of specificity and throughput in the presence of non-specific competition is important for
33 25 the design of artificial nano-channels and biosensors that are capable of molecular sorting and
34 26 detection under realistic conditions without fouling [193,306,307].
35
36
37
38
39
40
41

42 28 To include the competition for space and binding sites inside the channel, the translocation of
43 29 particles can be described via extensions of the hopping models described above, introducing full
44 30 or partial exclusion between particles at the same site. A number of methods have been devised to
45 31 treat such scenarios, using ASEP (asymmetric exclusion processes) models and other methods
46 32 [277,308–311]. In the mean field approximation, the rate equation for the average occupancies n
47 33 at site i can be written as
48
49
50

$$51 34$$

$$52 35 \dot{n}_i = -r_{i \rightarrow i+1} n_i (1 - n_{i+1}) - r_{i \rightarrow i-1} n_i (1 - n_{i+1}) + r_{i+1 \rightarrow i} n_{i+1} (1 - n_i) + r_{i-1 \rightarrow i} n_{i-1} (1 - n_i), (7)$$

$$53 36$$

54 37 where the $r_{i \rightarrow j}$ refer to transition rates from site i to site j (see Section 4.1.2.1 and Figure 24). The
55 38 models can be used to calculate the steady-state fluxes, and can be extended to compute single-
56 39 molecule quantities such as translocation times [281,292,312–314].
57
58
59
60
61
62
63
64
65

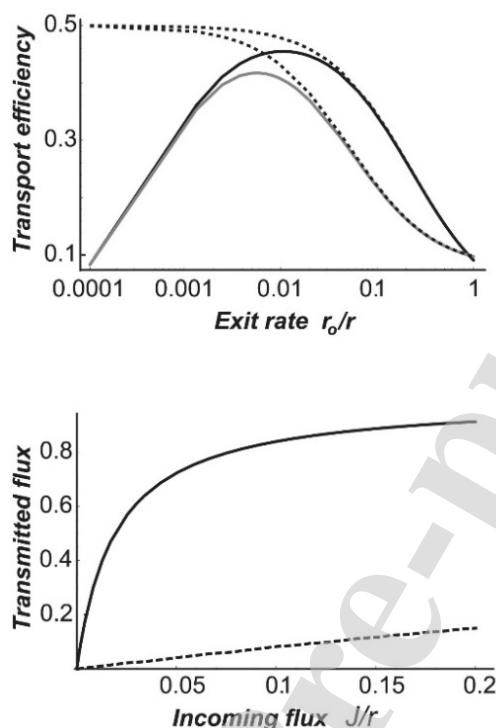


Figure 28. Effects of trapping in the channel on transport efficiency and transmitted flux. Top: transport efficiency, defined as the ratio of the transmitted flux to the incoming flux as a function of the interaction strength in the channel. The exit rate $\frac{r_0}{r} \approx \exp\left(-\frac{E}{k_B T}\right)$ where E is the potential well depth; r is the hopping rate within the channel. Bottom: Transmitted flux as a function of the incoming flux. Solid line: particles with strong attraction to the channel. Dashed line: neutral particles that do not interact attractively with the channel. **Reproduced from [312], permission pending.**

As explained above, the probability of translocation increases with the time that particles remain in the channel. However, longer residence times can lead to crowding and eventual blockage of the pore entrance, resulting in the saturation of the flux as a function of the concentration [49,277,285]. Accordingly, stronger particle-channel interactions initially increase the transport probability but lead to channel jamming and reduction in the flux at very deep potential wells. Balancing these two effects, the channel throughput may be optimized at a certain value of the potential depth/exit rate as shown in Figure 28. Interestingly, this implies that the flux through the channel is not maximized by attaining a relatively flat potential profile, as it might be expected. Instead, it is maximized for a net negative potential well [49,277,285]. These theoretical principles have been validated in micro-channel/micro-particle experiments with optically produced potentials, as well as in other experiments [295,296].

Crowding caused by transport proteins could also explain the specificity of transport when multiple protein species are present, and when the transport proteins compete for space and binding sites in

1 the channel with large numbers of other non-specific molecules. Some of these questions were
2 investigated with FG nup functionalized nanoporous membranes described in Section 3.3.3 [23]
3 and uncovered non-trivial non-linear interactions between fluxes of different species. Namely, the
4 transport of inert control proteins was significantly reduced by the presence of transport proteins
5 whereas the presence of inert proteins facilitated the translocation of transport proteins [23]. These
6 results can be understood within the simple kinetic models described in equation (7) and Figure
7 24, and were extended by multiple species containing a mechanism of preventing the transport of
8 non-specific competitor molecules [50]. Under these conditions, transport proteins, that bind
9 strongly within the channel (see Section 4.1.4.3 and Section 4.2.4), reduce the probability of the
10 translocation of non-specific proteins. Typically, if a specific molecule binds tightly to the channel
11 and is followed by a non-specific molecule with loose interactions, the latter will likely diffuse out
12 of the channel before the specific transport protein moves through. On the other hand, if the
13 transport protein is followed by another transport protein, it is likely that the latter will linger long
14 enough for the first one to clear through. Thus, the non-specific molecules are unlikely to
15 translocate through the channel, and their accumulation near the entrance creates an additional
16 density exclusion gradient that enhances the translocation of the specific transport proteins by
17 preventing their return to the cis compartment [50]. This indicates that the specificity conditions
18 strongly depend on the multi-species composition of the cargoes transported through the channel.

19
20 These theoretical predictions are in good agreement with the experimental results of Jovanovic-
21 Talisman *et al.* [23]. Moreover, the competitive selectivity effects have been confirmed in other
22 work using synthetic nanoporous materials for molecular separations [193,199]. Conceptually
23 similar phenomena have been described in ion channels, known as “anomalous mole fraction
24 effect”. In this case, ionic fluxes in the mixtures of ions are not proportional to the molar
25 concentrations of the ions in the feed solution, because the differences in their transport kinetics
26 are amplified through non-linear density coupling within the channel [315–317].

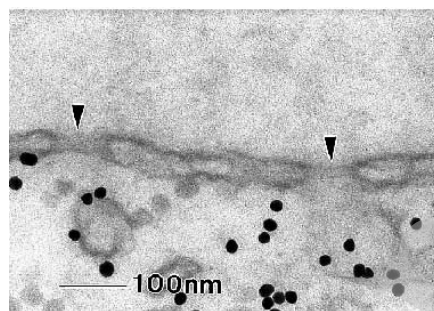
27 28 4.2. Physical insights into transport by NPCs in the cell

29
30 Actual NPCs are significantly more complex than even the most elaborate *in vitro* mimics.
31 Nevertheless, analysis of transport phenomena in reconstituted FG nup/transport protein
32 assemblies and nanofabricated NPC mimics using physical models helped identifying the key
33 principles of transport and resulted in computational tools that together provide an important
34 framework for the understanding of the structure and the function of NPCs in the cell.

35 36 4.2.3. Passive permeability barrier of the NPC

37
38 According to the common consensus, one primary function of the FG nup assembly in the NPC is
39 to provide a permeability barrier and filter for undesirable cargoes that are neither bound to the
40 transport proteins nor specifically bind the FG nups directly [67,75–77,235].

1
2
3
4 1 Early investigations of the passive permeability barrier were performed using electron microscopy
5 2 to visualize the localization of (PEGylated) gold nanoparticles that were micro-injected into living
6 3 cells on either side of the nuclear envelope, as illustrated in Figure 29 [235]. Whereas small
7 4 particles were able to translocate through the NPC, large particles did not penetrate the NPC to a
8 5 measurable degree even at long times after injection.
9 6



7
8 *Figure 29. EM image of the nuclear envelope perforated by nuclear pores (indicated by black arrows). Black dots are the gold*
9 *nanoparticles micro-injected into the cell. Reproduced from [235], permission pending.*

10
11 Further quantification of the size dependence and cutoff for passive permeability was provided
12 using an *ex vivo* setup [76]. The nuclear envelope of *Xenopus laevis* (frog) was mechanically
13 extracted from oocytes and spread out on a nanoporous surface, resulting in co-localization of
14 some of the NPCs with the nanopores. The permeability of the NPC was assessed by measuring
15 the flux of fluorescently labeled dextran cargoes through this composite structure. It was found
16 that the flux of the passive cargoes through the NPC diminished with the cargo size and became
17 almost non-existent at a molecular weight of around 40 kDa, corresponding to a particle radius of
18 approximately 2.5 nm [76].
19

20 The results were further refined in permeabilized cells using protein cargoes of different sizes [77].
21 These studies showed that the 40 kDa cutoff is not absolute, and the flux persists even for larger
22 cargo, although with a strong size dependence. Other studies [67,75] compared the passive
23 transport through the nuclear pore in yeast for different mutant cell lines with different FG nup
24 density and cohesiveness. These yeast experiments are summarized in Figure 30, bottom.
25 However, direct comparison of the results of these independent experimental studies using
26 different methods should be undertaken with caution. Nevertheless, in spite of the wide variety of
27 cell types and experimental techniques in these studies, the size-dependence of the passive
28 permeability appeared remarkably consistent.
29

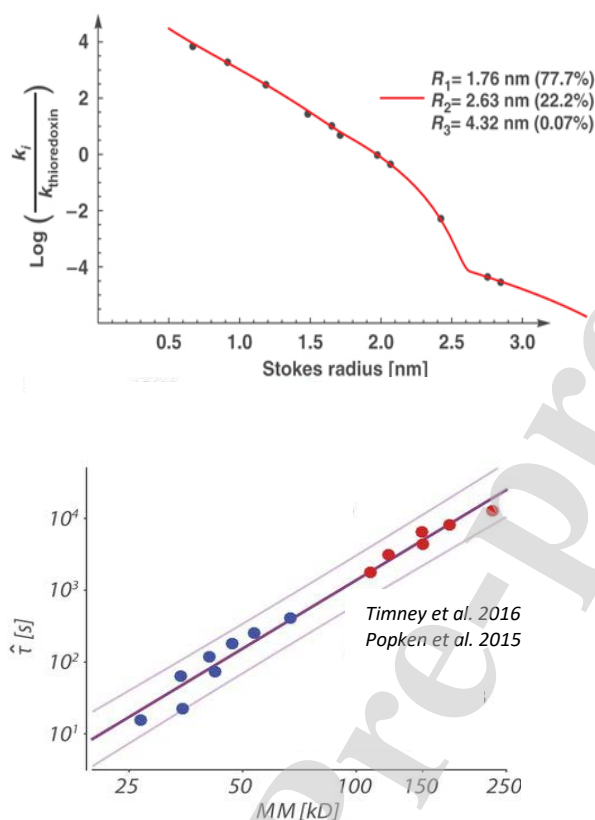


Figure 30. Transport of passive particles through the NPC. Top: Normalized kinetic constant k of cargo accumulation the nucleus as a function of the particle Stokes radius R . Red line: fit with the model of weighted diffusive fluxes through three independent fluid channels. Adapted from [77], permission pending. Bottom: inverse of the normalized kinetic constant of the neutral proteins transverse into the nucleus as a function of their molecular weight $MM \sim R^3$. Adapted from [75], permission pending.

Initially, passive fluxes of neutral particles were interpreted based on the assumption that the NPC passageway can be viewed as a collection of separate parallel liquid filled transport channels [76,77], inspired by early structural data [318].

These were superseded by theories based on the current knowledge of the physics of the FG nup assembly and kinetics transport described in the previous sections. Following the discussion of the FG nup covered nanochannels in Section 4.1.2, the experimental findings in NPCs in live cells could be interpreted in terms of the effective free energy profile that is experienced by the translocating particles. For neutral cargoes, the lack of affinity for the FG nups inside the NPC passageway results in a high (positive) effective potential barrier $U(x)$ for diffusing particles. According to equation (6) the flux in this case is proportional to

$$J \propto \frac{1}{2 + \alpha \frac{D_{out}}{RD_{in}} \int dx e^{\frac{U(x)}{k_B T}}} \simeq e^{-\frac{\Delta G}{k_B T}},$$

where $\Delta G \equiv k_B T \ln \left(\int dx e^{\frac{U(x)}{k_B T}} \right) > 0$ is a measure of the height of the free energy barrier. In this regime of barrier-limited penetration, the expression for the flux derives from the same physics as the classical Boltzmann, Arrhenius, Eyring, Polya and Kramers expression for barrier crossing rates in chemical reactions. In case of NPC, the distance along the channel axis serves as the “reaction coordinate” [25,75,319].

Both the one-bead-per-amino-acid model of Ghavami *et al.* [297] and the homopolymer model of Timney *et al.* [75] found that the free energy barrier ΔG scales with the particle radius as R^a , where $a \sim 1-2$. These observations are consistent with the theoretical estimates of the insertion cost of a neutral particle of radius R into a polymer assembly [226,320]. However, the exact scaling of the experimental results is still not fully understood due to the limited size range of the probed particles, experimental errors, and discrepancies between theory and experiments.

The transport barrier can be modulated, both in experiments and in computational models, using mutants, which are less cohesive and form a lower density of the FG nup cloud inside the pore [67,75]. As expected on theoretical grounds, the effective barrier for transport is lower in these mutants, and passive cargoes consequently exhibit higher flux. More specifically, Popken *et al.* [67] computed the FG nup density distribution in the model yeast NPC for different FG nup strains, and found an approximately linear decay of the experimental permeability with the computed average protein density in the center of the pore. Hence, the passive permeability can be related to the density and the intermolecular interactions of the FG nups in the NPC, described in Section 3.

4.2.4. Kinetics and energetics of the facilitated transport through NPCs in cells.

Here we describe how the models and concepts arising from the study of *in vitro* mimics also provide invaluable input into the analysis of facilitated/active transport in living cells.

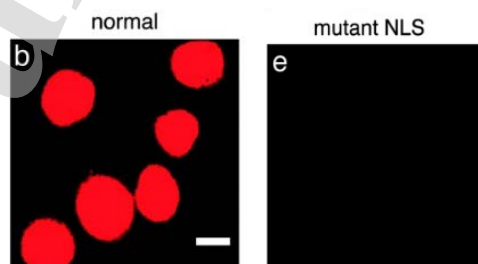
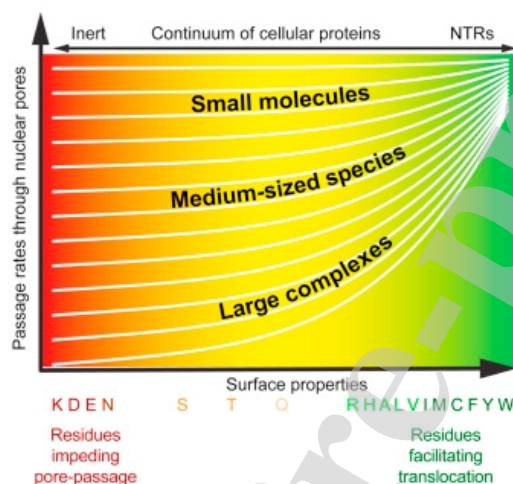


Figure 31. Illustration of a high selectivity of nuclear import. Left: nuclear accumulation of fluorescently (red) labeled cargoes possessing a NLS that enables them to bind the import proteins. Cell nuclei with accumulated cargo appear red. Right: import of

1
2
3
4 1 the same cargoes with a mutant NLS sequence that precludes their binding to transport proteins. Adapted from [78], permission
5 2 pending.

6 3 Transport through the NPC is both selective and rapid, producing fluxes of hundreds of molecules
7 4 per second per NPC [86,89]. The high specificity of the NPC is illustrated in Figure 31, which
8 5 illustrates the difference between the import of cargoes that possess a NLS (i.e., can bind transport
9 6 proteins) and cargoes with a mutation in this sequence (i.e., do not bind transport proteins).



7
8 Figure 32. Surface properties are responsible for the efficient translocation of cargoes through the NPC; see text. Reproduced
9 from [96], permission pending.

10 It has been long believed that the interactions between the transport proteins and the FG nups arise
11 predominantly from the phenylalanine binding to the hydrophobic grooves on the transport
12 proteins. However, as mentioned in Section 3.4.1 the exact number of binding sites on the
13 transport proteins is not fully known, [107,205,210,211,321]. Moreover, recent experimental work
14 has established that the permeability of the NPC with respect to various cargoes is determined not
15 only by the hydrophobic binding sites on their surface, but also by residues that form charged,
16 cation- π , and π - π interactions with the FG nups. Accordingly, artificial cargoes can be
17 engineered to tune their permeability into the NPC based on their surface properties; typically,
18 negative, hydrophobic and aromatic stacking residues promote transport, while positive residues
19 impede transport [96,97,214,233,322,323], summarized in Figure 32. This is consistent with
20 computational predictions [63] shown in Figure 33, which indicate that transport probability may
21 be tuned through the balance between hydrophobic and charged residues on the cargo surface.
22 Taken together, these experimental data and their theoretical analysis indicate that the specificity
23 of the transport protein/FG nup interaction relies on the balance of hydrophobic and charged
24 interactions.

25
26 However, these bulk measurements of fluxes do not provide information about the translocation
27 dynamics at the single-molecule level.
28

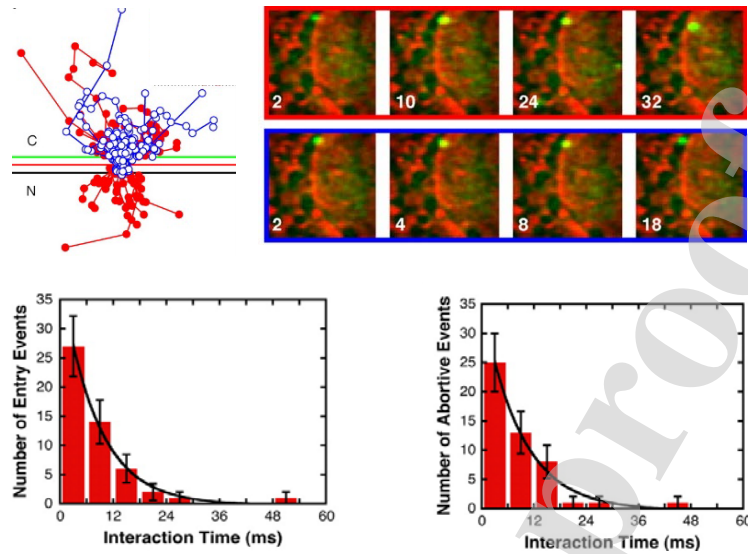


Figure 33. Single molecule studies of NPC transport. Top left: trajectories of fluorescently labeled transport protein in the vicinity of the nuclear envelope. Red: successful translocations. Blue: abortive translocation. Right top: snapshots of a movie of a successful and an abortive translocation. Bottom panel: distributions of successful (left) and abortive (right) transport events. Adapted from [78], permission pending.

First characterization of the dynamics of translocation of individual transport proteins originated from single molecule tracking in [78,324], and [81,91] (Figure 33) and established two important points. First, they directly confirmed that the translocation of transport proteins is a stochastic process, consistent with the model of thermally activated diffusion. In particular, it was observed that the translocations can be abortive whereby the transport protein returns to the cytoplasm rather than translocating into the nucleus. Second, the observed translocation times obeyed a distribution with an exponential tail, with a characteristic decay time of several milliseconds for both successful and abortive events. Notably, NPC mimics have been able to recapitulate these the durations of translocation events (Section 4.1.2), indicating that they capture the most salient features of NPC transport dynamics.

To further probe NPC transport dynamics, large cargoes have been constructed by fusing multiple proteins or using quantum dots [220,325,326]. These experiments also serve as the first step in understanding how large cargoes, such as large mRNA particles or viral capsids, navigate the NPC [12,327–329].

Musser and coworkers [220] used a large tetrameric protein complex with a total molecular weight 465 kDa, or approximately 10 nm in diameter. Each subunit carried one NLS, which allowed to load different numbers of transport proteins onto the construct and thus tune the strength of its interaction with the NPC. Using single molecule fluorescent microscopy, translocating complexes could then be tracked individually in permeabilized cell assays. This provided information about spatial densities and distributions of the accumulated cargoes in the NPC under different

1 experimental conditions, such as the presence or absence of RanGTP, including statistics of
2 successful and abortive transport events and their translocation times. The results were analyzed
3 in terms of diffusion in the effective potential model described in Section 4.1.4. The inferred
4 effective potential showed a barrier in the middle of the pore along the transport axis, and two
5 potential wells at the nuclear and the cytoplasmic “vestibules” of the NPC. When the number of
6 transport proteins attached to the cargo was increased, the barrier became lower due to stronger
7 interaction of the construct with the FG nups, in accord with the expectations. Addition of RanGTP
8 to the system increased the transport, likely caused by the reduction of the potential at the nuclear
9 vestibule. This observation is consistent with RanGTP function of catalyzing the release of the
10 cargoes from the NPC.

11
12 In a complementary approach, Weis, Liphardt and co-workers used quantum dot nanoparticles,
13 conjugated with up to ~40 transport proteins, resulting in a construct of 30-40 nm in size [325].
14 The transport and translocation of the nanoparticle through the NPC was tracked using optical
15 (fluorescence) microscopy. The quantum dot experiments are in good agreement with previous
16 experiment and also support the existence of the permeability barrier/bottleneck at the center of
17 the pore flanked by “docking” areas on the nuclear and cytoplasmic sides (see also Figure 20).

18 More recently, [326] used very large cargoes based on viral capsids that can reach up to 30 nm in
19 diameter and carry up to 100 NLS attached transport proteins. These studies support the previously
20 identified general trends - import efficiency increased with the number of transport proteins, and
21 larger cargoes required more attached proteins for efficient transport than the smaller ones.
22 Analysis of these results in terms of transport in an effective potential similar to [220] was also
23 consistent with the existence of a central free energy barrier and a cytoplasmic
24 “docking”/“vestibule” regions.

25
26 Notably, simulations of the FG nup distribution in the pore also predict higher effective potential
27 barrier for cargoes at the center of the pore, shown in Figure 34 [62,63], although the simulation
28 parameters do not fully resemble cellular conditions.

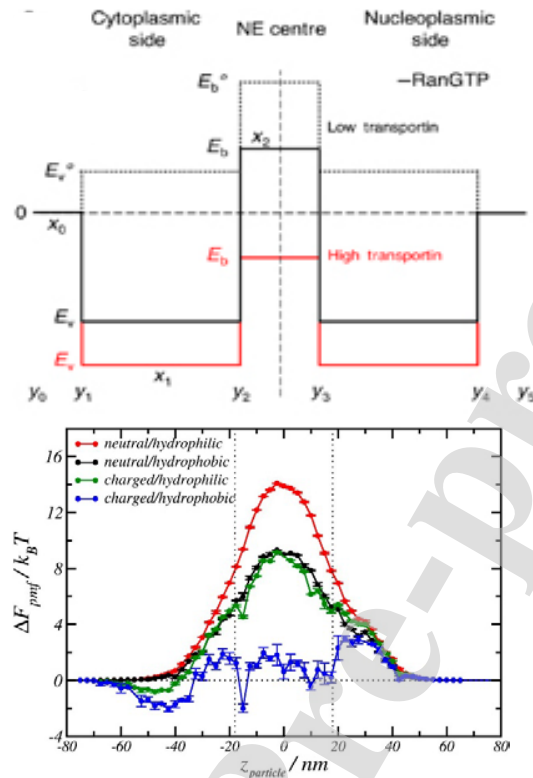


Figure 34. Inferred effective potential profiles along the axis of the NPC from single molecule trajectory tracking. Dashed lines: neutral particles. Black lines: particles with weak attraction to the FG nups. Red lines: particles with strong attraction with the FG nups. **Reproduced from** [330], **permission pending**. Bottom panel: Computational effective potential profile (pmf) along the NPC axis for particles of different surface properties. **Reproduced from** [63], **permission pending**.

Overall, *in vivo* studies support the picture arising from the *in vitro* experiments. The selectivity of the NPC transport is largely determined by the thermodynamic free energy of transport protein penetration into the FG nup assembly. This free energy defines an effective potential for diffusion inside the pore, which comprises the free energy cost of penetration due to entropic and osmotic effects, as well as the cost of breaking the cohesive interactions between the FG nups, which is balanced by the binding between the transport proteins and the FG nups.

When attempting to relate transport efficiency and speed to the molecular affinity between transport proteins and FG nups, various problems arise that require corrections to the simple picture of diffusion through an effective potential. One reason is that interactions not only determine the effective potential, but also affect the effective diffusion coefficient. Although it is still unknown how the diffusion coefficient depends on various parameters, the dynamic considerations can modulate the thermodynamic selectivity picture [52,257–262,267,268].

Initially, the short translocation times caused consternation because of the strong equilibrium effective binding affinities between the FG nup assemblies and transport proteins – sometimes

1
2
3
4 1 known as the “transport paradox” [134,206,219,331]. As explained earlier, this apparent
5 2 inconsistency can be attributed to the multivalency of the interactions between transport proteins
6 3 and FG nup and the FG nup flexibility, allowing the transport proteins to slide in a millipede-type
7 4 motion from one to another while breaking only a small number of bonds, resulting in relatively
8 5 high diffusion coefficients observed *in vitro* and *in vivo* as well as the high release rates from the
9 6 pore ends [103,134,224].
10 7

11 8 Additional factor is the potential spatial heterogeneity of the FG nup assembly in the NPC that has
12 9 been deduced from both *in vitro* and *in vivo* studies [7,36,43,100,101,173,220,332,333]. Because
13 10 the effective affinity of the transport proteins/FG nup, binding strongly depends on the local FG
14 11 nup concentration (see Section 3.4), it has been hypothesized that NPC regions with low FG nup
15 12 concentration contain a population of transport proteins with a lower effective binding affinity and
16 13 thus higher mobility, which are predominantly responsible for the fast cargo translocation through
17 14 the NPC [100,101]. Transport protein crowding might be also contributing to the resolution of the
18 15 paradox (see next section). However, full quantitative understanding of the NPC transport process
19 16 in its entirety is still lacking, and further computational and experimental work is necessary to fully
20 17 understand the mechanism of transport protein motion through the FG nup network.
21 18

22 19 3.4.2. Effects of transport protein crowding on NPC transport

23 20 Unlike the case of many other protein transporters, protein translocation through the NPC does not
24 21 occur one-by-one. Due to their affinity to the NPC interior, transport proteins tend to accumulate
25 22 within the pore, as illustrated in Figure 35, which shows enrichment of the fluorescently labeled
26 23 transport protein NTF2 within the nuclear envelope [23]. Similar accumulation can also be
27 24 observed for other transport proteins, such as Importin- β , with tens and possibly hundreds present
28 25 simultaneously in the NPC (e.g., [43]). Furthermore, NPC contains many different types of
29 26 transport proteins, and is engaged in bi-directional processes, including cargo-carrying import
30 27 proteins translocating into the nucleus, RanGTP-bound import proteins returning to the cytoplasm,
31 28 export proteins, and mRNA export particles [6,9].
32 29

33 30 While the presence of multiple transport proteins increases the NPC throughput on the one hand,
34 31 it also has a potential to block the pore. It remains to be fully understood how the NPC is able to
35 32 maintain high throughput and selective bi-directional transport under such conditions, and
36 33 different investigations provide somewhat contradictory evidence. One of the proposed solutions
37 34 has been a separation of transport pathways either through differential usage of different FG nups
38 35 types by different transport protein types, or by spatial segregation on the nanoscale
39 36 [43,44,83,100,101,173,252,253,324,334]; other mechanisms, such as dynamical switching
40 37 between export and import, have been proposed as well [281]. However, a consensus picture is
41 38 still lacking, with a number of controversies and discrepancies arising from different experiments.
42 39 We briefly summarize the current state of the art.
43 40
44 41

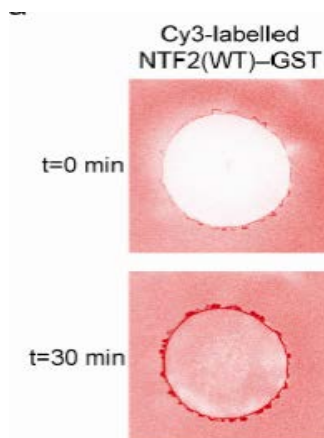


Figure 35. Accumulation of transport protein NTF2 in the nuclear envelope. Top: cell nucleus (white) surrounded by fluorescently labeled transport protein NTF2 in the cytoplasm. Bottom: after 30 minutes, significant fraction of the transport proteins accumulates in the NPCs at the nuclear envelope, as indicated by the bright red rim. Adapted from [23], permission pending.

Using permeabilized cells, single-molecule tracking showed that the transport efficiency and the speed of translocation of the transport protein Importin- β increases with increasing its concentration [324]. This counter-intuitive finding is at odds with the predictions of minimal theoretical models based on the exclusion process theory [281]. It is in line, however, with *in vitro* experiments on colloids that were engineered to carry transport proteins on their surface. On planar assemblies of FG nups, the two-dimensional mobility of these colloids was strongly dependent on the presence of free transport proteins in solution: by competitive binding to the FG nups, these free transport proteins reduced the number of accessible binding sites for the colloids and therefore effectively reduced their binding to the FG nup assembly and thus increasing the mobility [172].

With respect to the effects of the different types of translocating molecules on each other, the evidence is also still controversial. The presence of the transport proteins has been shown to reinforce the permeability barrier created by the FG nups towards neutral cargoes [23,43,83], consistent with the theoretical notions of Section 4.1.2.1. In particular, ref. [43] showed that an increase in the concentration of Importin- β decreased the passive transport of GFP monomers, dimers and trimers; this effect could be significantly modulated by the presence or absence of RanGTP in accord with its function as a catalyst of transport protein unbinding from the FG nups. On the other hand, previous studies [252,253] showed that passive cargoes (dextrans) do not significantly affect the translocation of BSA-NLS cargo facilitated by transport proteins. Similarly, earlier work indicates that two different transport proteins (Importin- β and Transportin) interact with different domains of the nuclear basket FG nup Nup153 [335]. The results were interpreted as the “uncoupling” between the passive and facilitated modes of transport. The pathway separation hypothesis is also supported by super-resolution measurements of the trajectories and

1
2
3
4 1 distributions of passive and facilitated transport pathways [44], but these results have been
5 2 criticized on technical grounds [92,336].
6 3

7 3
8 4 Although the precise nanoscale picture of the NPC is still incomplete, it is clear that both FG nups
9 5 and transport proteins (and potentially RanGTP) need to work together to achieve the unique
10 6 transport properties that characterize the NPC. Further combination of experimental, theoretical
11 7 and computational approaches is necessary. The progress in this area will have impact on the
12 8 understanding of other non-equilibrium spatially inhomogeneous nanoscale systems, such as
13 9 liquid droplets and other aggregates in the cell [159,160], as well as artificial composite
14 10 nanomaterials [337,338].
15 11

12 12 4.3. Nucleo-cytoplasmic transport cycle as a pump 13 13

14 14 In the previous sections, we have focused on the biophysical characterization of the assemblies of
15 15 the disordered proteins in the NPC, and on how their interactions with the transport proteins dictate
16 16 the dynamics of translocation of protein-transport complexes through the NPC channel, and thus
17 17 the transport efficiency and selectivity.
18 18

19 19 Although the translocation of transport proteins through the NPC is a key step in nucleo-
20 20 cytoplasmic transport, it is only one component in the transport cycle. In its entirety, a complete
21 21 transport cycle acts as an energy-driven pump that can generate import and export fluxes against
22 22 concentration gradients, and maintain the system in a non-equilibrium steady state. In this section
23 23 we discuss the current understanding of the biophysics, energetics and main principles of operation
24 24 of the active cycle of the nucleo-cytoplasmic transport machinery.
25 25

26 26 Overall, the directionality of the transport cycle relies on the consumption of GTP and on the
27 27 asymmetry in the nucleo-cytoplasmic partitioning of the protein Ran, with its RanGDP form being
28 28 abundant in the cytoplasm and its RanGTP form being abundant in the nucleus. This asymmetric
29 29 distribution of Ran relies on the asymmetric distribution of RanGAP and RanGEF, two factors
30 30 responsible for GTP hydrolysis in the cytoplasm and GDP-to-GTP exchange in the nucleus,
31 31 respectively [5,339]. The complete nucleo-cytoplasmic exchange cycle comprises three inter-
32 32 linked loops, shown Figure 36. These loops are the import cycle, the export cycle, and the
33 33 NTF2/Ran cycle that is responsible for recycling of RanGDP into the nucleus and for the
34 34 maintenance of the RanGTP/GTP gradient.
35 35

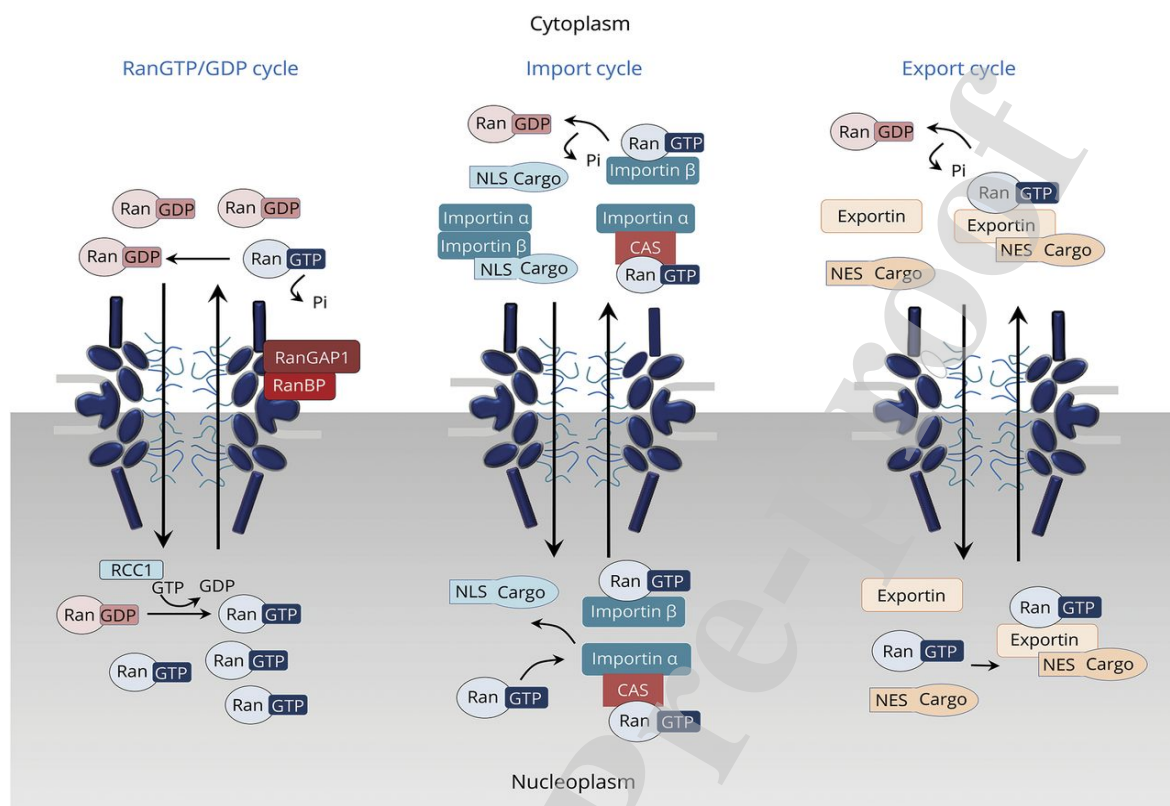
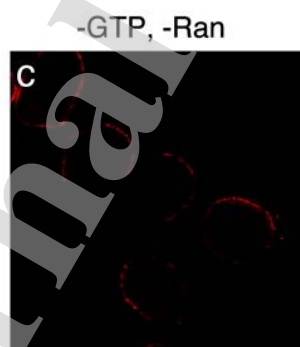


Figure 36. Full scheme of the nucleo-cytoplasmic transport pathways for Importin- β , including various adaptor molecules such as Importin- α , CAS and RanBP. For illustrative purposes, the various reactions are indicated by uni-directional arrows, corresponding to the “normal” operational cycle of the NPC. However, all these reactions are reversible, with the exception of the GTP hydrolysis, which is catalyzed by RanGAP in the cytoplasm and can be considered irreversible for all practical purposes. The irreversibility of GTP hydrolysis defines the directionality of the whole cycle, as indicated by the arrows in this figure. Reproduced from [339], permission pending.

The details of the import cycle and the Ran/NTF2 cycle are described in Section 2. The export cycle is similar to the import cycle, as shown in Figure 36. In the nucleus, export-specialized transport proteins (collectively known as Exportins) bind the export cargo through the Nuclear Export Sequence (NES), analogous to the NLS for import. However, unlike the import complexes, the export complexes also contain RanGTP bound to an Exportin. Upon translocation of the export complex to the cytoplasm, RanGTP is hydrolyzed by RanGAP, releasing the export cargo and the resulting RanGDP from the Exportin. It is crucial to emphasize that, with the exception of RanGTP hydrolysis, all the other reactions in the nucleo-cytoplasmic transport cycle are thermodynamically reversible [6,85,340]. It has also been shown that the accumulation gradient of certain cargoes can be reversed by reversing the gradient of RanGTP between the nucleus and the cytoplasm [341].

1
2
3
4 1 Figure 37 illustrates the generation of the non-equilibrium steady state concentration difference
5 2 between the nucleus and the cytoplasm by the nucleo-cytoplasmic transport “pump”. Cargo with
6 3 a nuclear localization sequence accumulates in the nucleus, but such accumulation does not occur
7 4 in the absence of GTP and Ran.
8
9

10 5
11 6 Notably, viewed as an import machine, the NPC operational cycle is not very efficient.
12 7 Experimentally measured ratios of nuclear and cytoplasmic concentrations of import cargoes are
13 8 in the range of $\frac{C_n}{C_c} \approx 10 - 30$ [85,86,340,342]. Under steady state conditions, this implies that
14 9 translocation of one cargo molecule across the nuclear envelope translates into a free energy
15 10 increase of approximately by $\Delta\mu = k_B T \ln(C_n/C_c) \approx 3 k_B T$ [90]. However, every translocation
16 11 requires hydrolysis of one GTP molecule (or an additional GTP molecule for the re-export of the
17 12 Importin- α adaptor), generating approximately $20 k_B T$ of energy [256], seven times more than
18 13 required to transport one cargo against the typical concentration gradient. This makes NPC import
19 14 rather inefficient compared with other bio-molecular machines, such as the sodium/potassium
20 15 pump or the bacterial flagellar motor that can harness almost all of the energy gained by ATP/GTP
21 16 hydrolysis towards the creation of a non-equilibrium concentration gradient or towards mechanical
22 17 work [90,343]. These observations come with the caveat that most of these concentration estimates
23 18 are based on measurements with artificial cargoes, such as GFP. These artificial cargoes do not
24 19 have a function in the nucleus, (e.g., binding to the DNA), and may therefore remain free to leak
25 20 back due to excess accumulation in the nucleus [85,344].
26
27
28
29
30
31
32
33
34
35
36
37
38
39
40
41
42
43
44
45
46
47
48
49
50
51
52
53
54
55
56
57
58
59
60
61
62
63
64
65



22
23 *Figure 37. Energy dependence of Nuclear Import. In the absence of GTP and Ran, the cargo reaches the nuclear envelope but*
24 *does not accumulate inside the nucleus. For comparison with normal import see Figure 31. Adapted from [78], permission*
25 *pending.*

26
27 Given the low efficiency of the transport cycle, it is possible that the import-export system is
28 simply hitch-hiking on the RanGTP/GDP de-mixing cycle, which has other important roles, such
29 as nucleosome positioning during cell division [340,345], and therefore is not necessarily
30 optimized to facilitate cargo de-mixing between the nucleus and the cytoplasm. This point of view,
31 which defines the “futile cycle” [346] of RanGTP/RanGDP conversion as a primary driver of the

1 nucleocytoplasmic transport cycle, has been useful in conceptualizing the principles of
2 nucleocytoplasmic de-mixing using the methods of non-equilibrium thermodynamics [347].

3
4 In principle, all the reactions involved in the nucleocytoplasmic exchange can be computationally
5 described with appropriate rate equations, but understanding of the full picture remains
6 complicated due to the large number of various molecular complexes involved. Therefore, the
7 predictions remain sensitive to the choice of parameters and assumptions, and are often at variance
8 with each other, both on the computational and experimental fronts [86,87,340,342,344,347–350].
9 All these experimental and computational studies mostly agree that the initial accumulation of
10 import cargo in the nucleus follows simple first order kinetics, and the initial accumulation
11 rate/flux is linearly proportional to the cargo concentration in the cytoplasm. On the other hand,
12 the various studies are less consistent about the saturation levels that are reached when the influx
13 of the cargo is balanced by the outflux. [340,344,349,350]

14
15 Similar uncertainty remains on how the relative concentrations of cargo in nucleus and cytoplasm
16 depend on the numbers of transport proteins, Ran, RanGAP/GEF and various other adapter
17 proteins in the cell. Timney *et al.* [86] found that the nucleo-cytoplasmic concentration ratio
18 increases with cytoplasmic concentration of the transport proteins, while Elbaum and coworkers
19 predict a non-monotonic function of the transport protein concentration [347,350]. Finally,
20 Riddick and Macara observed that the import rate is decreasing with the concentration of Importin-
21 β (due to the depletion of RanGTP), although the connection between the initial accumulation rate
22 and the relative concentrations at saturation is non-trivial [87,342]. It has also been shown that the
23 competition of the transport proteins for different cargoes might be important [344,349,350]

24
25 It is likely that different behaviors are observed in various regimes depending on relative
26 concentrations of individual components of the nucleocytoplasmic transport cycle. One can
27 speculate that the wide range of observed behaviors might endow the NPC transport with
28 additional flexibility, so that its function can be modulated in different conditions, such as different
29 stages of the cell cycle.

30 31 5. Conclusions and Discussion

32
33 NPC is a vital biological machine that regulates transport and communication between the cell
34 nucleus and the cytoplasm. The mechanism of its operation presents several physical puzzles,
35 among them its ability to rapidly, and yet selectively, simultaneously translocate many
36 macromolecules through a disordered, crowded and confined medium. Despite its enormous
37 complexity, theoretical and experimental physics approaches have been crucial in elucidating the
38 properties of NPC components, its internal spatial organization and the dynamics of transport.
39 These physical approaches, combined with the increasingly detailed picture of its biochemical and

1 structural aspects, have started to converge to unified physical principles of NPC organization and
2 transport, some of which have been successfully recapitulated in artificial nanochannel mimics of
3 the NPC. At the same time, these studies of the NPC have revealed and highlighted a rich set of
4 underlying physical behaviors that connect the NPC research to a wide range of areas of physics,
5 including collective polymer behavior in confinement, phase-separation in nano-confinement,
6 specificity of multivalent interactions, and crowding effects in stochastic nano-scale transport.

7
8 Several main questions have captivated the attention of the field in the past decade, and have
9 benefitted from physical approaches:

- 10
11 • What determines the ability of the NPC to combine high thermodynamic
12 specificity/selectivity with high rapidity and throughput in the steady fluctuating and multi-
13 species environment of the cell?
- 14 • What are the main biophysical properties of the intrinsically disordered components (FG
15 nups) of the NPC?
- 16 • What is the spatial organization of the assembly of polymer-like FG nups within the NPC?
- 17 • How do the collective dynamics and multivalent interactions of the transported molecules
18 and these intrinsically disordered heteropolymers answer the first question?

19
20 The intrinsically disordered proteins lining the NPC channel (known as FG nups) are the central
21 component of the NPC transport mechanism. They serve a twofold role of 1) providing the target
22 for the transport protein binding and shuttling through the NPC, and 2) providing a permeability
23 barrier for the excluded cargoes. The exact biophysical properties of the FG nups and their
24 assemblies have been a subject of intense controversy, in particular about the respective
25 importance of polymer-chain entropy on the one hand, and cohesiveness or even gelation, on the
26 other, in establishing the transport barrier. In the main, the research of the past decade has shown
27 that the behavior of individual FG nups and their assemblies can be well understood in terms of
28 physics of moderately cohesive polymers, and is well described by theoretical and computational
29 models of varying degrees of coarse-graining. In particular, interactions between the FG nup
30 chains often result in formation of condensed phases *in vitro*, whose morphology may be different
31 in different geometries (bulk phases, surface grafted layers and nanochannels). This has been
32 described in Sections 3.1-3.3. In actual NPCs, however, descriptions of the FG nup phase
33 behavior will also need to take into account the presence of cargo-carrying transport proteins.

34
35 The second crucial feature of the NPC transport is the transient multivalent binding of these
36 transport proteins to the FG nup assembly within the NPC, which plays a central role in the
37 selectivity of the NPC transport. While one-to-one intermolecular affinities are weak among the
38 FG nups themselves and between individual FG motifs and transport proteins, multivalency
39 facilitates high thermodynamic partitioning of transport proteins into FG nup assemblies, thus
40 creating the basis for strongly selective transport. Overall, the equilibrium permeability of the FG

1 nup assembly towards the transport proteins arises from the balance between, on one hand, the free
2 energy cost of insertion, which combines osmotic, entropic and steric effects, and, on the other
3 hand, the free energy gain arising predominantly from the attractive interactions of the transport
4 proteins with the FG nups. Thus, whereas larger inert molecules face a free energy barrier to cross
5 FG nup assemblies of the NPC, transport proteins face one or more free energy wells across the
6 NPC allowing their penetration and eventual translocation through the NPC. Minimal physical
7 models have succeeded in semi-quantitatively replicated data from *in vitro* experimental assays of
8 FG nup assemblies with transport proteins, including differences in the selective penetration by
9 transport proteins and inert molecules. These topics have been covered in Sections 3.4-3.5. These,
10 insights, obtained mostly from the studies of equilibrium or non-equilibrium steady state
11 assemblies, potentially can be modified under conditions of direct energy input through GTP
12 hydrolysis in the active cycle of the NPC.

13
14 In addition to the thermodynamics of transport protein partitioning into the NPC, kinetics of their
15 translocation is another crucial factor in determining NPC selectivity, speed and throughput. At
16 the molecular scale, the translocation of the multivalent transport proteins through the spatially
17 inhomogeneous polymer assembly of FG nups within the NPC passageway is a complex process,
18 which is still incompletely understood. However, multivalency of transport protein/FG nup
19 interactions and the flexibility of the FG nups are likely to play important roles here as well. Their
20 combination enables apparently strong thermodynamic binding and partitioning without inhibiting
21 the lateral “millipede” (or “slide-and-exchange”) – like motion of the particle through the FG nup
22 assembly that allows the transport proteins to rapidly translocate and exit from the NPC. These
23 topics have been covered in Sections 4.1-4.2

24
25 Remarkably, much can be understood about the NPC transport mechanism even in the absence of
26 a complete picture of the microscopic motion. The dynamics of particle translocation through the
27 NPC can be viewed as a thermally activated diffusive transport in an effective free energy profile,
28 determined, the interactions between the transport proteins and the FG nups, by the local density
29 of the FG nups and their local cohesiveness. Transport proteins, experiencing an attractive
30 effective potential profile, dwell longer within the NPC, increasing the likelihood of successful
31 translocation events and increasing the total particle flux rate. This mechanism has been known in
32 many contexts as “facilitated diffusion”.

33
34 Overall, the selectivity of the NPC (and other similar nanochannels) arises from the balance of two
35 opposing effects: attractive interaction with the pore enhances the flux through the pore at
36 moderate interaction strengths and low concentrations, while stronger interactions and higher
37 concentrations can block the transport. Importantly, accumulation of the transport proteins in the
38 pore can also impede the translocation of inert molecules, thus further enhancing the transport
39 selectivity in the presence of non-specific competitors. Theoretical, computational and
40 experimental models based on these ideas, implemented and studied through a variety of

1 computational and experimental techniques, successfully capture the dynamics of transport in *in*
2 *vitro* nanopore NPC mimics and other selective nanochannels. Remarkably, these ideas work well
3 even for very large cargoes whose size approaches the inner diameter of the NPC channel.

4
5 The robust nature of the physical concepts underlying the principles of the NPC transport might
6 also explain the robustness of its transport mechanism with respect to structural perturbations, as
7 well as its high conservation among different species, despite substantial evolutionary divergence
8 of its molecular components. On the other hand, the precise aspects of transport can be modulated
9 via specific chemical modifications, such as glycosylation or phosphorylation of the FG nups,
10 further enhancing its flexibility and adaptability to various cellular conditions.

11
12 While much of this review and much of biophysical research in the past decade has focused on the
13 properties of FG nup assemblies and the thermally activated diffusion of the transport proteins
14 through the NPC channel, it should be emphasized that the NPC is only a part of a more extensive
15 nucleo-cytoplasmic transport cycle. This cycle operates as an active thermodynamic pump,
16 powered by GTP hydrolysis and relying on the nucleo-cytoplasmic asymmetry in the distribution
17 of certain enzymes. Only few studies have attempted to tackle this problem so far. Although in
18 general it can be thought of as a very large chemical reaction network, we currently lack
19 understanding on the coupling between the kinetics, energy consumption and the structural and
20 dynamic properties of the NPC. Such understanding will be of paramount importance when
21 considering the NPC in a wider biological and biomedical context and its function in various health
22 and disease processes. This topic has been covered in Section 5.

23
24 The overall conceptual physical understanding has reached the stage that it can be applied to
25 outstanding specific biological and biomedical problems such as involvement of the NPC in
26 cancer, neurodegenerative diseases, gene regulation and device fabrication inspired by the NPC
27 for selective sensing, sorting and transport of macromolecules. However, with the field converging
28 to an overall consensus about how molecular properties and physical concepts translate into the
29 functional behavior of the NPC, several open questions remain. A full quantitative understanding
30 of how transport through the NPC is affected by various forms of crowding, caused by different
31 types of cargo-bound and free transport proteins moving into and out of the nucleus cargoes, is
32 still lacking. Another equally important subject that has yet received only minimal attention from
33 the physics perspective is mRNA export - a crucially important topic from the biological and
34 biomedical perspectives. Other effects such as the mechanics of potential conformational changes
35 of the NPC structural scaffold during transport have also not been covered in this review [351,352].
36 These subjects are likely to be areas of exciting new discoveries in the future.

37
38 Finally, the quest for understanding NPC function has motivated and inspired a range of physical
39 questions and models. Such models are now ready for further in-depth analysis of questions related
40 to equilibrium and non-equilibrium thermodynamics and kinetics at the nano-scale. The NPC may

1
2
3
4 1 thus provide a fruitful venue for understanding the coupling of nano-mechanics, fluctuations and
5 2 chemical reactions.
6
7 3

8
9 4 **Acknowledgement** . The authors express deep gratitude to all the colleagues in the field for
10 5 numerous illuminating discussions, and apologize in advance for any potential omissions. We also
11 6 thank Aritra Chowdhury and Tom Scheidt for their input into this work, Tiantian Zheng for
12 7 comments on the manuscript, and the anonymous reviewer for incisive comments. BWH
13 8 acknowledges funding from UK BBSRC (BB/J014567/1) and EPSRC (EP/L015277/1;
14 9 EP/L504889/1). LH acknowledges funding from NIH R35 GM119755 and NSF 1943488. RYHL
15 10 acknowledges support from the Swiss National Science Foundation, the Biozentrum and
16 11 the Swiss Nanoscience Institute. PRO acknowledges funding from the Zernike Institute for
17 12 Advanced Materials (University of Groningen) and the Dutch Research Council (NWO). AZ
18 13 acknowledges the support from the National Science and Engineering Research Council of Canada
19 14 (NSERC) through Discovery Grant RGPIN-2016-06591. EAL acknowledges funding from
20 15 SMPFv2.0, as well as SFB1129 and SPP2191 of the Deutsche Forschungsgemeinschaft (DFG).
21 16 AZ and BWH acknowledge joint funding from the UCL-University of Toronto Strategic Partner
22 17 Fund.
23 18
24 19
25 20
26 21
27
28
29
30
31
32
33
34
35
36
37
38
39
40
41
42
43
44
45
46
47
48
49
50
51
52
53
54
55
56
57
58
59
60
61
62
63
64
65

1
2
3
4
5 **References**
6
7
8
9
10
11
12
13
14
15
16
17
18
19
20
21
22
23
24
25
26
27
28
29
30
31
32
33
34
35
36
37
38
39
40
41
42
43
44
45
46
47
48
49
50
51
52
53
54
55
56
57
58
59
60
61
62
63
64
65

- [1] B. Alberts et al., *Molecular Biology of the Cell*, 4th edition, Garland Science, New York, 2002. <https://www.ncbi.nlm.nih.gov/books/NBK21054/> (accessed November 4, 2020).
- [2] B. Mans, V. Anantharaman, L. Aravind, E. V. Koonin, *Comparative Genomics, Evolution and Origins of the Nuclear Envelope and Nuclear Pore Complex, Cell Cycle*. 3 (2004) 1625–1650. doi:10.4161/cc.3.12.1316.
- [3] M.C. Field, M.P. Rout, Pore timing: the evolutionary origins of the nucleus and nuclear pore complex., *F1000Research*. 8 (2019). doi:10.12688/f1000research.16402.1.
- [4] J.M. Berg, J.L. Tymoczko, L. Stryer, L. Stryer, *Biochemistry*, W.H. Freeman, 2002.
- [5] B. Cautain, R. Hill, N. de Pedro, W. Link, Components and regulation of nuclear transport processes, *FEBS J*. 282 (2015) 445–462. doi:10.1111/febs.13163.
- [6] T. Jovanovic-Talisman, A. Zilman, Protein Transport by the Nuclear Pore Complex: Simple Biophysics of a Complex Biomachine, *Biophys. J*. 113 (2017) 6–14. doi:10.1016/j.bpj.2017.05.024.
- [7] S.J. Kim, J. Fernandez-Martinez, I. Nudelman, Y. Shi, W. Zhang, B. Raveh, T. Herricks, B.D. Slaughter, J.A. Hogan, P. Upla, I.E. Chemmama, R. Pellarin, I. Echeverria, M. Shivaraju, A.S. Chaudhury, J. Wang, R. Williams, J.R. Unruh, C.H. Greenberg, E.Y. Jacobs, Z. Yu, M.J. de la Cruz, R. Mironska, D.L. Stokes, J.D. Aitchison, M.F. Jarrold, J.L. Gerton, S.J. Ludtke, C.W. Akey, B.T. Chait, A. Sali, M.P. Rout, Integrative structure and functional anatomy of a nuclear pore complex, *Nature*. 555 (2018) 475–482. doi:10.1038/nature26003.
- [8] A. Hoelz, E.W. Debler, G. Blobel, The Structure of the Nuclear Pore Complex, *Annu. Rev. Biochem.* 80 (2011) 613–643. doi:10.1146/annurev-biochem-060109-151030.
- [9] J.D. Aitchison, M.P. Rout, The yeast nuclear pore complex and transport through it, *Genetics*. 190 (2012) a000562.
- [10] A. Dickmanns, R.H. Kehlenbach, B. Fahrenkrog, Nuclear Pore Complexes and Nucleocytoplasmic Transport: From Structure to Function to Disease, *Int. Rev. Cell Mol. Biol.* (2015). doi:10.1016/bs.ircmb.2015.07.010.
- [11] H.J. Kim, J.P. Taylor, Lost in Transportation: Nucleocytoplasmic Transport Defects in ALS and Other Neurodegenerative Diseases, *Neuron*. 96 (2017) 285–297. doi:10.1016/j.neuron.2017.07.029.
- [12] A.A. Labokha, A. Fassati, Viruses Challenge Selectivity Barrier of Nuclear Pores., *Viruses*. 5 (2013) 2410–2423. doi:10.3390/v5102410.
- [13] K.H. Chow, R.E. Factor, K.S. Ullman, The nuclear envelope environment and its cancer connections, *Nat. Rev. Cancer*. 12 (2012) 196–209. doi:10.1038/nrc3219.
- [14] D.N. Simon, M.P. Rout, Cancer and the Nuclear Pore Complex, in: Springer, New York, NY, 2014: pp. 285–307. doi:10.1007/978-1-4899-8032-8_13.
- [15] E.J. Tran, M.C. King, A.H. Corbett, Macromolecular transport between the nucleus and the cytoplasm: Advances in mechanism and emerging links to disease., *Biochim. Biophys. Acta*. 1843 (2014) 2784–2795. doi:10.1016/j.bbamcr.2014.08.003.
- [16] A.H. Lang, H. Li, J.J. Collins, P. Mehta, J. Gong, Epigenetic Landscapes Explain Partially Reprogrammed Cells and Identify Key Reprogramming Genes, *PLoS Comput. Biol.* 10 (2014) e1003734. doi:10.1371/journal.pcbi.1003734.
- [17] A. Mor, M.A. White, B.M.A. Fontoura, Nuclear trafficking in health and disease., *Curr. Opin. Cell Biol.* 28 (2014) 28–35. doi:10.1016/j.ceb.2014.01.007.

- 1
2
3
4 1 [18] J.A. DeGrasse, K.N. DuBois, D. Devos, T.N. Siegel, A. Sali, M.C. Field, M.P. Rout, B.T.
5 2 Chait, Evidence for a shared nuclear pore complex architecture that is conserved from the
6 3 last common eukaryotic ancestor., *Mol. Cell. Proteomics*. 8 (2009) 2119–30.
7 4 doi:10.1074/mcp.M900038-MCP200.
8 5 [19] A. Ori, N. Banterle, M. Iskar, A. Andrés-Pons, C. Escher, H. Khanh Bui, L. Sparks, V.
9 6 Solis-Mezarino, O. Rinner, P. Bork, E.A. Lemke, M. Beck, Cell type-specific nuclear
10 7 pores: a case in point for context-dependent stoichiometry of molecular machines., *Mol.*
11 8 *Syst. Biol.* 9 (2013) 648. doi:10.1038/msb.2013.4.
12 9 [20] R. Hayama, M.P. Rout, J. Fernandez-Martinez, The nuclear pore complex core scaffold
13 10 and permeability barrier: variations of a common theme Introduction: the nuclear pore
14 11 complex and nuclear transport, *Curr. Opin. Cell Biol.* 46 (2017) 110–118.
15 12 doi:10.1016/j.ceb.2017.05.003.
16 13 [21] Y. Shav-Tal, T. Tripathi, Yeast and Human Nuclear Pore Complexes: Not So Similar
17 14 After All, *Trends Cell Biol.* 28 (2018) 589–591. doi:10.1016/j.TCB.2018.06.004.
18 15 [22] G. Holzer, W. Antonin, Nuclear Pore Complexes: Global Conservation and Local
19 16 Variation, *Curr. Biol.* 28 (2018) R674–R677. doi:10.1016/j.cub.2018.04.032.
20 17 [23] T. Jovanovic-Talisman, J. Tetenbaum-Novatt, A.S. McKenney, A. Zilman, R. Peters, M.P.
21 18 Rout, B.T. Chait, Artificial nanopores that mimic the transport selectivity of the nuclear
22 19 pore complex, *Nature*. 457 (2009) 1023–1027. doi:10.1038/nature07600.
23 20 [24] P. Ketterer, A.N. Ananth, D.S. Laman Trip, A. Mishra, E. Bertosin, M. Ganji, J. van der
24 21 Torre, P. Onck, H. Dietz, C. Dekker, DNA origami scaffold for studying intrinsically
25 22 disordered proteins of the nuclear pore complex, *Nat. Commun.* 9 (2018) 902.
26 23 doi:10.1038/s41467-018-03313-w.
27 24 [25] A.N. Ananth, A. Mishra, S. Frey, A. Dwarkasing, R. Versloot, E. van der Giessen, D. Gö
28 25 rlich, P. Onck, C. Dekker, Spatial structure of disordered proteins dictates conductance
29 26 and selectivity in nuclear pore complex mimics, (2018). doi:10.7554/eLife.31510.001.
30 27 [26] S.W.W. Kowalczyk, L. Kapinos, T.R.R. Blosser, T. Magalhães, P. van Nies, R.Y.H.Y.H.
31 28 Lim, C. Dekker, Single-molecule transport across an individual biomimetic nuclear pore
32 29 complex, *Nat. Nanotechnol.* 6 (2011) 433–438. doi:10.1038/nnano.2011.88.
33 30 [27] Y. Caspi, D. Zbaida, H. Cohen, M. Elbaum, Synthetic Mimic of Selective Transport
34 31 Through the Nuclear Pore Complex, *Nano Lett.* 8 (2008) 3728–3734.
35 32 [28] P.D.E. Fisher, Q. Shen, B. Akpınar, L.K. Davis, K.K.H. Chung, D. Baddeley, A. Šarić,
36 33 T.J. Melia, B.W. Hoogenboom, C. Lin, C.P. Lusk, A Programmable DNA Origami
37 34 Platform for Organizing Intrinsically Disordered Nucleoporins within Nanopore
38 35 Confinement, *ACS Nano*. 12 (2018) 1508–1518. doi:10.1021/acsnano.7b08044.
39 36 [29] M.P. Rout, G. Blobel, Isolation of the yeast nuclear pore complex, *J. Cell Biol.* 123 (1993)
40 37 771–783. doi:10.1083/jcb.123.4.771.
41 38 [30] R. Reichelt, A. Holzenburg, E.L. Buhle, M. Jarnik, A. Engel, U. Aebi, Correlation
42 39 between structure and mass distribution of the nuclear pore complex and of distinct pore
43 40 complex components, *J. Cell Biol.* 110 (1990) 883–894. doi:10.1083/jcb.110.4.883.
44 41 [31] M. Beck, E. Hurt, The nuclear pore complex: understanding its function through structural
45 42 insight, *Nat. Rev. Mol. Cell Biol.* 18 (2017) 73–89. doi:10.1038/nrm.2016.147.
46 43 [32] A. Hoelz, J.S. Glavy, M. Beck, Toward the atomic structure of the nuclear pore complex:
47 44 when top down meets bottom up, *Nat. Struct. Mol. Biol.* 23 (2016) 624–630.
48 45 doi:10.1038/nsmb.3244.
49 46 [33] M. Eibauer, M. Pellanda, Y. Turgay, A. Dubrovsky, A. Wild, O. Medalia, Structure and
50
51
52
53
54
55
56
57
58
59
60
61
62
63
64
65

- gating of the nuclear pore complex., *Nat. Commun.* 6 (2015) 7532.
doi:10.1038/ncomms8532.
- [34] A. von Appen, J. Kosinski, L. Sparks, A. Ori, A.L. DiGuilio, B. Vollmer, M.-T. Mackmull, N. Banterle, L. Parca, P. Kastritis, K. Buczak, S. Mosalaganti, W. Hagen, A. Andres-Pons, E. Lemke, P. Bork, W. Antonin, J.S. Glavy, K.H. Bui, M. Beck, In situ structural analysis of the human nuclear pore complex, *Nature*. 526 (2015) 140–143. doi:10.1038/nature15381.
- [35] D.H. Lin, T. Stuwe, S. Schilbach, E.J. Rundlet, T. Perriches, G. Mobbs, Y. Fan, K. Thierbach, F.M. Huber, L.N. Collins, A.M. Davenport, Y.E. Jeon, A. Hoelz, Architecture of the symmetric core of the nuclear pore., *Science*. 352 (2016) aaf1015. doi:10.1126/science.aaf1015.
- [36] F. Alber, S. Dokudovskaya, L.M. Veenhoff, W. Zhang, J. Kipper, D. Devos, A. Suprpto, O. Karni-Schmidt, R. Williams, B.T. Chait, The molecular architecture of the nuclear pore complex, *Nature*. 450 (2007) 695–701.
- [37] E.A. Lemke, The Multiple Faces of Disordered Nucleoporins, *J. Mol. Biol.* 428 (2016) 2011–2024. doi:10.1016/J.JMB.2016.01.002.
- [38] M. Macossay-Castillo, G. Marvelli, M. Guharoy, A. Jain, D. Kihara, P. Tompa, S.J. Wodak, The Balancing Act of Intrinsically Disordered Proteins: Enabling Functional Diversity while Minimizing Promiscuity, *J. Mol. Biol.* 431 (2019) 1650–1670. doi:10.1016/J.JMB.2019.03.008.
- [39] R. van der Lee, M. Buljan, B. Lang, R.J. Weatheritt, G.W. Daughdrill, A.K. Dunker, M. Fuxreiter, J. Gough, J. Gsponer, D.T. Jones, P.M. Kim, R.W. Kriwacki, C.J. Oldfield, R. V Pappu, P. Tompa, V.N. Uversky, P.E. Wright, M.M. Babu, Classification of intrinsically disordered regions and proteins., *Chem. Rev.* 114 (2014) 6589–631. doi:10.1021/cr400525m.
- [40] D.P. Denning, S.S. Patel, V. Uversky, A.L. Fink, M. Rexach, Disorder in the nuclear pore complex: the FG repeat regions of nucleoporins are natively unfolded, *Proc. Natl. Acad. Sci.* 100 (2003) 2450–2455. doi:10.1073/pnas.0437902100.
- [41] S.S. Patel, B.J. Belmont, J.M. Sante, M.F. Rexach, Natively unfolded nucleoporins gate protein diffusion across the nuclear pore complex, *Cell*. 129 (2007) 83–96.
- [42] Y. Sakiyama, A. Mazur, L.E. Kapinos, R.Y.H. Lim, Spatiotemporal dynamics of the nuclear pore complex transport barrier resolved by high-speed atomic force microscopy, *Nat. Nanotechnol.* 11 (2016) 719–723. doi:10.1038/nnano.2016.62.
- [43] A.R. Lowe, J.H. Tang, J. Yassif, M. Graf, W.Y.C. Huang, J.T. Groves, K. Weis, J.T. Liphardt, Importin- β modulates the permeability of the nuclear pore complex in a Ran-dependent manner., *Elife*. 4 (2015) e04052. doi:10.7554/eLife.04052.
- [44] J. Ma, A. Goryaynov, W. Yang, Super-resolution 3D tomography of interactions and competition in the nuclear pore complex, *Nat. Struct. Mol. Biol.* 23 (2016) 239–247. doi:10.1038/nsmb.3174.
- [45] A. Bestembayeva, A. Kramer, A.A. Labokha, D. Osmanović, I. Liashkovich, E. V Orlova, I.J. Ford, G. Charras, A. Fassati, B.W. Hoogenboom, Nanoscale stiffness topography reveals structure and mechanics of the transport barrier in intact nuclear pore complexes., *Nat. Nanotechnol.* 10 (2015) 60–4. doi:10.1038/nnano.2014.262.
- [46] G.J. Stanley, A. Fassati, B.W. Hoogenboom, Atomic force microscopy reveals structural variability amongst nuclear pore complexes, *Life Sci. Alliance*. 1 (2018) e201800142. doi:10.26508/lsa.201800142.

- 1
2
3
4 1 [47] F. Cardarelli, L. Lanzano, E. Gratton, Capturing directed molecular motion in the nuclear
5 2 pore complex of live cells, *Proc Natl Acad Sci U S A.* 109 (2012) 9863–9868.
6 3 www.pnas.org/lookup/suppl/doi:10.1073/pnas.1200486109/-
7 4 [/DCSupplemental.www.pnas.org/cgi/doi/10.1073/pnas](http://DCSupplemental.www.pnas.org/cgi/doi/10.1073/pnas) (accessed July 22, 2019).
8 5 [48] F. Cardarelli, L. Lanzano, E. Gratton, Nanoscale Fluorescence Correlation Spectroscopy
9 6 of Intact Nuclear Pore Complexes, *Biophys. J.* 101 (2011) L27–L29.
10 7 doi:10.1016/j.bpj.2011.04.057.
11 8 [49] A. Zilman, S. Di Talia, B.T.B.T. Chait, M.P.M.P. Rout, M.O.M.O. Magnasco, Efficiency,
12 9 Selectivity, and Robustness of Nucleocytoplasmic Transport, *PLoS Comput Biol.* 3 (2007)
13 10 e125. doi:10.1371/journal.pcbi.0030125.
14 11 [50] A. Zilman, S. di Talia, T. Jovanovic-Talisman, B.T. Chait, M.P. Rout, M.O. Magnasco,
15 12 Enhancement of transport selectivity through nano-channels by non-specific competition,
16 13 *PLoS Comp. Biol.* 6 (2010) e1000804. doi:10.1371/journal.pcbi.1000804.
17 14 [51] T. Kustanovich, Y. Rabin, Metastable network model of protein transport through nuclear
18 15 pores., *Biophys. J.* 86 (2004) 2008–16. doi:10.1016/S0006-3495(04)74262-9.
19 16 [52] T. Bickel, R. Bruinsma, The Nuclear Pore Complex Mystery and Anomalous Diffusion in
20 17 Reversible Gels, 83 (2002) 3079–3087.
21 18 [53] D. Ando, R. Zandi, Y.W. Kim, M. Colvin, M. Rexach, A. Gopinathan, Nuclear Pore
22 19 Complex Protein Sequences Determine Overall Copolymer Brush Structure and Function,
23 20 *Biophys. J.* 106 (2014) 1997–2007. doi:10.1016/J.BPJ.2014.03.021.
24 21 [54] R. Moussavi-Baygi, Y. Jamali, R. Karimi, M.R.K. Mofrad, Brownian dynamics
25 22 simulation of nucleocytoplasmic transport: a coarse-grained model for the functional state
26 23 of the nuclear pore complex., *PLoS Comput. Biol.* 7 (2011) e1002049.
27 24 doi:10.1371/journal.pcbi.1002049.
28 25 [55] R. Gamini, W. Han, J.E. Stone, K. Schulten, Assembly of Nsp1 Nucleoporins Provides
29 26 Insight into Nuclear Pore Complex Gating, *PLoS Comput. Biol.* 10 (2014) e1003488.
30 27 doi:10.1371/journal.pcbi.1003488.
31 28 [56] A. Vovk, C. Gu, M.G. Opferman, L.E. Kapinos, R.Y.H. Lim, R.D. Coalson, D. Jasnow,
32 29 A. Zilman, Simple biophysics underpins collective conformations of the intrinsically
33 30 disordered proteins of the Nuclear Pore Complex, *Elife.* 5 (2016) 12.
34 31 doi:10.7554/eLife.10785.
35 32 [57] R. Zahn, D. Osmanović, S. Ehret, C. Araya Callis, S. Frey, M. Stewart, C. You, D.
36 33 Görlich, B.W. Hoogenboom, R.P. Richter, A physical model describing the interaction of
37 34 nuclear transport receptors with FG nucleoporin domain assemblies., *Elife.* 5 (2016) 695–
38 35 701. doi:10.7554/eLife.14119.
39 36 [58] D. Osmanović, A. Fassati, I. Ford, B. Hogenboom, Physical Modelling of the Nuclear
40 37 Pore Complex, *Soft Matter.* 9 (2013) 10442–10451. doi:10.1039/c3sm50722j.
41 38 [59] J. Pulupa, M. Rachh, M.D. Tomasini, J.S. Mincer, S.M. Simon, A coarse-grained
42 39 computational model of the nuclear pore complex predicts Phe-Gly nucleoporin dynamics,
43 40 *J. Gen. Physiol.* 149 (2017) 951–966. doi:10.1085/jgp.201711769.
44 41 [60] D. Osmanović, I.J. Ford, B.W. Hoogenboom, Model inspired by nuclear pore complex
45 42 suggests possible roles for nuclear transport receptors in determining its structure.,
46 43 *Biophys. J.* 105 (2013) 2781–9. doi:10.1016/j.bpj.2013.11.013.
47 44 [61] J.S. Mincer, S.M. Simon, Simulations of nuclear pore transport yield mechanistic insights
48 45 and quantitative predictions., *Proc. Natl. Acad. Sci. U. S. A.* 108 (2011) E351-8.
49 46 doi:10.1073/pnas.1104521108.
50
51
52
53
54
55
56
57
58
59
60
61
62
63
64
65

- 1
2
3
4 1 [62] A. Ghavami, L.M. Veenhoff, E. van der Giessen, P.R. Onck, Probing the Disordered
5 2 Domain of the Nuclear Pore Complex through Coarse-Grained Molecular Dynamics
6 3 Simulations., *Biophys. J.* 107 (2014) 1393–402. doi:10.1016/j.bpj.2014.07.060.
7 4 [63] M. Tagliacruzchi, O. Peleg, M. Kröger, Y. Rabin, I. Szleifer, Effect of charge,
8 5 hydrophobicity, and sequence of nucleoporins on the translocation of model particles
9 6 through the nuclear pore complex., *Proc. Natl. Acad. Sci. U. S. A.* 110 (2013) 3363–8.
10 7 doi:10.1073/pnas.1212909110.
11 8 [64] M. Delaleau, K.L.B. Borden, Multiple Export Mechanisms for mRNAs, *Cells.* 4 (2015)
12 9 452–473. doi:10.3390/cells4030452.
13 10 [65] P. Wendler, C. Enekel, Nuclear transport of yeast proteasomes, *Front. Mol. Biosci.* 6
14 11 (2019) 34. doi:10.3389/fmolb.2019.00034.
15 12 [66] D. Grünwald, R.H. Singer, M. Rout, Nuclear export dynamics of RNA-"protein
16 13 complexes, *Nature.* 475 (2011) 333–341. doi:10.1038/nature10318.
17 14 [67] P. Popken, A. Ghavami, P.R. Onck, B. Poolman, L.M. Veenhoff, Size-dependent leak of
18 15 soluble and membrane proteins through the yeast nuclear pore complex., *Mol. Biol. Cell.*
19 16 26 (2015) 1386–94. doi:10.1091/mbc.E14-07-1175.
20 17 [68] L.A. Strawn, T. Shen, N. Shulga, D.S. Goldfarb, S.R. Wenten, Minimal nuclear pore
21 18 complexes define FG repeat domains essential for transport, *Nat. Cell Biol.* 6 (2004) 197–
22 19 206.
23 20 [69] S.R. Wenten, M.P. Rout, The nuclear pore complex and nuclear transport., *Cold Spring*
24 21 *Harb. Perspect. Biol.* 2 (2010) a000562. doi:10.1101/cshperspect.a000562.
25 22 [70] J. Kosinski, S. Mosalaganti, A. Von Appen, R. Teimer, A.L. Digulio, W. Wan, K.H. Bui,
26 23 W.J.H. Hagen, J.A.G. Briggs, J.S. Glavy, E. Hurt, M. Beck, Molecular architecture of the
27 24 inner ring scaffold of the nuclear pore complex, *Science* (80-.). 352 (2016) 363–365.
28 25 [71] K.H. Bui, A. von Appen, A.L. DiGuilio, A. Ori, L. Sparks, M.-T. Mackmull, T. Bock, W.
29 26 Hagen, A. Andrés-Pons, J.S. Glavy, M. Beck, Integrated Structural Analysis of the Human
30 27 Nuclear Pore Complex Scaffold, *Cell.* 155 (2013) 1233–1243.
31 28 doi:10.1016/J.CELL.2013.10.055.
32 29 [72] S.R. Wenten, M.P. Rout, G. Blobel, A new family of yeast nuclear pore complex proteins,
33 30 *J. Cell Biol.* 119 (1992) 705–723. doi:10.1083/jcb.119.4.705.
34 31 [73] R.Y.H. Lim, N.-P.P. Huang, J. Köser, J. Deng, K.H.A. Lau, K. Schwarz-Herion, B.
35 32 Fahrenkrog, U. Aebi, Flexible phenylalanine-glycine nucleoporins as entropic barriers to
36 33 nucleocytoplasmic transport, *Proc. Natl. Acad. Sci.* 103 (2006) 9512–9517.
37 34 doi:10.1073/pnas.0603521103.
38 35 [74] L.K. Davis, I.J. Ford, A.D.S. Šarić, B.W. Hoogenboom, Intrinsically disordered nuclear
39 36 pore proteins show ideal-polymer morphologies and dynamics, *Phys. Rev. E.* 101 (2020)
40 37 022420. doi:10.1103/PhysRevE.101.022420.
41 38 [75] B.L. Timney, B. Raveh, R. Mironska, J.M. Trivedi, S.J. Kim, D. Russel, S.R. Wenten, A.
42 39 Sali, M.P. Rout, Simple rules for passive diffusion through nuclear pore complex, *J. Cell*
43 40 *Biol.* 215 (2016) 57–76. doi:10.1083/jcb.201601004.
44 41 [76] O. Keminer, R. Peters, Permeability of Single Nuclear Pores, *Biophys. J.* 77 (1999) 217–
45 42 228. doi:10.1016/S0006-3495(99)76883-9.
46 43 [77] D. Mohr, S. Frey, T. Fischer, T. Güttler, D. Görlich, Characterisation of the passive
47 44 permeability barrier of nuclear pore complexes, *EMBO J.* 28 (2009) 2541–2553.
48 45 doi:10.1038/emboj.2009.200.
49 46 [78] W. Yang, J. Gelles, S. Musser, Imaging of single-molecule translocation through nuclear

- 1
2
3
4 1 pore complexes, Proc. Natl. Acad. Sci. USA. 101 (2004) 12887–12892.
5 2 [79] K. Ribbeck, U. Kutay, E. Paraskeva, D. Görlich, The translocation of transportin--cargo
6 3 complexes through nuclear pores is independent of both Ran and energy, Curr. Biol. 9
7 4 (1999) 47--S1. <http://www.ncbi.nlm.nih.gov/pubmed/9889126>.
8 5 [80] M. Rexach, G. Blobel, Protein import into nuclei: association and dissociation reactions
9 6 involving transport substrate, transport factors, and nucleoporins, Cell. 83 (1995) 683–
10 7 692.
11 8 [81] U. Kubitscheck, D. Grünwald, A. Hoekstra, D. Rohleder, T. Kues, J.P. Siebrasse, R.
12 9 Peters, Nuclear transport of single molecules: dwell times at the nuclear pore complex, J.
13 10 Cell. Biol. 168 (2005) 233. doi:10.1083/jcb.200411005.
14 11 [82] D. Görlich, U. Kutay, Transport between the Cell Nucleus and the Cytoplasm, Ann. REV.
15 12 Cell. Dev. Biol. 15 (1999) 607.
16 13 [83] L.E. Kapinos, B. Huang, C. Rencurel, R.Y.H. Lim, Karyopherins regulate nuclear pore
17 14 complex barrier and transport function., J. Cell Biol. 216 (2017) 3609–3624.
18 15 doi:10.1083/jcb.201702092.
19 16 [84] I. Ben-Efraim, L. Gerace, Gradient of Increasing Affinity of Importin b for Nucleoporins
20 17 along the Pathway of Nuclear Import, 152 (2001) 411–417.
21 18 [85] R.B. Kopito, M. Elbaum, Reversibility in nucleocytoplasmic transport, Proc. Natl. Acad.
22 19 Sci. 104 (2007) 12743.
23 20 [86] B.L. Timney, J. Tetenbaum-Novatt, D.S. Agate, R. Williams, W. Zhang, B.T. Chait, M.P.
24 21 Rout, Simple kinetic relationships and nonspecific competition govern nuclear import
25 22 rates in vivo., J. Cell Biol. 175 (2006) 579–93. doi:10.1083/jcb.200608141.
26 23 [87] G. Riddick, I.G. Macara, A systems analysis of importin- α - β mediated nuclear
27 24 protein import., J. Cell Biol. 168 (2005) 1027–38. doi:10.1083/jcb.200409024.
28 25 [88] I.G. Macara, Transport into and out of the nucleus, Microbiol. Mol. Biol. Revs. 65 (2001)
29 26 570.
30 27 [89] K. Ribbeck, D. Görlich, Kinetic analysis of translocation through nuclear pore complexes,
31 28 EMBO J. 20 (2001) 1320–1330.
32 29 [90] R. Phillips, J. Kondev, J. Theriot, H. Garcia, Physical Biology of the Cell, Garland
33 30 Science, New York, 2012. doi:10.1201/9781134111589.
34 31 [91] T. Dange, D. Grünwald, A. Grünwald, R. Peters, U. Kubitscheck, D. Grünwald, A.
35 32 Grünwald, R. Peters, U. Kubitscheck, Autonomy and robustness of translocation through
36 33 the nuclear pore complex: a single-molecule study., J. Cell Biol. 183 (2008) 77–86.
37 34 doi:10.1083/jcb.200806173.
38 35 [92] S.M. Musser, D. Grünwald, Deciphering the Structure and Function of Nuclear Pores
39 36 Using Single-Molecule Fluorescence Approaches, J. Mol. Biol. 428 (2016) 2091–2119.
40 37 doi:10.1016/J.JMB.2016.02.023.
41 38 [93] A. Mor, S. Suliman, R. Ben-Yishay, S. Yunger, Y. Brody, Y. Shav-Tal, Dynamics of
42 39 single mRNP nucleocytoplasmic transport and export through the nuclear pore in living
43 40 cells, Nat. Cell Biol. 12 (2010) 543–552. doi:10.1038/ncb2056.
44 41 [94] B.B. Hülsmann, A.A. Labokha, D. Görlich, The permeability of reconstituted nuclear
45 42 pores provides direct evidence for the selective phase model., Cell. 150 (2012) 738–51.
46 43 doi:10.1016/j.cell.2012.07.019.
47 44 [95] M. Stewart, Molecular mechanism of the nuclear protein import cycle, Nat. Rev. Mol.
48 45 Cell Biol. 8 (2007) 195–208. doi:10.1038/nrm2114.
49 46 [96] S. Frey, R. Rees, J. Schünemann, S.C. Ng, K. Fünfgeld, T. Huyton, D. Görlich, Surface

- 1
2
3
4 1 Properties Determining Passage Rates of Proteins through Nuclear Pores, *Cell*. 174 (2018)
5 2 202–217.e9. doi:10.1016/J.CELL.2018.05.045.
6 3 [97] S. Frey, D. Görlich, A saturated FG-repeat hydrogel can reproduce the permeability
7 4 properties of nuclear pore complexes, *Cell*. 130 (2007) 512–523.
8 5 [98] H.B. Schmidt, D. Görlich, Transport Selectivity of Nuclear Pores, Phase Separation, and
9 6 Membraneless Organelles, *Trends Biochem. Sci.* 41 (2016) 46–61.
10 7 <https://www.sciencedirect.com/science/article/pii/S0968000415002091> (accessed March
11 8 28, 2018).
12 9 [99] R.L. Schoch, L.E. Kapinos, R.Y.H. Lim, Nuclear transport receptor binding avidity
13 10 triggers a self-healing collapse transition in FG-nucleoporin molecular brushes., *Proc.*
14 11 *Natl. Acad. Sci. U. S. A.* 109 (2012) 16911–6. doi:10.1073/pnas.1208440109.
15 12 [100] R.Y.H. Lim, B. Huang, L.E. Kapinos, How to operate a nuclear pore complex by Kap-
16 13 centric control, *Nucleus*. 6 (2015) 366–372. doi:10.1080/19491034.2015.1090061.
17 14 [101] J. Yamada, J.L. Phillips, S. Patel, G. Goldfien, A. Calestagne-Morelli, H. Huang, R. Reza,
18 15 J. Acheson, V. V Krishnan, S. Newsam, others, A bimodal distribution of two distinct
19 16 categories of intrinsically disordered structures with separate functions in FG
20 17 nucleoporins, *Mol. Cell. Proteomics*. 9 (2010) 2205.
21 18 [102] M.P. Rout, J.D. Aitchison, M.O. Magnasco, B.T. Chait, Virtual gating and nuclear
22 19 transport: the hole picture, *Trends Cell Biol.* 13 (2003) 622–628.
23 20 [103] L.E. Hough, K. Dutta, S. Sparks, D.B. Temel, A. Kamal, J. Tetenbaum-Novatt, M.P. Rout,
24 21 D. Cowburn, The molecular mechanism of nuclear transport revealed by atomic-scale
25 22 measurements, *Elife*. 4 (2015) e10027. doi:10.7554/eLife.10027.
26 23 [104] H.B. Schmidt, D. Görlich, Nup98 FG domains from diverse species spontaneously phase-
27 24 separate into particles with nuclear pore-like permselectivity., *Elife*. 4 (2015) e04251.
28 25 doi:10.7554/eLife.04251.
29 26 [105] L.J. Colwell, M.P. Brenner, K. Ribbeck, M. Gilson, Charge as a Selection Criterion for
30 27 Translocation through the Nuclear Pore Complex, *PLoS Comput Biol.* 6 (2010) e1000747.
31 28 [106] R. Bayliss, T. Littlewood, L.A. Strawn, S.R. Wentz, M. Stewart, GLFG and FxFG
32 29 nucleoporins bind to overlapping sites on importin- β , *J. Biol. Chem.* 277 (2002) 50597–
33 30 50606.
34 31 [107] R. Bayliss, K. Ribbeck, D. Akin, H.M. Kent, C.M. Feldherr, D. Görlich, M. Stewart,
35 32 Interaction between NTF2 and xFxFG-containing nucleoporins is required to mediate
36 33 nuclear import of RanGDP., *J. Mol. Biol.* 293 (1999) 579–93.
37 34 doi:10.1006/jmbi.1999.3166.
38 35 [108] N.B. Eisele, A.A. Labokha, S. Frey, D. Görlich, R.P. Richter, Cohesiveness tunes
39 36 assembly and morphology of FG nucleoporin domain meshworks - Implications for
40 37 nuclear pore permeability, *Biophys. J.* 105 (2013) 1860–1870.
41 38 doi:10.1016/j.bpj.2013.09.006.
42 39 [109] S. Frey, R.P. Richter, D. Görlich, FG-rich repeats of nuclear pore proteins form a three-
43 40 dimensional meshwork with hydrogel-like properties., *Science*. 314 (2006) 815–7.
44 41 doi:10.1126/science.1132516.
45 42 [110] M. Peyro, M. Soheilypour, A. Ghavami, M.R.K. Mofrad, Nucleoporin's Like Charge
46 43 Regions Are Major Regulators of FG Coverage and Dynamics Inside the Nuclear Pore
47 44 Complex, *PLoS One*. 10 (2015) e0143745. doi:10.1371/journal.pone.0143745.
48 45 [111] D. Ando, M. Colvin, M. Rexach, A. Gopinathan, Physical Motif Clustering within
49 46 Intrinsically Disordered Nucleoporin Sequences Reveals Universal Functional Features,

- 1 PLoS One. 8 (2013) e73831. doi:10.1371/journal.pone.0073831.
- 2 [112] W.G. Chen, J. Witten, S.C. Grindy, N. Holten-Andersen, K. Ribbeck, Charge Influences
3 Substrate Recognition and Self-Assembly of Hydrophobic FG Sequences, *Biophys. J.* 113
4 (2017) 2088–2099. doi:10.1016/j.bpj.2017.08.058.
- 5 [113] R.Y.H. Lim, B. Fahrenkrog, J. Koser, K. Schwarz-Herion, J. Deng, U. Aebi, J. Köser, K.
6 Schwarz-Herion, J. Deng, U. Aebi, J. Koser, Nanomechanical Basis of Selective Gating
7 by the Nuclear Pore Complex, *Science* (80-.). 318 (2007) 640.
- 8 [114] C. Gu, A. Vovk, T. Zheng, R.D.R.D. Coalson, A. Zilman, The Role of Cohesiveness in
9 the Permeability of the Spatial Assemblies of FG Nucleoporins, *Biophys. J.* 116 (2019) 1–
10 12. doi:10.1016/J.BPJ.2019.02.028.
- 11 [115] V.N. Uversky, Natively unfolded proteins: A point where biology waits for physics,
12 *Protein Sci.* 11 (2002) 739–756.
- 13 [116] R.K. Das, K.M. Ruff, R. V Pappu, Relating sequence encoded information to form and
14 function of intrinsically disordered proteins., *Curr. Opin. Struct. Biol.* 32 (2015) 102–112.
15 doi:10.1016/j.sbi.2015.03.008.
- 16 [117] C. Camilloni, A. De Simone, W.F. Vranken, M. Vendruscolo, Determination of
17 Secondary Structure Populations in Disordered States of Proteins Using Nuclear Magnetic
18 Resonance Chemical Shifts, *Biochemistry.* 51 (2012) 2224–2231. doi:10.1021/bi3001825.
- 19 [118] J.A. Marsh, V.K. Singh, Z. Jia, J.D. Forman-Kay, Sensitivity of secondary structure
20 propensities to sequence differences between α - and γ -synuclein: Implications for
21 fibrillation, *Protein Sci.* 15 (2006) 2795–2804. doi:10.1110/ps.062465306.
- 22 [119] S. Milles, D. Mercadante, I.V. Aramburu, M.R. Jensen, N. Banterle, C. Koehler, S. Tyagi,
23 J. Clarke, S.L. Shammash, M. Blackledge, F. Gräter, E.A. Lemke, Plasticity of an Ultrafast
24 Interaction between Nucleoporins and Nuclear Transport Receptors., *Cell.* 163 (2015) 1–
25 12. doi:10.1016/j.cell.2015.09.047.
- 26 [120] M. Doi, S.F. Edwards, *The Theory of Polymer Dynamics*, Clarendon Press, 1998.
- 27 [121] P.J. Flory, *Principles of Polymer Chemistry*, Cornell University Press, 1953.
- 28 [122] C.M. Kok, A. Rudin, Relationship between the hydrodynamic radius and the radius of
29 gyration of a polymer in solution, *Die Makromol. Chemie, Rapid Commun.* 2 (1981) 655–
30 659. doi:10.1002/marc.1981.030021102.
- 31 [123] P. Bernadó, D.I. Svergun, Structural analysis of intrinsically disordered proteins by small-
32 angle X-ray scattering, *Mol. BioSyst.* 8 (2012) 151–167. doi:10.1039/C1MB05275F.
- 33 [124] G. Fuertes, N. Banterle, K.M. Ruff, A. Chowdhury, D. Mercadante, C. Koehler, M.
34 Kachala, G. Estrada Girona, S. Milles, A. Mishra, P.R. Onck, F. Gräter, S. Esteban-
35 Martín, R. V Pappu, D.I. Svergun, E.A. Lemke, Decoupling of size and shape fluctuations
36 in heteropolymeric sequences reconciles discrepancies in SAXS vs. FRET measurements.,
37 *Proc. Natl. Acad. Sci. U. S. A.* 114 (2017) E6342–E6351. doi:10.1073/pnas.1704692114.
- 38 [125] M. Brucale, B. Schuler, B. Samorì, Single-molecule studies of intrinsically disordered
39 proteins., *Chem. Rev.* 114 (2014) 3281–317. doi:10.1021/cr400297g.
- 40 [126] K. Gast, C. Fiedler, *Dynamic and Static Light Scattering of Intrinsically Disordered
41 Proteins*, in: *Intrinsically Disord. Protein Anal.*, Springer New York, New York, NY,
42 2012: pp. 137–161. doi:10.1007/978-1-4614-3704-8_9.
- 43 [127] P.G. de Gennes, *Scaling Concepts in Polymer Science*, Cornell University Press, 1979.
- 44 [128] H.S. Ashbaugh, H.W. Hatch, Natively unfolded protein stability as a coil-to-globule
45 transition in charge/hydrophobicity space., *J. Am. Chem. Soc.* 130 (2008) 9536–42.
46 doi:10.1021/ja802124e.

- 1
2
3
4 1 [129] E. Sherman, G. Haran, Coil-globule transition in the denatured state of a small protein.,
5 2 Proc. Natl. Acad. Sci. U. S. A. 103 (2006) 11539–43. doi:10.1073/pnas.0601395103.
6 3 [130] N.B. Eisele, S. Frey, J. Piehler, D. Görlich, R.P. Richter, Ultrathin nucleoporin
7 4 phenylalanine--glycine repeat films and their interaction with nuclear transport receptors,
8 5 EMBO Rep. 11 (2010) 366–372.
9 6 [131] A.Y. Grosberg, A.R. Khokhlov, Giant Molecules, WORLD SCIENTIFIC, 2010.
10 7 doi:10.1142/7199.
11 8 [132] A.S. Holehouse, R. V. Pappu, Collapse Transitions of Proteins and the Interplay Among
12 9 Backbone, Sidechain, and Solvent Interactions, Annu. Rev. Biophys. 47 (2018) 19–39.
13 10 doi:10.1146/annurev-biophys-070317-032838.
14 11 [133] L. Miao, K. Schulten, Transport-related structures and processes of the nuclear pore
15 12 complex studied through molecular dynamics., Structure. 17 (2009) 449–59.
16 13 doi:10.1016/j.str.2008.12.021.
17 14 [134] B. Raveh, J.M. Karp, S. Sparks, K. Dutta, M.P. Rout, A. Sali, D. Cowburn, Slide-and-
18 15 exchange mechanism for rapid and selective transport through the nuclear pore complex.,
19 16 Proc. Natl. Acad. Sci. U. S. A. 113 (2016) E2489–97. doi:10.1073/pnas.1522663113.
20 17 [135] D. Mercadante, S. Milles, G. Fuertes, D.I. Svergun, E.A. Lemke, F. Gräter, Kirkwood-
21 18 Buff Approach Rescues Overcollapse of a Disordered Protein in Canonical Protein Force
22 19 Fields, J. Phys. Chem. B. 119 (2015) 7975–7984. doi:10.1021/acs.jpcc.5b03440.
23 20 [136] S. Piana, A.G. Donchev, P. Robustelli, D.E. Shaw, Water dispersion interactions strongly
24 21 influence simulated structural properties of disordered protein states, J. Phys. Chem. B.
25 22 119 (2015) 5113–5123. doi:10.1021/jp508971m.
26 23 [137] A. Gooneie, S. Schuschnigg, C. Holzer, A review of multiscale computational methods in
27 24 polymeric materials, Polymers (Basel). 9 (2017) 16. doi:10.3390/polym9010016.
28 25 [138] L. Aggarwal, P. Biswas, Hydration Water Distribution around Intrinsically Disordered
29 26 Proteins, J. Phys. Chem. B. 122 (2018) 4206–4218. doi:10.1021/acs.jpcc.7b11091.
30 27 [139] P. Rani, P. Biswas, Local Structure and Dynamics of Hydration Water in Intrinsically
31 28 Disordered Proteins, J. Phys. Chem. B. 119 (2015) 10858–10867. doi:10.1021/jp511961c.
32 29 [140] P. Rani, P. Biswas, Diffusion of Hydration Water around Intrinsically Disordered
33 30 Proteins, J. Phys. Chem. B. 119 (2015) 13262–13270. doi:10.1021/acs.jpcc.5b07248.
34 31 [141] F.X. Gallat, A. Laganowsky, K. Wood, F. Gabel, L. Van Eijck, J. Wuttke, M. Moulin, M.
35 32 Härtle, D. Eisenberg, J.P. Colletier, G. Zaccai, M. Weik, Dynamical coupling of
36 33 intrinsically disordered proteins and their hydration water: Comparison with folded
37 34 soluble and membrane proteins, Biophys. J. 103 (2012) 129–136.
38 35 doi:10.1016/j.bpj.2012.05.027.
39 36 [142] J. Huang, S. Rauscher, G. Nawrocki, T. Ran, M. Feig, B.L. de Groot, H. Grubmüller, A.D.
40 37 MacKerell, CHARMM36m: an improved force field for folded and intrinsically
41 38 disordered proteins, Nat. Methods. 14 (2017) 71–73. doi:10.1038/nmeth.4067.
42 39 [143] J. Yoo, A. Aksimentiev, New tricks for old dogs: improving the accuracy of biomolecular
43 40 force fields by pair-specific corrections to non-bonded interactions, Phys. Chem. Chem.
44 41 Phys. 20 (2018) 8432–8449. doi:10.1039/C7CP08185E.
45 42 [144] K. Huang, M. Tagliacruzchi, S.H. Park, Y. Rabin, I. Szleifer, Nanocompartmentalization of
46 43 the Nuclear Pore Lumen, Biophys. J. 118 (2019) 219–231. doi:10.1016/j.bpj.2019.11.024.
47 44 [145] L.K. Davis, A.A. Šarić, B.W. Hoogenboom, A. Zilman, Physical modelling of multivalent
48 45 interactions in the nuclear pore complex, bioRxiv, 2020. doi:10.1101/2020.10.01.322156.
49 46 [146] M. Tagliacruzchi, I. Szleifer, eds., Chemically modified nanopores and nanochannels,
50
51
52
53
54
55
56
57
58
59
60
61
62
63
64
65

- 1
2
3
4
5
6
7
8
9
10
11
12
13
14
15
16
17
18
19
20
21
22
23
24
25
26
27
28
29
30
31
32
33
34
35
36
37
38
39
40
41
42
43
44
45
46
47
48
49
50
51
52
53
54
55
56
57
58
59
60
61
62
63
64
65
- Elsevier, 2017.
- [147] A. Ghavami, E. van der Giessen, P.R. Onck, Coarse-Grained Potentials for Local Interactions in Unfolded Proteins, *J. Chem. Theory Comput.* 9 (2013) 432–440. doi:10.1021/ct300684j.
- [148] B. Carrasco, J. García de la Torre, Hydrodynamic properties of rigid particles: comparison of different modeling and computational procedures., *Biophys. J.* 76 (1999) 3044–57. doi:10.1016/S0006-3495(99)77457-6.
- [149] J. Garcia de la Torre, S. Navarro, M.C. Lopez Martinez, F.G. Diaz, J.J. Lopez Cascales, HYDRO: a computer program for the prediction of hydrodynamic properties of macromolecules., *Biophys. J.* 67 (1994) 530–1. doi:10.1016/S0006-3495(94)80512-0.
- [150] S. Milles, E.A. Lemke, Single molecule study of the intrinsically disordered FG-repeat nucleoporin 153., *Biophys. J.* 101 (2011) 1710–9. doi:10.1016/j.bpj.2011.08.025.
- [151] A. Chowdhury, S.A. Kovalenko, I.V. Aramburu, P.S. Tan, N.P. Ernsting, E.A. Lemke, I. Valle Aramburu, P.S. Tan, N.P. Ernsting, E.A. Lemke, Mechanism-Dependent Modulation of Ultrafast Interfacial Water Dynamics in Intrinsically Disordered Protein Complexes, *Angew. Chemie Int. Ed.* 58 (2019) 4720–4724. doi:10.1002/anie.201813354.
- [152] P.S. Tan, I.V. Aramburu, D. Mercadante, S. Tyagi, A. Chowdhury, D. Spitz, S.L. Shammass, F. Gräter, E.A. Lemke, Two Differential Binding Mechanisms of FG-Nucleoporins and Nuclear Transport Receptors, *Cell Rep.* 22 (2018) 3660–3671. doi:10.1016/J.CELREP.2018.03.022.
- [153] D. Mercadante, J.A. Wagner, I. V. Aramburu, E.A. Lemke, F. Gräter, Sampling Long-versus Short-Range Interactions Defines the Ability of Force Fields To Reproduce the Dynamics of Intrinsically Disordered Proteins, *J. Chem. Theory Comput.* 13 (2017) 3964–3974. doi:10.1021/acs.jctc.7b00143.
- [154] H.M. Watkins, A.J. Simon, T.R. Sosnick, E.A. Lipman, R.P. Hjelm, K.W. Plaxco, Random coil negative control reproduces the discrepancy between scattering and FRET measurements of denatured protein dimensions., *Proc. Natl. Acad. Sci. U. S. A.* 112 (2015) 6631–6. doi:10.1073/pnas.1418673112.
- [155] J.F. Marko, E.D. Siggia, Stretching DNA, *Macromolecules.* 28 (1995) 8759–8770. doi:10.1021/ma00130a008.
- [156] A. Zilman, Aggregation, Phase Separation and Spatial Morphologies of the Assemblies of FG Nucleoporins, *J. Mol. Biol.* 430 (2018) 4730–4740. doi:10.1016/J.JMB.2018.07.011.
- [157] A. Ghavami, E. Van Der Giessen, P.R. Onck, Sol-gel transition in solutions of FG-Nups of the nuclear pore complex, *Extrem. Mech. Lett.* 22 (2018) 36–41. doi:10.1016/j.eml.2018.04.006.
- [158] M. Beck, V. Lučić, F. Förster, W. Baumeister, O. Medalia, Lu, V. Ccaron, Snapshots of nuclear pore complexes in action captured by cryo-electron tomography, *Nature.* 449 (2007) 611–615. doi:10.1038/nature06170.
- [159] C.P.P. Brangwynne, P. Tompa, R.V. V. Pappu, Polymer physics of intracellular phase transitions, *Nat. Phys.* 11 (2015) 899–904. doi:10.1038/nphys3532.
- [160] A.A. Hyman, C.A. Weber, F. Jülicher, Liquid-Liquid Phase Separation in Biology, *Annu. Rev. Cell Dev. Biol.* 30 (2014) 39–58. doi:10.1146/annurev-cellbio-100913-013325.
- [161] C. Ader, S. Frey, W. Maas, H.B. Schmidt, D. Görlich, M. Baldus, Amyloid-like interactions within nucleoporin FG hydrogels., *Proc. Natl. Acad. Sci. U. S. A.* 107 (2010) 6281–5. doi:10.1073/pnas.0910163107.
- [162] S. Milles, K. Huy Bui, C. Koehler, M. Eltsov, M. Beck, E.A. Lemke, Facilitated

- 1
2
3
4 1 aggregation of FG nucleoporins under molecular crowding conditions., *EMBO Rep.* 14
5 2 (2013) 178–83. doi:10.1038/embor.2012.204.
6 3 [163] A.A. Labokha, S. Gradmann, S. Frey, B.B. Hülsmann, H. Urlaub, M. Baldus, D. Görlich,
7 4 Systematic analysis of barrier-forming FG hydrogels from *Xenopus* nuclear pore
8 5 complexes., *EMBO J.* 32 (2013) 204–18. doi:10.1038/emboj.2012.302.
9 6 [164] G. Celetti, G. Paci, J. Caria, V. VanDelinder, G. Bachand, E.A. Lemke, The liquid state of
10 7 FG-nucleoporins mimics permeability barrier properties of nuclear pore complexes, *J. Cell*
11 8 *Biol.* 219 (2020). doi:10.1083/jcb.201907157.
12 9 [165] A.G. Zilman, S.A. Safran, Thermodynamics and structure of self-assembled networks,
13 10 *Phys. Rev. E - Stat. Nonlinear, Soft Matter Phys.* 66 (2002) 051107.
14 11 doi:10.1103/PhysRevE.66.051107.
15 12 [166] A. Zilman, T. Tlusty, S.A. Safran, Entropic networks in colloidal, polymeric and
16 13 amphiphilic systems, *J. Phys. Condens. Matter.* 15 (2003) S57. doi:10.1088/0953-
17 14 8984/15/1/306.
18 15 [167] F. Tanaka, Theoretical study of molecular association and thermoreversible gelation in
19 16 polymers, *Polym. J.* 34 (2002) 479–509. doi:10.1295/polymj.34.479.
20 17 [168] R.F. Boyer, E. Baer, A. Hiltner, Concerning Gelation Effects in Atactic Polystyrene
21 18 Solutions, *Macromolecules.* 18 (1985) 427–434. doi:10.1021/ma00145a022.
22 19 [169] K. Huang, M. Tagliazucchi, S.H. Park, Y. Rabin, I. Szleifer, Molecular model of the
23 20 nuclear pore complex reveals a thermoreversible FG-network with distinct territories
24 21 occupied by different FG motifs, *BioRxiv.* (2019) 568865. doi:10.1101/568865.
25 22 [170] R. Moussavi-Baygi, M.R.K. Mofrad, Rapid Brownian Motion Primes Ultrafast
26 23 Reconstruction of Intrinsically Disordered Phe-Gly Repeats Inside the Nuclear Pore
27 24 Complex, *Sci. Rep.* 6 (2016) 29991. doi:10.1038/srep29991.
28 25 [171] N.B. Eisele, F.I. Andersson, S. Frey, R.P. Richter, Viscoelasticity of thin biomolecular
29 26 films: a case study on nucleoporin phenylalanine-glycine repeats grafted to a histidine-tag
30 27 capturing QCM-D sensor., *Biomacromolecules.* 13 (2012) 2322–32.
31 28 doi:10.1021/bm300577s.
32 29 [172] K.D. Schleicher, S.L. Dettmer, L.E. Kapinos, S. Pagliara, U.F. Keyser, S. Jeney, R.Y.H.
33 30 Lim, Selective transport control on molecular velcro made from intrinsically disordered
34 31 proteins., *Nat. Nanotechnol.* 9 (2014) 525–30. doi:10.1038/nnano.2014.103.
35 32 [173] L.E. Kapinos, R.L. Schoch, R.S. Wagner, K.D. Schleicher, R.Y.H. Lim, Karyopherin-
36 33 centric control of nuclear pores based on molecular occupancy and kinetic analysis of
37 34 multivalent binding with FG nucleoporins., *Biophys. J.* 106 (2014) 1751–62.
38 35 doi:10.1016/j.bpj.2014.02.021.
39 36 [174] R.S. Wagner, L.E. Kapinos, N.J. Marshall, M. Stewart, R.Y.H. Lim, Promiscuous Binding
40 37 of Karyopherin β 1 Modulates FG Nucleoporin Barrier Function and Expedites NTF2
41 38 Transport Kinetics, *Biophys. J.* 108 (2015) 918–927. doi:10.1016/j.bpj.2014.12.041.
42 39 [175] S.T. Milner, *Polymer Brushes*, *Science* (80-.). 251 (1991) 905–914.
43 40 doi:10.1002/3527603824.
44 41 [176] E.B. Zhulina, O. V. Borisov, V.A. Pryamitsyn, T.M. Birshtein, Coil-globule type
45 42 transitions in polymers. 1. Collapse of layers of grafted polymer chains, *Macromolecules.*
46 43 24 (1991) 140–149. doi:10.1021/ma00001a023.
47 44 [177] T. Suo, M.D. Whitmore, Self-consistent field theory of tethered polymers: one
48 45 dimensional, three dimensional, strong stretching theories and the effects of excluded-
49 46 volume-only interactions., *J. Chem. Phys.* 141 (2014) 204903. doi:10.1063/1.4901925.

- 1
2
3
4 1 [178] J.N. Bright, T.B. Woolf, J.H. Hoh, Predicting properties of intrinsically unstructured
5 2 proteins, *Prog. Biophys. Mol. Biol.* 76 (2001) 131–173. doi:10.1016/S0079-
6 3 6107(01)00012-8.
7 4 [179] T.M. Birshtein, Y. V Lyatskaya, Polymer brush in a mixed solvent, *Colloids Surfaces A*
8 5 *Physicochem. Eng. Asp.* 86 (1994) 77–83.
9 6 [180] A. Halperin, M. Kr\ddot{ot}oger, E.B. Zhulina, Colloid-Brush Interactions: The Effect of
10 7 Solvent Quality, *Macromolecules.* 44 (2011) 3622.
11 8 [181] S.T. Milner, T.A. Witten, M.E. Cates, Theory of the Grafted Polymer Brush,
12 9 *Macromolecules.* 21 (1988) 2610–2619.
13 10 [182] M.G. Opferman, R.D. Coalson, D. Jasnow, A. Zilman, Morphology of polymer brushes
14 11 infiltrated by attractive nanoinclusions of various sizes., *Langmuir.* 29 (2013) 8584–8591.
15 12 doi:10.1021/la4013922.
16 13 [183] L.C.H. Moh, M.D. Losego, P. V Braun, Solvent quality effects on scaling behavior of
17 14 poly(methyl methacrylate) brushes in the moderate- and high-density regimes., *Langmuir.*
18 15 27 (2011) 3698–702. doi:10.1021/la2002139.
19 16 [184] D. Osmanovic, J. Bailey, A.H. Harker, A. Fassati, B.W. Hoogenboom, I.J. Ford, Bistable
20 17 collective behavior of polymers tethered in a nanopore, *Phys. Rev. E.* 85 (2012) 61917.
21 18 [185] A. Eskandari Nasrabad, D. Jasnow, A. Zilman, R.D. Coalson, Precise control of polymer
22 19 coated nanopores by nanoparticle additives: Insights from computational modeling, 145
23 20 (2016) 064901. doi:10.1063/1.4955191.
24 21 [186] O. Peleg, M. Tagliacruzchi, M. Kröger, Y. Rabin, I. Szleifer, Morphology Control of Hairy
25 22 Nanopores, *ACS Nano.* 5 (2011) 4737–4747. doi:10.1021/nn200702u.
26 23 [187] R. Panatala, S. Barbato, T. Kozai, J. Luo, L.E. Kapinos, R.Y.H. Lim, Nuclear Pore
27 24 Membrane Proteins Self-Assemble into Nanopores, *Biochemistry.* 58 (2019) 484–488.
28 25 doi:10.1021/acs.biochem.8b01179.
29 26 [188] I. Tokareva, S. Minko, J.H. Fendler, E. Hutter, Nanosensors based on responsive polymer
30 27 brushes and gold nanoparticle enhanced transmission surface plasmon resonance
31 28 spectroscopy, *J. Am. Chem. Soc.* 126 (2004) 15950–15951.
32 29 [189] M. Ali, B. Schiedt, R. Neumann, W. Ensinger, Biosensing with functionalized single
33 30 asymmetric polymer nanochannels., *Macromol. Biosci.* 10 (2010) 28–32.
34 31 doi:10.1002/mabi.200900198.
35 32 [190] S. Howorka, S. Cheley, H. Bayley, Sequence-specific detection of individual DNA strands
36 33 using engineered nanopores., *Nat. Biotechnol.* 19 (2001) 636–9. doi:10.1038/90236.
37 34 [191] E.N. Savariar, K. Krishnamoorthy, S. Thayumanavan, Molecular discrimination inside
38 35 polymer nanotubules, *Nat. Nanotech.* 3 (2008) 112. doi:10.1038/nnano.2008.6.
39 36 [192] M. Tagliacruzchi, I. Szleifer, Stimuli-responsive polymers grafted to nanopores and other
40 37 nano-curved surfaces: structure, chemical equilibrium and transport, *Soft Matter.* 8 (2012)
41 38 7292. doi:10.1039/c2sm25777g.
42 39 [193] I. Sadeghi, A. Asatekin, Membranes with Functionalized Nanopores for Aromaticity-
43 40 Based Separation of Small Molecules, *ACS Appl. Mater. Interfaces.* (2019)
44 41 *acsami.9b00090.* doi:10.1021/acsami.9b00090.
45 42 [194] K. Luo, T. Ala-Nissila, S.-C. Ying, A. Bhattacharya, Sequence Dependence of DNA
46 43 Translocation through a Nanopore, *Phys. Rev. Lett.* 100 (2008) 058101.
47 44 doi:10.1103/PhysRevLett.100.058101.
48 45 [195] M. Soskine, A. Biesemans, B. Moeyaert, S. Cheley, H. Bayley, G. Maglia, An Engineered
49 46 ClyA Nanopore Detects Folded Target Proteins by Selective External Association and
50
51
52
53
54
55
56
57
58
59
60
61
62
63
64
65

- 1
2
3
4 1 Pore Entry., *Nano Lett.* 12 (2012) 4895–900. doi:10.1021/nl3024438.
- 5 2 [196] M. Firnkes, D. Pedone, J. Knezevic, M. Döblinger, U. Rant, Electrically facilitated
6 3 translocations of proteins through silicon nitride nanopores: conjoint and competitive
7 4 action of diffusion, electrophoresis, and electroosmosis., *Nano Lett.* 10 (2010) 2162–7.
8 5 doi:10.1021/nl100861c.
- 9 6 [197] P. Kohli, C.C. Harrell, Z. Cao, G. R., W. Tan, C.R. Martin, DNA-Functionalized
10 7 Nanotube Membranes with Single-Base Mismatch Selectivity, *Science* (80-.). 305 (2004)
11 8 984–986.
- 12 9 [198] G. Emilsson, K. Xiong, Y. Sakiyama, B. Malekian, V. Ahlberg Gagnér, R.L. Schoch,
13 10 R.Y.H. Lim, A.B. Dahlin, Polymer brushes in solid-state nanopores form an impenetrable
14 11 entropic barrier for proteins, *Nanoscale.* 10 (2018) 4663–4669.
15 12 doi:10.1039/C7NR09432A.
- 16 13 [199] A. Asatekin, K.K. Gleason, Polymeric Nanopore Membranes for Hydrophobicity-Based
17 14 Separations by Conformal Initiated Chemical Vapor Deposition, *Nano Lett.* 11 (2011)
18 15 677–686. doi:10.1021/nl103799d.
- 19 16 [200] K. Binder, A. Milchev, Polymer brushes on flat and curved surfaces: How computer
20 17 simulations can help to test theories and to interpret experiments, *J. Polym. Sci. Part B*
21 18 *Polym. Phys.* 50 (2012) 1515–1555. doi:10.1002/polb.23168.
- 22 19 [201] C.-W. Li, H. Merlitz, C.-X. Wu, J.-U. Sommer, Nanopores as Switchable Gates for
23 20 Nanoparticles: A Molecular Dynamics Study, *Macromolecules.* 51 (2018) 6238–6247.
24 21 doi:10.1021/acs.macromol.8b01149.
- 25 22 [202] C.W. Li, H. Merlitz, J.U. Sommer, Mean-Field Model of the Collapse Transition of
26 23 Brushes inside Cylindrical Nanopores, *Macromolecules.* 53 (2020) 6711–6719.
27 24 doi:10.1021/acs.macromol.0c00618.
- 28 25 [203] R.D. Coalson, A. Eskandari Nasrabad, D. Jasnow, A. Zilman, A Polymer-Brush-Based
29 26 Nanovalve Controlled by Nanoparticle Additives: Design Principles., *J. Phys. Chem. B.*
30 27 119 (2015) 11858–66. doi:10.1021/acs.jpcc.5b02623.
- 31 28 [204] G.J. Stanley, B. Akpınar, Q. Shen, P.D.E. Fisher, C.P. Lusk, C. Lin, B.W. Hoogenboom,
32 29 Quantification of Biomolecular Dynamics inside Real and Synthetic Nuclear Pore
33 30 Complexes using Time-Resolved Atomic Force Microscopy, *ACS Nano.* (2019)
34 31 acsnano.9b02424. doi:10.1021/acsnano.9b02424.
- 35 32 [205] R. Bayliss, T. Littlewood, M. Stewart, Structural basis for the interaction between FxFG
36 33 nucleoporin repeats and importin-beta in nuclear trafficking., *Cell.* 102 (2000) 99–108.
37 34 <http://www.ncbi.nlm.nih.gov/pubmed/10929717>.
- 38 35 [206] J. Tetenbaum-Novatt, L.E. Hough, R. Mironska, A.S. McKenney, M.P. Rout,
39 36 Nucleocytoplasmic transport: a role for nonspecific competition in karyopherin-
40 37 nucleoporin interactions., *Mol. Cell. Proteomics.* 11 (2012) 31–46.
41 38 doi:10.1074/mcp.M111.013656.
- 42 39 [207] D. Gilchrist, M. Rexach, Molecular basis for the rapid dissociation of nuclear localization
43 40 signals from karyopherin alpha in the nucleoplasm., *J. Biol. Chem.* 278 (2003) 51937–49.
44 41 doi:10.1074/jbc.M307371200.
- 45 42 [208] B. Pyhtila, M. Rexach, A Gradient of Affinity for the Karyopherin Kap95p along the
46 43 Yeast Nuclear Pore Complex*, *J. Biol. Chem.* 278 (2003) 42699–42709.
47 44 doi:10.1074/jbc.M307135200.
- 48 45 [209] R. Hayama, S. Sparks, L.M. Hecht, K. Dutta, J.M. Karp, C.M. Cabana, M.P. Rout, D.
49 46 Cowburn, Thermodynamic characterization of the multivalent interactions underlying

- 1
2
3
4 1 rapid and selective translocation through the nuclear pore complex., *J. Biol. Chem.* 293
5 2 (2018) 4555–4563. doi:10.1074/jbc.AC117.001649.
6 3 [210] T.A. Isgro, K. Schulten, Cse1p-Binding Dynamics Reveal a Binding Pattern for FG-
7 4 Repeat Nucleoporins on Transport Receptors, *Structure*. 15 (2007) 977–991.
8 5 doi:10.1016/J.STR.2007.06.011.
9 6 [211] T.A. Isgro, K. Schulten, Binding dynamics of isolated nucleoporin repeat regions to
10 7 importin- β , *Structure*. 13 (2005) 1869–1879.
11 8 [212] T.A. Isgro, K. Schulten, Association of Nuclear Pore FG-repeat Domains to NTF2 Import
12 9 and Export Complexes, *J. Mol. Biol.* 366 (2007) 330–345.
13 10 doi:10.1016/J.JMB.2006.11.048.
14 11 [213] M. Kumeta, H. Yamaguchi, S.H. Yoshimura, K. Takeyasu, Karyopherin-independent
15 12 spontaneous transport of amphiphilic proteins through the nuclear pore, *J. Cell Sci.* 125
16 13 (2012) 4979–4984. doi:10.1242/jcs.109520.
17 14 [214] J. Kim, A. Izadyar, N. Nioradze, S. Amemiya, Nanoscale mechanism of molecular
18 15 transport through the nuclear pore complex as studied by scanning electrochemical
19 16 microscopy., *J. Am. Chem. Soc.* 135 (2013) 2321–9. doi:10.1021/ja311080j.
20 17 [215] J. Tetenbaum-Novatt, M.P. Rout, The Mechanism of Nucleocytoplasmic Transport
21 18 through the Nuclear Pore Complex, in: *Cold Spring Harb. Symp. Quant. Biol.*, 2010: pp.
22 19 567–584.
23 20 [216] S. Milles, E.A. Lemke, Mapping Multivalency and Differential Affinities within Large
24 21 Intrinsically Disordered Protein Complexes with Segmental Motion Analysis., *Angew.*
25 22 *Chemie Int. Ed.* 53 (2014) 7364–7367. doi:10.1002/anie.201403694.
26 23 [217] A. Sethi, B. Goldstein, S. Gnanakaran, Quantifying intramolecular binding in multivalent
27 24 interactions: a structure-based synergistic study on Grb2-Sos1 complex., *PLoS Comput.*
28 25 *Biol.* 7 (2011) e1002192. doi:10.1371/journal.pcbi.1002192.
29 26 [218] D.H. De Jong, L. V. Schäfer, A.H. De Vries, S.J. Marrink, H.J.C. Berendsen, H.
30 27 Grubmüller, Determining equilibrium constants for dimerization reactions from molecular
31 28 dynamics simulations, *J. Comput. Chem.* 32 (2011) 1919–1928. doi:10.1002/jcc.21776.
32 29 [219] P. Nelson, *Biological Physics*, WH Freeman, New York, 2004.
33 30 [220] L.-C. Tu, G. Fu, A. Zilman, S.M. Musser, Large cargo transport by nuclear pores:
34 31 implications for the spatial organization of FG-nucleoporins., *EMBO J.* 32 (2013) 3220–
35 32 30. doi:10.1038/emboj.2013.239.
36 33 [221] M.G. Opferman, R.D. Coalson, D. Jasnow, A. Zilman, No Title, *Phys. Rev. E.* 86 (2012)
37 34 31806.
38 35 [222] K.P. Wall, L.E. Hough, In-Cell NMR within Budding Yeast Reveals Cytoplasmic
39 36 Masking of Hydrophobic Residues of FG Repeats, *Biophys. J.* 115 (2018) 1690–1695.
40 37 doi:10.1016/J.BPJ.2018.08.049.
41 38 [223] R.K. Pathria, *Statistical Mechanics*, 2nd Edition, Elsevier, 1996.
42 39 [224] I.V. Aramburu, E.A. Lemke, Floppy but not sloppy: Interaction mechanism of FG-
43 40 nucleoporins and nuclear transport receptors, *Semin. Cell Dev. Biol.* 68 (2017) 34–41.
44 41 doi:10.1016/J.SEMCDB.2017.06.026.
45 42 [225] P. Tompa, M. Fuxreiter, Fuzzy complexes: polymorphism and structural disorder in
46 43 protein–protein interactions, *Trends Biochem. Sci.* 33 (2008) 2–8.
47 44 doi:10.1016/J.TIBS.2007.10.003.
48 45 [226] C. Gu, R.D. Coalson, D. Jasnow, A. Zilman, Free Energy of Nanoparticle Binding to
49 46 Multivalent Polymeric Substrates, *J. Phys. Chem. B.* 121 (2017) 6425–6435.
50
51
52
53
54
55
56
57
58
59
60
61
62
63
64
65

- 1
2
3
4 1 doi:10.1021/acs.jpcc.7b00868.
5 2 [227] M.G. Opferman, R.D. Coalson, D. Jasnow, A. Zilman, Morphological control of grafted
6 3 polymer films via attraction to small nanoparticle inclusions, *Phys. Rev. E*. 86 (2012) 1–7.
7 4 doi:10.1103/PhysRevE.86.031806.
8 5 [228] T.M. Birshtein, V.M. Amoskov, L.I. Klushin, A.A. Mercurieva, A.A. Polotsky, P.A.
9 6 Iakovlev, Microphase coexistence in polymeric brushes, in: *Macromol. Symp.*, 2003: pp.
10 7 51–58.
11 8 [229] A. Galuschko, J.-U. Sommer, Co-Nonsolvency Response of a Polymer Brush: A
12 9 Molecular Dynamics Study, *Macromolecules*. 52 (2019) 4120–4130.
13 10 doi:10.1021/acs.macromol.9b00569.
14 11 [230] H. Yong, S. Rauch, K.-J. Eichhorn, P. Uhlmann, A. Fery, J.-U. Sommer, H. Yong, S.
15 12 Rauch, K.-J. Eichhorn, P. Uhlmann, A. Fery, J.-U. Sommer, Cononsolvency Transition of
16 13 Polymer Brushes: A Combined Experimental and Theoretical Study, *Materials (Basel)*. 11
17 14 (2018) 991. doi:10.3390/ma11060991.
18 15 [231] N.B. Eisele, A. Labokha, S. Frey, D. Görlich, R.P. Richter, The Supramolecular Assembly
19 16 of Intrinsically Disordered Nucleoporin Domains is Tuned by Inter-Chain Interactions,
20 17 *Biophys. J.* 104 (2013) 120a. doi:10.1016/j.bpj.2012.11.693.
21 18 [232] M. Ozmaian, D. Jasnow, A. Eskandari Nasrabad, A. Zilman, R.D.R.D. Coalson, Effects of
22 19 cross-linking on partitioning of nanoparticles into a polymer brush: Coarse-grained
23 20 simulations test simple approximate theories, *J. Chem. Phys.* 148 (2018).
24 21 doi:10.1063/1.4990796.
25 22 [233] K. Ribbeck, D. Görlich, The permeability barrier of nuclear pore complexes appears to
26 23 operate via hydrophobic exclusion., *EMBO J.* 21 (2002) 2664–71.
27 24 doi:10.1093/emboj/21.11.2664.
28 25 [234] L. Miao, K. Schulten, Probing a Structural Model of the Nuclear Pore Complex Channel
29 26 through Molecular Dynamics, *Biophys. J.* 98 (2010) 1658–1667.
30 27 doi:10.1016/J.BPJ.2009.12.4305.
31 28 [235] C.M. Feldherr, D. Akin, The location of the transport gate in the nuclear pore complex., *J.*
32 29 *Cell Sci.* 110 (Pt 2 (1997) 3065–70. <http://www.ncbi.nlm.nih.gov/pubmed/9365276>.
33 30 [236] Y. Sakiyama, R. Panatala, R.Y.H. Lim, Structural dynamics of the nuclear pore complex,
34 31 *Semin. Cell Dev. Biol.* 68 (2017) 27–33. doi:10.1016/J.SEMCDB.2017.05.021.
35 32 [237] C.E. Atkinson, A.L. Matheyses, M. Kampmann, S.M. Simon, Conserved spatial
36 33 organization of FG domains in the nuclear pore complex., *Biophys. J.* 104 (2013) 37–50.
37 34 doi:10.1016/j.bpj.2012.11.3823.
38 35 [238] M.S. Mohamed, A. Kobayashi, A. Taoka, T. Watanabe-Nakayama, Y. Kikuchi, M.
39 36 Hazawa, T. Minamoto, Y. Fukumori, N. Kodera, T. Uchihashi, T. Ando, R.W. Wong,
40 37 High-Speed Atomic Force Microscopy Reveals Loss of Nuclear Pore Resilience as a
41 38 Dying Code in Colorectal Cancer Cells, *ACS Nano*. 11 (2017) 5567–5578.
42 39 doi:10.1021/acsnano.7b00906.
43 40 [239] H. Oberleithner, E. Brinckmann, A. Schwab, G. Krohne, Imaging nuclear pores of
44 41 aldosterone-sensitive kidney cells by atomic force microscopy., *Proc. Natl. Acad. Sci.* 91
45 42 (1994) 9784–9788. doi:10.1073/pnas.91.21.9784.
46 43 [240] R.D. Jäggi, A. Franco-Obregón, P. Mühlhäusser, F. Thomas, U. Kutay, K. Ensslin,
47 44 Modulation of nuclear pore topology by transport modifiers., *Biophys. J.* 84 (2003) 665–
48 45 70. doi:10.1016/S0006-3495(03)74886-3.
49 46 [241] D. Stoffler, B. Feja, B. Fahrenkrog, J. Walz, D. Typke, U. Aebi, Cryo-electron
50
51
52
53
54
55
56
57
58
59
60
61
62
63
64
65

- 1
2
3
4 1 Tomography Provides Novel Insights into Nuclear Pore Architecture: Implications for
5 2 Nucleocytoplasmic Transport, *J. Mol. Biol.* 328 (2003) 119–130. doi:10.1016/S0022-
6 3 2836(03)00266-3.
- 8 4 [242] A. Kramer, Y. Ludwig, V. Shahin, H. Oberleithner, A pathway separate from the central
9 5 channel through the nuclear pore complex for inorganic ions and small macromolecules.,
10 6 *J. Biol. Chem.* 282 (2007) 31437–43. doi:10.1074/jbc.M703720200.
- 12 7 [243] A. Kramer, I. Liashkovich, H. Oberleithner, S. Ludwig, I. Mazur, V. Shahin, Apoptosis
13 8 leads to a degradation of vital components of active nuclear transport and a dissociation of
14 9 the nuclear lamina., *Proc. Natl. Acad. Sci. U. S. A.* 105 (2008) 11236–41.
15 10 doi:10.1073/pnas.0801967105.
- 16 11 [244] J.O. Bustamante, A. Liepins, R.A. Prendergast, J.A. Hanover, H. Oberleithner, Patch
17 12 clamp and atomic force microscopy demonstrate TATA-binding protein (TBP)
18 13 interactions with the nuclear pore complex, *J. Membr. Biol.* 146 (1995) 263–272.
19 14 doi:10.1007/BF00233946.
- 21 15 [245] I. Liashkovich, D. Pasrednik, V. Prystopiuk, G. Rosso, H. Oberleithner, V. Shahin,
22 16 Clathrin inhibitor Pitstop-2 disrupts the nuclear pore complex permeability barrier, *Sci.*
23 17 *Rep.* 5 (2015) 1–9. doi:10.1038/srep09994.
- 25 18 [246] M. Eibauer, M. Pellanda, Y. Turgay, A. Dubrovsky, A. Wild, O. Medalia, Structure and
26 19 gating of the nuclear pore complex - Supplementary, *Nat. Commun.* 6 (2015) 7532.
27 20 doi:10.1038/ncomms8532.
- 28 21 [247] G.J. Stanley, A. Fassati, B.W. Hoogenboom, Biomechanics of the transport barrier in the
29 22 nuclear pore complex, *Semin. Cell Dev. Biol.* 68 (2017) 42–51.
30 23 doi:10.1016/j.semcdb.2017.05.007.
- 32 24 [248] C.W. Akey, Visualization of transport-related configurations of the nuclear pore
33 25 transporter, *Biophys. J.* 58 (1990) 341–355. doi:10.1016/S0006-3495(90)82381-X.
- 34 26 [249] G. Rabut, V. Doye, J. Ellenberg, Mapping the dynamic organization of the nuclear pore
35 27 complex inside single living cells., *Nat. Cell Biol.* 6 (2004) 1114–21.
36 28 doi:10.1038/ncb1184.
- 38 29 [250] A. Loschberger, S. van de Linde, M.-C. Dabauvalle, B. Rieger, M. Heilemann, G. Krohne,
39 30 M. Sauer, Super-resolution imaging visualizes the eightfold symmetry of gp210 proteins
40 31 around the nuclear pore complex and resolves the central channel with nanometer
41 32 resolution, *J. Cell Sci.* 125 (2012) 570–575. doi:10.1242/jcs.098822.
- 43 33 [251] J. Hüve, R. Wesselmann, M. Kahms, R. Peters, 4Pi microscopy of the nuclear pore
44 34 complex, *Biophys. J.* 95 (2008) 877–885. doi:10.1529/biophysj.107.127449.
- 45 35 [252] J. Fiserova, S.A. Richards, S.R. Wentz, M.W. Goldberg, Facilitated transport and
46 36 diffusion take distinct spatial routes through the nuclear pore complex., *J. Cell Sci.* 123
47 37 (2010) 2773–80. doi:10.1242/jcs.070730.
- 49 38 [253] B. Naim, V. Brumfeld, R. Kapon, V. Kiss, R. Nevo, Z. Reich, Passive and facilitated
50 39 transport in nuclear pore complexes is largely uncoupled., *J. Biol. Chem.* 282 (2007)
51 40 3881–8. doi:10.1074/jbc.M608329200.
- 53 41 [254] U. Rand, M. Rinas, J. Schwerk, G. Nöhren, M. Linnes, A. Kröger, M. Flossdorf, K. Kály-
54 42 Kullai, H. Hauser, T. Höfer, M. Köster, Multi-layered stochasticity and paracrine signal
55 43 propagation shape the type-I interferon response., *Mol. Syst. Biol.* 8 (2012) 584.
56 44 doi:10.1038/msb.2012.17.
- 58 45 [255] D.S. Banks, C. Fradin, Anomalous Diffusion of Proteins Due to Molecular Crowding,
59 46 *Biophys. J.* 89 (2005) 2960–2971. doi:10.1529/BIOPHYSJ.104.051078.

- 1
2
3
4 1 [256] R.P. R. Milo, Cell Biology by the Numbers, (n.d.). <http://book.bionumbers.org/> (accessed
5 2 July 7, 2019).
- 6 3 [257] L.L.-H. Cai, S. Panyukov, M. Rubinstein, Mobility of Nonsticky Nanoparticles in
7 4 Polymer Liquids, *Macromolecules*. 44 (2011) 7853–7863. doi:10.1021/ma201583q.
- 8 5 [258] C.P. Goodrich, M.P. Brenner, K. Ribbeck, Enhanced diffusion by binding to the crosslinks
9 6 of a polymer gel, *Nat. Commun.* 9 (2018) 4348. doi:10.1038/s41467-018-06851-5.
- 10 7 [259] J. Witten, K. Ribbeck, The particle in the spider's web: transport through biological
11 8 hydrogels, *Nanoscale*. 9 (2017) 8080–8095. doi:10.1039/C6NR09736G.
- 12 9 [260] S.K. Ghosh, A.G. Cherstvy, R. Metzler, Non-universal tracer diffusion in crowded media
13 10 of non-inert obstacles, *Phys. Chem. Chem. Phys.* 17 (2015) 1847–1858.
14 11 doi:10.1039/C4CP03599B.
- 15 12 [261] B. Carroll, V. Bocharova, J.-M.Y. Carrillo, A. Kisliuk, S. Cheng, U. Yamamoto, K.S.
16 13 Schweizer, B.G. Sumpter, A.P. Sokolov, Diffusion of Sticky Nanoparticles in a Polymer
17 14 Melt: Crossover from Suppressed to Enhanced Transport, *Macromolecules*. 51 (2018)
18 15 2268–2275. doi:10.1021/acs.macromol.7b02695.
- 19 16 [262] Q. Xu, L. Feng, R. Sha, N. Seeman, P. Chaikin, Subdiffusion of a Sticky Particle on a
20 17 Surface, *Phys. Rev. Lett.* 106 (2011) 5–8. doi:10.1103/PhysRevLett.106.228102.
- 21 18 [263] U. Yamamoto, J.-M.Y.M.Y. Carrillo, V. Bocharova, A.P. Sokolov, B.G. Sumpter, K.S.
22 19 Schweizer, Theory and Simulation of Attractive Nanoparticle Transport in Polymer Melts,
23 20 *Macromolecules*. 51 (2018) 2258–2267. doi:10.1021/acs.macromol.7b02694.
- 24 21 [264] L.-H. Cai, S. Panyukov, M. Rubinstein, Hopping Diffusion of Nanoparticles in Polymer
25 22 Matrices, *Macromolecules*. 48 (2015) 847–862. doi:10.1021/ma501608x.
- 26 23 [265] X.-Z. Cao, H. Merlitz, C.-X. Wu, Tuning Adsorption Duration To Control the Diffusion
27 24 of a Nanoparticle in Adsorbing Polymers, *J. Phys. Chem. Lett.* 8 (2017) 2629–2633.
28 25 doi:10.1021/acs.jpcclett.7b01049.
- 29 26 [266] J. van der Gucht, N. Besseling, W. Knoben, L. Bouteiller, M. Cohen Stuart, Brownian
30 27 particles in supramolecular polymer solutions, *Phys. Rev. E*. 67 (2003) 1–10.
31 28 doi:10.1103/PhysRevE.67.051106.
- 32 29 [267] M.W. Stefferson, S.L. Norris, F.J. Vernerey, M.D. Betterton, L.E. Hough, Effects of soft
33 30 interactions and bound mobility on diffusion in crowded environments: a model of sticky
34 31 and slippery obstacles, *Phys. Biol.* 14 (2017) 045008. doi:10.1088/1478-3975/aa7869.
- 35 32 [268] L. Maguire, M. Stefferson, M.D. Betterton, L.E. Hough, Design principles of selective
36 33 transport through biopolymer barriers, 100 (2019).
37 34 <https://journals.aps.org/pre/abstract/10.1103/PhysRevE.100.042414> (accessed August 13,
38 35 2019).
- 39 36 [269] J. Ramirez, T.J. Dursch, B.D. Olsen, A Molecular Explanation for Anomalous Diffusion
40 37 in Supramolecular Polymer Networks, *Macromolecules*. 51 (2018) 2517–2525.
41 38 doi:10.1021/acs.macromol.7b02465.
- 42 39 [270] Y.J. Yang, D.J. Mai, T.J. Dursch, B.D. Olsen, Nucleopore-Inspired Polymer Hydrogels
43 40 for Selective Biomolecular Transport, *Biomacromolecules*. 19 (2018) 3905–3916.
44 41 doi:10.1021/acs.biomac.8b00556.
- 45 42 [271] L. Leibler, M. Rubinstein, R.H. Colby, Dynamics of reversible networks, (2002).
46 43 doi:10.1021/MA00016A034.
- 47 44 [272] L. Maguire, M.D. Betterton, L.E. Hough, Bound-State Diffusion due to Binding to
48 45 Flexible Polymers in a Selective Biofilter, *Biophys. J.* 118 (2020) 376–385.
49 46 doi:10.1016/j.bpj.2019.11.026.
- 50
51
52
53
54
55
56
57
58
59
60
61
62
63
64
65

- 1
2
3
4 1 [273] A. Giometto, A. Rinaldo, F. Carrara, F. Altermatt, Emerging predictable features of
5 2 replicated biological invasion fronts., *Proc. Natl. Acad. Sci. U. S. A.* 111 (2014) 297–301.
6 3 doi:10.1073/pnas.1321167110.
7 4 [274] C. Plesa, S.W. Kowalczyk, R. Zinsmeister, A.Y. Grosberg, Y. Rabin, C. Dekker, Fast
8 5 Translocation of Proteins through Solid State Nanopores, *Nano Lett.* 13 (2013) 658–663.
9 6 doi:10.1021/nl3042678.
10 7 [275] F. Tanakat, F. Edwards, R.M. Received, Viscoelastic Properties of Physically Cross-
11 8 Linked Networks. *Transient Network Theory*, (1992) 1516–1523.
12 9 [276] C. Gu, C. Gu, Coarse-grained Theory and Simulation of Assemblies of Intrinsically-
13 10 disordered Nucleoporins, Ph. D. Thesis, University of Toronto, 2019.
14 11 [277] A. Zilman, Effects of Multiple Occupancy and Interparticle Interactions on Selective
15 12 Transport through Narrow Channels: Theory versus Experiment, *Biophys. J.* 96 (2009)
16 13 1235–1248. doi:10.1016/j.bpj.2008.09.058.
17 14 [278] Paul Bressloff, P.C. Bressloff, *Stochastic processes in cell biology*, Springer, Heidelberg,
18 15 2014. doi:10.1007/978-3-319-08488-6.
19 16 [279] S. Iyer-Biswas, A. Zilman, *First-Passage Processes in Cellular Biology*, *Adv. Chem. Phys.*
20 17 160 (2016) 261. doi:10.1002/9781119165156.ch5.
21 18 [280] C.W. Gardiner, *Stochastic Processes in Physics, Chemistry and Biology*, Springer-
22 19 Verlag, Heidelberg, 2003.
23 20 [281] R. Kapon, A. Topchik, D. Mukamel, Z. Reich, A possible mechanism for self-
24 21 coordination of bidirectional traffic across nuclear pores, *Phys. Biol.* 5 (2008) 036001.
25 22 doi:10.1088/1478-3975/5/3/036001.
26 23 [282] J. Wyman, Facilitated diffusion and the possible role of myoglobin as a transport
27 24 mechanism, *J. Biol. Chem.* 211 (1966) 114–121.
28 25 [283] A.M. Berezhkovskii, M.A. Pustovoit, S.M. Bezrukov, Channel-facilitated membrane
29 26 transport: Average lifetimes in the channel, *J. Chem. Phys.* 119 (2003) 3943.
30 27 doi:10.1063/1.1590957.
31 28 [284] S.M. Bezrukov, A.M. Berezhkovskii, M.A. Pustovoit, A. Szabo, Particle number
32 29 fluctuations in a membrane channel, *J. Chem. Phys.* 113 (2000) 8206.
33 30 [285] A. Berezhkovskii, S. Bezrukov, Optimizing Transport of Metabolites through Large
34 31 Channels: Molecular Sieves with and without Binding, *Biophys. J.* 88 (2005) L17–L19.
35 32 [286] J. Keizer, Diffusion Effects on Rapid Bimolecular Chemical Reactions, *Chem. Rev.* 87
36 33 (1987) 167–180. doi:10.1021/cr00077a009.
37 34 [287] H.C. Berg, *Random walks in biology*, Princeton University Press, 1993.
38 35 [288] A.M. Berezhkovskii, S.M. Bezrukov, Channel-facilitated membrane transport:
39 36 Constructive role of particle attraction to the channel pore, *Chem. Phys.* 319 (2005) 342.
40 37 [289] P. Hänggi, M. Borkovec, Reaction-rate theory: fifty years after Kramers, *Rev. Mod. Phys.*
41 38 62 (1990) 251–341. doi:10.1103/RevModPhys.62.251.
42 39 [290] H.C. Berg, *Random Walks in Biology*, Princeton University Press, 2001.
43 40 [291] A.M. Berezhkovskii, M.A. Pustovoit, S.M. Bezrukov, Channel-facilitated membrane
44 41 transport: Average lifetimes in the channel, *J. Chem. Phys.* 119 (2003) 3943.
45 42 doi:10.1063/1.1590957.
46 43 [292] A. Zilman, G. Bel, Crowding effects in non-equilibrium transport through nano-channels.,
47 44 *J. Phys. Condens. Matter.* 22 (2010) 454130. doi:10.1088/0953-8984/22/45/454130.
48 45 [293] W.D. Stein, *Channels, Carriers, and Pumps: An Introduction to Membrane Transport*,
49 46 Academic Press, New York, 1990.

- 1
2
3
4 1 [294] A.M. Berezhkovskii, M.A. Pustovoit, S.M. Bezrukov, M.A. Pustovoit, Channel-facilitated
5 2 membrane transport: Transit probability and interaction with the channel, *J. Chem. Phys.*
6 3 116 (2002) 9952–9956. doi:10.1063/1.1475758.
7 4 [295] S. Pagliara, S.L. Dettmer, U.F. Keyser, Channel-Facilitated Diffusion Boosted by Particle
8 5 Binding at the Channel Entrance, *Phys. Rev. Lett.* 113 (2014) 048102.
9 6 doi:10.1103/PhysRevLett.113.048102.
10 7 [296] S. Pagliara, C. Schwall, U.F. Keyser, Optimizing Diffusive Transport Through a Synthetic
11 8 Membrane Channel, *Adv. Mater.* 25 (2013) 844–849. doi:10.1002/adma.201203500.
12 9 [297] A. Ghavami, E. van der Giessen, P.R. Onck, Energetics of Transport through the Nuclear
13 10 Pore Complex, *PLoS One.* 11 (2016) e0148876. doi:10.1371/journal.pone.0148876.
14 11 [298] Z. Zhu, D. Wang, Y. Tian, L. Jiang, Ion/molecule transportation in nano- pore/channels:
15 12 From critical principles to diverse functions, *J. Am. Chem. Soc.* (2019) jacs.9b00086.
16 13 doi:10.1021/jacs.9b00086.
17 14 [299] J.-M. Pagès, C.E. James, M. Winterhalter, The porin and the permeating antibiotic: a
18 15 selective diffusion barrier in Gram-negative bacteria., *Nat. Rev. Microbiol.* 6 (2008) 893–
19 16 903. doi:10.1038/nrmicro1994.
20 17 [300] C. Danelon, E.M. Nestorovich, M. Winterhalter, M. Ceccarelli, S.M. Bezrukov,
21 18 Interaction of zwitterionic penicillins with the OmpF channel facilitates their
22 19 translocation, *Biophys. J.* 90 (2006) 1617–1627.
23 20 [301] E.M. Nestorovich, C. Danelon, M. Winterhalter, S.M. Bezrukov, Designed to penetrate:
24 21 Time-resolved interaction of single antibiotic molecules with bacterial pores, *Proc. Natl.*
25 22 *Acad. Sci.* 99 (2002) 9789–9794.
26 23 [302] S.M. Bezrukov, L. Kullman, M. Winterhalter, Probing sugar translocation through
27 24 maltoporin at the single channel level, *FEBS Lett.* 476 (2000) 224–228.
28 25 [303] Y.M. Chook, K.E. Süel, Nuclear import by karyopherin- β s: Recognition and inhibition,
29 26 *Biochim. Biophys. Acta - Mol. Cell Res.* 1813 (2011) 1593–1606.
30 27 doi:10.1016/j.bbamcr.2010.10.014.
31 28 [304] M. Kimura, N. Imamoto, Biological Significance of the Importin- β Family-Dependent
32 29 Nucleocytoplasmic Transport Pathways, *Traffic.* 15 (2014) 727–748.
33 30 doi:10.1111/tra.12174.
34 31 [305] R. Peters, Translocation Through the Nuclear Pore Complex: Selectivity and Speed by
35 32 Reduction-of-Dimensionality, *Traffic.* 6 (2005) 421.
36 33 [306] B.N. Miles, A.P. Ivanov, K.A. Wilson, F. Doğan, D. Japrun, J.B. Edel, Single molecule
37 34 sensing with solid-state nanopores: novel materials, methods, and applications., *Chem.*
38 35 *Soc. Rev.* 42 (2013) 15–28. doi:10.1039/c2cs35286a.
39 36 [307] X. Hou, W. Guo, L. Jiang, Biomimetic smart nanopores and nanochannels., *Chem. Soc.*
40 37 *Rev.* 40 (2011) 2385–401. doi:10.1039/c0cs00053a.
41 38 [308] B. Derrida, E. Domany, D. Mukamel, An exact solution of a one-dimensional asymmetric
42 39 exclusion model with open boundaries, *J. Stat. Phys.* 69 (1992) 667–687.
43 40 [309] S. Nowak, P.-W. Fok, T. Chou, Dynamic boundaries in asymmetric exclusion processes,
44 41 *Phys. Rev. E.* 76 (2007) 1–11. doi:10.1103/PhysRevE.76.031135.
45 42 [310] G. Lakatos, J. O'Brien, T. Chou, Hydrodynamic mean-field solutions of 1D exclusion
46 43 processes with spatially varying hopping rates, *J. Phys. A. Math. Gen.* 39 (2006) 2253–
47 44 2264. doi:10.1088/0305-4470/39/10/002.
48 45 [311] G.M. Schuetz, Single-file diffusion far from equilibrium, *Diffus. Fundam.* 2 (2005) 1–5.
49 46 [312] A. Zilman, J. Pearson, G. Bel, Effects of jamming on nonequilibrium transport times in
50
51
52
53
54
55
56
57
58
59
60
61
62
63
64
65

- 1
2
3
4 1 nanochannels, *Phys. Rev. Lett.* 103 (2009) 128103. doi:10.1103/PhysRevLett.103.128103.
5 2 [313] C. Rödenbeck, J. Kärger, K. Hahn, Exact analytical description of tracer exchange and
6 3 particle conversion in single-file systems, *Phys. Rev. E.* 55 (1997) 5697.
7 4 [314] T. Chou, Kinetics and thermodynamics across single-file pores: Solute permeability and
8 5 rectified osmosis, *J. Chem. Phys.* 110 (1999) 606.
9 6 [315] D. Gillespie, D. Boda, The Anomalous Mole Fraction Effect in Calcium Channels: A
10 7 Measure of Preferential Selectivity, *Biophys. J.* 95 (2008) 2658–2672.
11 8 doi:10.1529/BIOPHYSJ.107.127977.
12 9 [316] D. Gillespie, D. Boda, Y. He, P. Apel, Z.S. Siwy, Synthetic nanopores as a test case for
13 10 ion channel theories: The anomalous mole fraction effect without single filing, *Biophys. J.*
14 11 95 (2008) 609–619. doi:10.1529/BIOPHYSJ.107.127985.
15 12 [317] S.W. Lockless, Determinants of cation transport selectivity: Equilibrium binding and
16 13 transport kinetics., *J. Gen. Physiol.* (2015) jgp.201511371-. doi:10.1085/jgp.201511371.
17 14 [318] J.E. Hinshaw, B.O. Carragher, R.A. Milligan, R.A. Milligan, Architecture and Design
18 15 of the Nuclear Pore Complex, *Cell Press*, 1992. doi:10.1016/0092-8674(92)90635-P.
19 16 [319] P.S. Burada, P. Hänggi, F. Marchesoni, G. Schmid, P. Talkner, Diffusion in confined
20 17 geometries., *Chem.Phys.Chem a Eur. J. Chem. Phys. Phys. Chem.* 10 (2009) 45–54.
21 18 doi:10.1002/cphc.200800526.
22 19 [320] H. Merlitz, C.-X. Wu, J.-U. Sommer, Inclusion Free Energy of Nanoparticles in Polymer
23 20 Brushes, *Macromolecules.* 45 (2012) 8494–8501. doi:10.1021/ma301781b.
24 21 [321] J. Bednenko, G. Cingolani, L. Gerace, Importin β contains a COOH-terminal nucleoporin
25 22 binding region important for nuclear transport, *J. Cell Biol.* 162 (2003) 391–401.
26 23 doi:10.1083/jcb.200303085.
27 24 [322] A. Goryaynov, W. Yang, Role of Molecular Charge in Nucleocytoplasmic Transport,
28 25 *PLoS One.* 9 (2014) e88792. doi:10.1371/journal.pone.0088792.
29 26 [323] B. Naim, D. Zbaida, S. Dagan, R. Kapon, Z. Reich, Cargo surface hydrophobicity is
30 27 sufficient to overcome the nuclear pore complex selectivity barrier., *EMBO J.* 28 (2009)
31 28 2697–705. doi:10.1038/emboj.2009.225.
32 29 [324] W. Yang, S.M. Musser, Nuclear import time and transport efficiency depend on importin
33 30 beta concentration., *J. Cell Biol.* 174 (2006) 951–61. doi:10.1083/jcb.200605053.
34 31 [325] A.R. Lowe, J.J. Siegel, P. Kalab, M. Siu, K. Weis, J.T. Liphardt, Selectivity mechanism of
35 32 the nuclear pore complex characterized by single cargo tracking., *Nature.* 467 (2010) 600–
36 33 3. doi:10.1038/nature09285.
37 34 [326] G. Paci, T. Zheng, J. Caria, A. Zilman, E.A. Lemke, Molecular determinants of large
38 35 cargo transport into the nucleus, *Elife.* 9 (2020) 1–24. doi:10.7554/eLife.55963.
39 36 [327] N. Panté, M. Kann, Nuclear pore complex is able to transport macromolecules with
40 37 diameters of ~ 39 nm, *Mol. Biol. Cell.* 13 (2002) 425–434. doi:10.1091/mbc.01-06-0308.
41 38 [328] C.A. Niño, L. Hérisant, A. Babour, C. Dargemont, mRNA Nuclear Export in Yeast.,
42 39 *Chem. Rev.* (2013). doi:10.1021/cr400002g.
43 40 [329] D. Grünwald, R.H. Singer, M. Rout, Nuclear export dynamics of RNA-protein
44 41 complexes., *Nature.* 475 (2011) 333–41. doi:10.1038/nature10318.
45 42 [330] D.L. Nelson, A.L. Lehninger, M.M. Cox, *Lehninger Principles of Biochemistry*, 2nd ed.,
46 43 Addison-Wesley, 2008.
47 44 [331] M. Schlosshauer, D. Baker, Realistic protein–protein association rates from a simple
48 45 diffusional model neglecting long-range interactions, free energy barriers, and
49 46 landscape ruggedness, *Protein Sci.* (2009) 1660–1669.

- doi:10.1110/ps.03517304.luchowski.
- [332] G. Chatel, S.H. Desai, A.L. Mattheyses, M.A. Powers, B. Fahrenkrog, Domain topology of nucleoporin Nup98 within the nuclear pore complex., *J. Struct. Biol.* 177 (2012) 81–9. doi:10.1016/j.jsb.2011.11.004.
- [333] B. Fahrenkrog, B. Maco, A.M. Fager, J. Köser, U. Sauder, K.S. Ullman, U. Aepli, Domain-specific antibodies reveal multiple-site topology of Nup153 within the nuclear pore complex., *J. Struct. Biol.* 140 (2002) 254–67. <http://www.ncbi.nlm.nih.gov/pubmed/12490173>.
- [334] J. Ma, A. Goryaynov, A. Sarma, W. Yang, Self-regulated viscous channel in the nuclear pore complex., *Proc. Natl. Acad. Sci. U. S. A.* 109 (2012) 7326–31. doi:10.1073/pnas.1201724109.
- [335] S. Shah, D.J. Forbes, Separate nuclear import pathways converge on the nucleoporin Nup153 and can be dissected with dominant-negative inhibitors, *Curr. Biol.* 8 (1998) 1376–1386. doi:10.1016/S0960-9822(98)00018-9.
- [336] L.-C. Tu, M. Huisman, Y.-C. Chung, C.S. Smith, D. Grunwald, Deconstructing transport-distribution reconstruction in the nuclear-pore complex, *Nat. Struct. Mol. Biol.* 25 (2018) 1061–1062. doi:10.1038/s41594-018-0161-2.
- [337] B. Mishra, B.B. Patel, S. Tiwari, Colloidal nanocarriers: a review on formulation technology, types and applications toward targeted drug delivery, *Nanomedicine Nanotechnology, Biol. Med.* 6 (2010) 9–24. doi:10.1016/j.nano.2009.04.008.
- [338] I. Luzinov, S. Minko, V. V Tsukruk, Responsive brush layers: from tailored gradients to reversibly assembled nanoparticles, *Soft Matter.* 4 (2008) 714–725.
- [339] E.E. Benarroch, Nucleocytoplasmic transport, *Neurology.* 92 (2019) 757–764. doi:10.1212/WNL.0000000000007305.
- [340] D. Görlich, M.J. Seewald, K. Ribbeck, Characterization of Ran-driven cargo transport and the RanGTPase system by kinetic measurements and computer simulation., *EMBO J.* 22 (2003) 1088–100. doi:10.1093/emboj/cdg113.
- [341] M. V. Nachury, K. Weis, K. Zerf, R. Peters, The direction of transport through the nuclear pore can be inverted, *Proc. Natl. Acad. Sci.* 96 (1999) 9622–9627. doi:10.1073/pnas.96.17.9622.
- [342] G. Riddick, I.G. Macara, The adapter importin- α provides flexible control of nuclear import at the expense of efficiency., *Mol. Syst. Biol.* 3 (2007) 118. doi:10.1038/msb4100160.
- [343] W.S. Ryu, R.M. Berry, H.C. Berg, Torque-generating units of the flagellar motor of *Escherichia coli* have a high duty ratio., *Nature.* 403 (2000) 444–7. doi:10.1038/35000233.
- [344] R.B. Kopito, M. Elbaum, Nucleocytoplasmic transport: A thermodynamic mechanism, *HFSP J.* 3 (2009) 130–141. doi:10.2976/1.3080807.
- [345] T. Cavazza, I. Vernos, The RanGTP Pathway: From Nucleo-Cytoplasmic Transport to Spindle Assembly and Beyond, *Front. Cell Dev. Biol.* 3 (2016) 82. doi:10.3389/fcell.2015.00082.
- [346] A. Goldbeter, D.E. Koshland, A.P. Arkin, An amplified sensitivity arising from covalent modification in biological systems., *Proc. Natl. Acad. Sci. U. S. A.* 78 (1981) 6840–4. doi:10.1073/pnas.78.11.6840.
- [347] C.-H. Wang, P. Mehta, M. Elbaum, Thermodynamic Paradigm for Solution Demixing Inspired by Nuclear Transport in Living Cells, *Phys. Rev. Lett.* 118 (2017) 158101.

- 1
2
3
4
5
6
7
8
9
10
11
12
13
14
15
16
17
18
19
20
21
22
23
24
25
26
27
28
29
30
31
32
33
34
35
36
37
38
39
40
41
42
43
44
45
46
47
48
49
50
51
52
53
54
55
56
57
58
59
60
61
62
63
64
65
- 1 doi:10.1103/PhysRevLett.118.158101.
2 [348] A.E. Smith, B.M. Slepchenko, J.C. Schaff, L.M. Loew, I.G. Macara, Systems analysis of
3 Ran transport., *Science*. 295 (2002) 488–91. doi:10.1126/science.1064732.
4 [349] S. Kim, M. Elbaum, A Simple Kinetic Model with Explicit Predictions for Nuclear
5 Transport, *Biophys. J.* 105 (2013) 565–569. doi:10.1016/J.BPJ.2013.04.025.
6 [350] S. Kim, M. Elbaum, Enzymatically Driven Transport: A Kinetic Theory for Nuclear
7 Export, *Biophys. J.* 105 (2013) 1997–2005. doi:10.1016/J.BPJ.2013.09.011.
8 [351] S.R. Solmaz, R. Chauhan, G. Blobel, I. Melčák, Molecular Architecture of the Transport
9 Channel of the Nuclear Pore Complex, *Cell*. 147 (2011) 590–602.
10 <http://www.sciencedirect.com/science/article/pii/S0092867411011457> (accessed January
11 24, 2014).
12 [352] A. Elosegui-Artola, I. Andreu, A.E.M. Beedle, A. Lezamiz, M. Uroz, A.J. Kosmalka, R.
13 Oria, J.Z. Kechagia, P. Rico-Lastres, A.L. Le Roux, C.M. Shanahan, X. Trepas, D.
14 Navajas, S. Garcia-Manyes, P. Roca-Cusachs, Force Triggers YAP Nuclear Entry by
15 Regulating Transport across Nuclear Pores, *Cell*. 171 (2017) 1397-1410.e14.
16 doi:10.1016/j.cell.2017.10.008.

Declaration of interests

The authors declare that they have no known competing financial interests or personal relationships that could have appeared to influence the work reported in this paper.

The authors declare the following financial interests/personal relationships which may be considered as potential competing interests: